

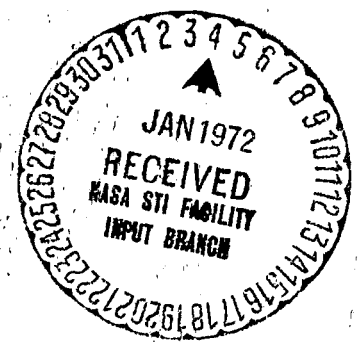
NASA CR-122359

(NASA-CR-122359) MAGNETOSPHERIC ACCESS OF
SOLAR PARTICLES AND THE CONFIGURATION OF
THE DISTANT GEOMAGNETIC FIELD, VOLUME 1
Ph.D. Thesis L.C. Evans (California Inst.
of Tech.) 1972 164 p
CSCL 03B G3/29
N72-25726
Unclas
30737

Get D

CALIFORNIA INSTITUTE OF TECHNOLOGY

Reproduced by
NATIONAL TECHNICAL
INFORMATION SERVICE
U.S. Department of Commerce
Springfield, VA 22151



MAGNETOSPHERIC ACCESS OF SOLAR PARTICLES
AND THE CONFIGURATION OF THE DISTANT GEOMAGNETIC FIELD

Thesis by
Lawrence Curtis Evans

Volume One

MAGNETOSPHERIC ACCESS OF SOLAR PARTICLES
AND THE CONFIGURATION OF THE DISTANT GEOMAGNETIC FIELD

Thesis by
Lawrence Curtis Evans

In Partial Fulfillment of the Requirements
for the Degree of
Doctor of Philosophy

California Institute of Technology
Pasadena, California

1972

(Submitted 22 September 1971)

to Janet,

for her patience, cooperation, and devotion;

to Carolyn and David,

for their enthusiasm, curiosity, and interest;

to my parents,

for their motivation, counsel, and faith;

to Vernon,

for his inspiration, advice, and concern; and

to them all,

for their love is what gives meaning to the fulfillment of goals.

ACKNOWLEDGMENTS

I am indebted to my faculty sponsor, Professor Edward C. Stone, for the time which he has taken from an increasingly busy schedule to provide guidance and encouragement throughout this research project.

I am grateful for many stimulating discussions with Dr. J. L. Fanselow. Some of these discussions solved the world's fundamental problems, while most, though more mundane, were more pertinent to the study reported in this thesis. Of particular note are the fortitude he demonstrated by volunteering to read the rough drafts of this thesis, and the appropriate and helpful comments he made as a result.

It is also a pleasure to acknowledge rewarding discussions with Professor L. Davis, Jr., Dr. S. S. Murray, and Messrs. J. E. Lupton, J. W. Brown, and T. L. Garrard.

All of the design and construction and most of the calibrations of the instrument being used here were completed prior to my involvement with the project. I am most grateful to Professor J. A. Simpson, principal investigator, and the staff of the Laboratory for Astrophysics and Space Research at the University of Chicago, who, along with Professor Stone, were responsible for the successful completion of these phases of this experiment. The electron response of a detector system similar to that flown on OGO-4 was measured at California Institute of Technology

by Mr. J. E. Lupton and the data were analyzed by Mr. J. W. Brown.

The formidable tasks of bookkeeping and routine data processing of the large number of data tapes associated with a satellite experiment have been performed admirably by Mmes. E. Aguilar and F. Pickett.

I am grateful to Professor J. A. Simpson and Messrs. J. D. Sullivan and H. J. Crawford of the University of Chicago for their help in providing some interplanetary proton data from IMP-4 for comparison with the OGO-4 data.

I am also grateful to Drs. D. H. Fairfield and N. F. Ness of the Goddard Space Flight Center for providing one hour averages of interplanetary magnetic field parameters for a period encompassing most of the lifetime of the OGO-4 satellite. These data were collected by Explorer 33, Explorer 35, and IMP-4.

I am appreciative of the fine work done by all those associated with the National Aeronautics and Space Administration OGO Project Office.

Financial aid during my graduate studies has been provided by the National Science Foundation, the State of California, and California Institute of Technology, for which I and my family are indebted. The research described in this thesis was supported by the National Aeronautics and Space Administration under contract NAS 5-3095 and grant NGL 05-002-007.

ABSTRACT

The access of 1.2-40 MeV protons and 0.4-1.0 MeV electrons from interplanetary space to the polar cap regions has been investigated with an experiment on board a low altitude, polar orbiting satellite (OGO-4).

A total of 333 quiet time observations of the electron polar cap boundary give a mapping of the boundary between open and closed geomagnetic field lines which is an order of magnitude more comprehensive than previously available.

Persistent features (north/south asymmetries) in the polar cap proton flux, which are established as normal during solar proton events, are shown to be associated with different flux levels on open geomagnetic field lines than on closed field lines. The pole in which these persistent features are observed is strongly correlated to the sector structure of the interplanetary magnetic field and uncorrelated to the north/south component of this field. The features were observed in the north (south) pole during a negative (positive) sector 91% of the time, while the solar field had a southward component only 54% of the time. In addition, changes in the north/south component have no observable effect on the persistent features.

Observations of events associated with co-rotating regions of enhanced proton flux in interplanetary space are used to establish the

characteristics of the 1.2-40 MeV proton access windows: the access window for low polar latitudes is near the earth, that for one high polar latitude region is $\sim 250 R_{\oplus}$ behind the earth, while that for the other high polar latitude region is $\sim 1750 R_{\oplus}$ behind the earth. All of the access windows are of approximately the same extent ($\sim 120 R_{\oplus}$). The following phenomena contribute to persistent polar cap features: limited interplanetary regions of enhanced flux propagating past the earth, radial gradients in the interplanetary flux, and anisotropies in the interplanetary flux.

These results are compared to the particle access predictions of the distant geomagnetic tail configurations proposed by Michel and Dessler, Dungey, and Frank. The data are consistent with neither the model of Michel and Dessler nor that of Dungey. The model of Frank can yield a consistent access window configuration provided the following constraints are satisfied: the merging rate for open field lines at one polar neutral point must be ~ 5 times that at the other polar neutral point, related to the solar magnetic field configuration in a consistent fashion, the migration time for open field lines to move across the polar cap region must be the same in both poles, and the open field line merging rate at one of the polar neutral points must be at least as large as that required for almost all the open field lines to have merged in $O(\text{one hour})$. The possibility of satisfying these constraints is investigated in some detail.

The role played by interplanetary anisotropies in the observation

of persistent polar cap features is discussed. Special emphasis is given to the problem of non-adiabatic particle entry through regions where the magnetic field is changing direction. The degree to which such particle entry can be assumed to be nearly adiabatic is related to the particle rigidity, the angle through which the field turns, and the rate at which the field changes direction; this relationship is established for the case of polar cap observations.

TABLE OF CONTENTS

I. INTRODUCTION	1
II. INSTRUMENT	6
Vertical Telescope	7
Horizontal Telescope	11
Electronics and Data Formatting	14
Thresholds and Calibrations	17
III. SATELLITE	30
IV. DATA ANALYSIS	39
V. OBSERVATIONS	47
Electron Observations	47
Proton Observations	53
EDP Event of 1 December 1967	57
Solar Flare Event of 2 November 1967	70
Comparison of Electron and Proton Observations	76
VI. BACKGROUND	86
Interplanetary Environment	86
Geomagnetic Field and Magnetic Merging	92

VII. DISCUSSION	104
Electron Polar Cap	105
Access of 1.2-40 MeV Protons	107
EDP Events	114
Flare Events	120
Models of the Distant Geomagnetic Field Configuration	122
Closed Magnetospheric Configuration -- MODEL A	123
Magnetic Merging at the Sub-solar Point -- MODEL B	129
Magnetic Merging at the Polar Neutral Points -- MODEL C	132
Interplanetary Anisotropies	143
VIII. CONCLUSIONS	149
APPENDIX A: Additional Observations	154
APPENDIX B: Particle Trajectories in a Turning Magnetic Field	192
APPENDIX C: Magnetic Merging at the Polar Neutral Points	207
Assumptions	209
Assumption A	216
Assumption B	219
Assumption C	220
Derivation of Merging Rates -- General	221
Assumption A	228
Assumption B	235
Assumption C	240
Results	244
REFERENCES	256

I. INTRODUCTION

An investigation of the physical processes involved in the access of low energy particles from interplanetary space into the interior of the earth's magnetic field is of special significance to several geophysical and astrophysical questions. Such an investigation bears directly on the question of the configuration of the distant geomagnetic field and the relation between this field and the polar cap region. A definition of this configuration is perhaps the only means available for the determination of the degree to which magnetic field merging plays a rôle in the interaction between solar and terrestrial plasmas and magnetic fields. Constraints placed on the extent of magnetic merging in this interaction would have far-reaching implications for other phenomena involving solar magnetic fields and for some phenomena involving galactic magnetic fields.

Since the discovery, in 1964 [1], that the solar wind distorts the geomagnetic field to the extent of forming a "tail" in the anti-solar direction, there has been a good deal of speculation concerning the configuration of the magnetic field in this tail at large distances from the earth. The models which have been presented for this configuration by Dungey (1961) [2], Dessler (1964) [3], and Frank (1971) [4] differ in their estimates of the length of the tail by one or two orders of magnitude. As Dessler pointed out, charged particle observations in the polar

caps constitute one of the most efficient and appropriate means of determining the structure of the distant geomagnetic field, since it is not practical to use satellite-born magnetometers to map this structure in detail.

Since the fundamental theoretical difference between the three models of the distant geomagnetic field is the assumption made about the extent and/or mechanism by which the solar and terrestrial fields merge, a resolution of questions concerning the configuration of the distant field can have a direct bearing, through these models, on the question of whether magnetic field merging is a significant process in the interaction between the solar wind and the geomagnetic field. Since it has been suggested that magnetic field merging may play an important role in, for instance, the generation of solar [5] and/or galactic [6] flares, a determination of the possibility or impossibility of magnetic merging in astrophysical plasmas, even over a limited range of plasma parameters, would be quite significant. The interaction between the solar wind plasma and the geomagnetic field is the only readily available system for which this can be determined.

Although charged particle measurements cannot determine the extent of magnetic merging directly, they can lead to the establishment of constraints to be placed on magnetospheric models. Several studies have been conducted with this goal in mind. Observations of >50 keV and >20 keV electrons in the magnetotail have been interpreted by Van Allen [7,8] and Anderson and Lin [9] as evidence that these electrons gain access to the magnetotail along geomagnetic field lines which are

connected to the interplanetary field. These results have, however, been interpreted differently by Michel and Dessler [10], who have modified the closed field configuration model (e.g. no merging) to account for these electron observations. In any case, the mode of access for >1 MeV protons may be quite different than that for >50 keV electrons, owing to the large differences in magnetic rigidity (~ 0.05 MV for the electrons *vs.* ~ 100 MV for the protons) and velocity ($0.43c$ (electrons) *vs.* $0.046c$ (protons)). The observation by Evans and Stone [11] of a large north/south difference in the proton polar cap flux lasting for more than twenty hours showed that the question of proton access was still unresolved.

Prior to the observations reported by Evans and Stone [11], some evidence of structure in observed polar cap proton fluxes was available [12-21], but the observations were too sparse to lead to comprehensive analysis. Since this preliminary report, several observations of persistent north/south asymmetries have been reported [22-26], and several of the most recent (Englemann, *et al.* [24], Van Allen, *et al.* [25], and Morfill and Quenby [26]) have been interpreted in the context of the Dungey open field configuration, relating the north/south polar cap flux differences to interplanetary flux anisotropies. Van Allen, *et al.* [25], for instance, report observations which seem to follow this relationship closely, but only for a period of about six hours during one solar flare event. This emphasizes a limitation which is common to all the previous observations cited above: none of these studies deal with observations from more than two events. Results obtained from the analysis of only one or two flare events are subject to the severe limitation that the

solar and interplanetary parameters which determine the behavior of the particle flux near the earth can vary significantly from one solar flare event to the next. Thus, although it is now well established that large scale structure in the polar cap flux of low energy protons is not uncommon, aside from the indications that interplanetary flux anisotropies play a role in the observations of north/south asymmetries, the relationship between polar cap fluxes and interplanetary particle fluxes is still unresolved.

The high time, energy, and flux resolution of the data presented in this thesis make them particularly appropriate to an investigation of low energy charged particle access to the polar caps. As suggested by Vampola [27], low rigidity electron observations can be used to map the geomagnetic tail field lines onto the polar caps in order to determine the polar cap boundary between open and closed geomagnetic field lines; the 333 observations of this boundary reported here will result in a much more comprehensive mapping than the 25 such observations previously available [27]. The proton observations reported herein differ from the observations cited above in at least two important aspects: (1) the availability of data throughout an eighteen month period has resulted in the compilation and analysis of fifty-four solar proton events rather than one or two, and (2) some of these events represent the first polar cap observations of fluxes associated with regions of enhanced flux in interplanetary space which are co-rotating past the earth. These observations will be interpreted in terms of the locations of the access windows for 1.2-40 MeV protons for the different regions of the polar

caps. The configuration of these access windows will then be related to the magnetospheric models mentioned above, and hence to the question of magnetic field merging.

II. INSTRUMENT

The detector system used in this study consists of two independent particle telescopes, each designed (a) to optimize charge and energy resolution within a range of incident particle energies, and (b) to be sensitive and operable over a wide range of incident particle fluxes. Because of their orientations on the spacecraft (see Section III), these telescopes are referred to as the vertical telescope and the horizontal telescope. Measurements consist of the counting rates, energy loss, and range of incident particles [28].

The rapid motion of a polar orbiting satellite with respect to the geomagnetic field subjects a detector system on board to rapid fluctuations in incident fluxes, due to changing geomagnetic cutoffs and trapped particles. This tends to place an upper limit on the sampling period for the various rates monitored by the system. In order to obtain adequate resolution of these fluctuations, the rates for this experiment were averaged over a maximum of 288 msec, during which time the spacecraft will have moved, typically, 1.1 minutes in latitude. Although this averaging rate represents the situation for the bulk of the data reported here (data which were collected on the on-board tape recorder), when the spacecraft telemetry was in the real time mode the averaging time is either 72 msec or 18 msec, depending on the exact telemetry configuration. Data collected in the real time mode are particularly

suitable to the study of phenomena closely related to the geomagnetic field, such as cutoffs.

Vertical Telescope

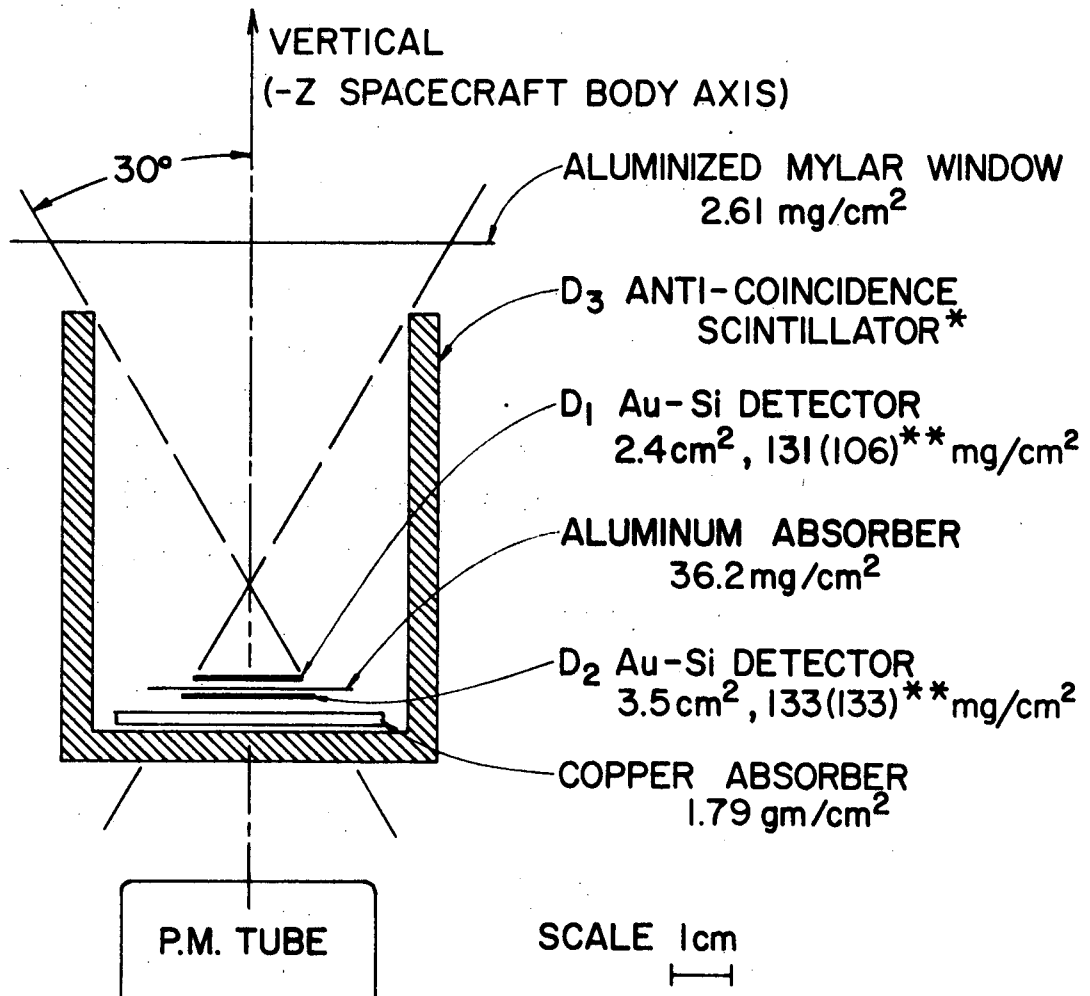
Figure II-1 shows a schematic cross sectional view of the vertical telescope, which consists of a stack of circular detectors and absorbers. From top to bottom, they are: a gold-silicon surface barrier detector, an aluminum absorber, another gold-silicon surface barrier detector, and a copper absorber. Such solid state detectors measure the energy lost by a charged particle passing through the sensitive region of the detector; the physical characteristics of these detectors and absorbers are given in table II-1. The detector stack is completely surrounded, except for the entrance aperture, by a cylindrical plastic scintillator cup, which serves to (1) collimate the response of the telescope, (2) help discriminate against side showers and nuclear interactions within the stack, and (3) determine the high energy analysis limit (~ 40 MeV/nucleon) for the system. The entrance aperture is covered by a 3/4 mil (0.00075 in) aluminized mylar light baffle; the thickness of this baffle contributes significantly to the low energy threshold (1.21 MeV/nucleon) of the telescope.

Incident particles are analyzed only if not registered in the anti-coincidence detector D_3 . The number of particles with energy losses above an electronically determined threshold in D_1 and D_2 are recorded, along with the number of $D_1 D_2$ coincidences. In addition, the energy

Figure II-1

Schematic cross section of vertical telescope.

OGO-II, IV VERTICAL PARTICLE TELESCOPE



* SCINTILLATOR IS SURROUNDED BY 138
mg/cm² OF MAGNESIUM.

** VALUES FOR OGO-IV ARE IN PARENTHESES.

D₁ AND D₂ BOTH HAVE DEPLETION
DEPTHS OF 56 mg/cm².

Table II-1

Physical Properties of Detectors and Absorbers
in the Vertical and Horizontal Telescopes

Detector/Absorber	Material	Thickness (mg/cm ²)	Sensitive Area (cm ²)
Window (Vertical)	Mylar	2.6 ± 0.2	-
D ₁ (Total) (Depletion region)	Silicon	106 ± 2 56 ± 5	2.4 (nom.)
Absorber	Aluminum	36 ± 4	-
D ₂ (Total) (Depletion region)	Silicon	133 (nom.) 56 (est.)	3.5 (nom.)
Absorber	Copper	1790 ± 45	-
Inner housing	Magnesium	138 ± 9	-
D ₃	Plastic Scintillator	505 ± 27	-
Window (Horizontal)	Mylar	1.22 (nom.)	
H ₁ (Total) (Depletion region)	Silicon	11.7 (nom.) 5.8 (nom.)	0.079 (nom.)

lost in D_1 is measured for one event during each sample period. The number of particles measured by D_3 are also recorded. The electronic configuration and the geometrical factors for the various rates are discussed in more detail below.

As noted in table II-1, the detectors used in this experiment are not fully depleted; fully depleted detectors with such large sensitive areas were not available when this experiment was designed. As will be noted below, the non-uniformity of the depletion depth over the sensitive area of the detector was one of the principle factors which limited the resolution of the pulse height analysis of the output from D_1 .

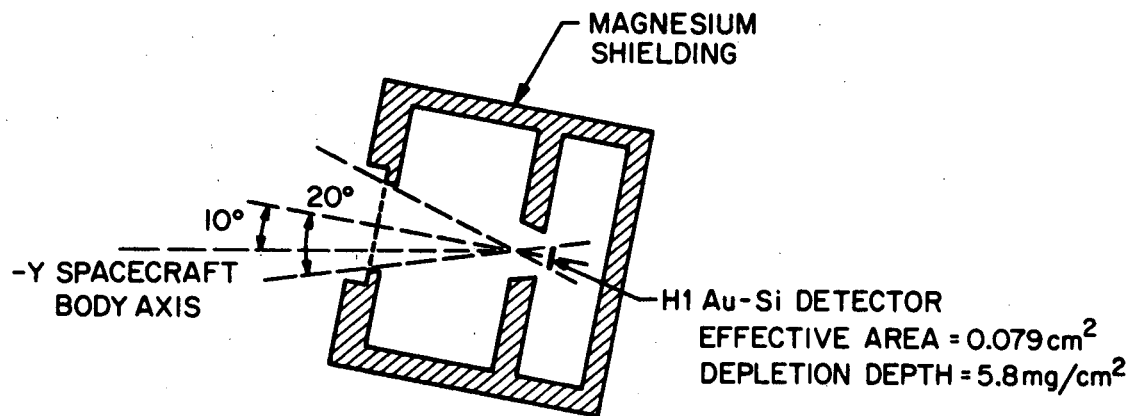
Horizontal Telescope

A schematic cross section of the horizontal telescope is shown in figure II-2. This telescope, which is considerably smaller than the vertical telescope, consists of a single gold-silicon surface barrier detector completely surrounded, except for the entrance aperture, by a magnesium shield. As in the vertical telescope, the entrance aperture is covered by a 0.00035 in. aluminumized mylar light baffle. The physical characteristics of the horizontal detector and window are included in table II-1. It should be noted that the collimation for this telescope is passive, in contrast to the active collimator available for the vertical telescope. The effect of this difference on the response of these two telescopes is indicated below in connection with the energy dependent geometrical factors. All charged particles losing more energy

Figure II-2

Schematic cross section of horizontal telescope. Note that the scale used here is different than that used in figure II-1.

OGO-II, IV HORIZONTAL PARTICLE TELESCOPE



in the sensitive region of the detector than the electronically determined threshold are counted.

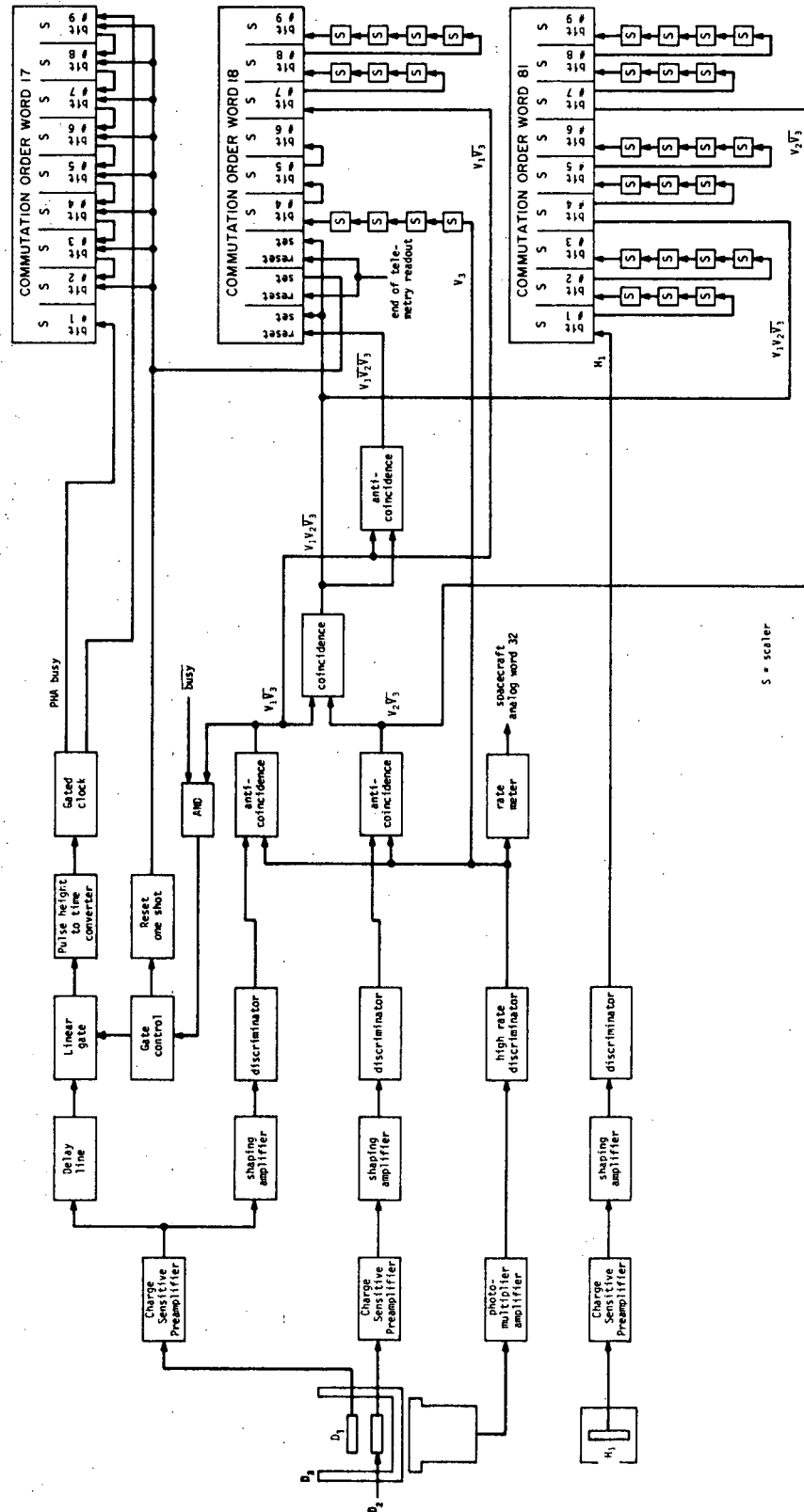
Electronics and Data Formatting

The block diagram in figure II-3 illustrates the logic configuration of the electronics system associated with the two charged particle telescopes and the format in which the data are stored in the spacecraft. The details of the electronic components are similar to those for Experiment F-20 on OGO-6 which were specified in a paper presented to the Fourteenth Nuclear Science Symposium of the IEEE in 1967 [29]. As indicated on this figure, the following information is stored by this experiment:

1. The 2^0 , 2^4 , and 2^9 bits of the recycling scalars corresponding to the number of counts from the following four logic configurations: $V_1\overline{V_3}$, $V_2\overline{V_3}$, $V_1V_2\overline{V_3}$, and H_1 ($V_1 \equiv D_1$, $V_2 \equiv D_2$, $V_3 \equiv D_3$).
2. The 2^4 , 2^5 , and 2^6 bits of a recycling scalar associated with the number of V_3 counts.
3. A 256-channel pulse height analysis of the amount of energy deposited in D_1 . Only one such analysis can be stored; the contents of word 17 are erased prior to storing a new event analysis. Thus only the last event analyzed before each readout is available.
4. Flags indicating whether the pulse height analyzed event is a new event (since the last telemetry readout) and whether the threshold of D_2 was exceeded on the event analyzed.

Figure II-3

Functional block diagram of electronics system.



5. A digitization of an analog rate meter connected to the output of the V_3 discriminator.

The spacecraft telemetry will be discussed in Section III.

Thresholds and Calibrations

The electronic thresholds associated with the discriminators of the four detectors were set so as to minimize the contamination due to background noise. The values of these thresholds in terms of detector output and of incident particle energy were determined by electronic and particle calibrations. The electronic calibrations give a precise determination of the discriminator thresholds and pulse height analyzer response as a function of charge at the input to the charge sensitive pre-amplifier, while the particle calibrations enable a determination of the response and resolution of the detectors.

In order to interpret these calibrations in terms of the response of the telescope, interpolations were made in the range-energy loss tables given by Janni [30] wherever necessary. These tables were generated by integrating a semi-empirical expression for the energy loss of a charged particle passing through a homogeneous material. The calibrations are described in more detail in a Space Radiation Laboratory Internal Report [31].

The results of the electronic calibrations of the detector thresholds are given in table II-2.

Table II-2

Energy loss thresholds for OGO-4 detectors

Detector	Threshold (25 °C)	Temperature Coefficient
D ₁	424±22 keV	0.0 keV/°C
D ₂	253±23 keV	0.3 keV/°C
D ₃	53±3 mV	-0.1 mV/°C
H ₁	377±14 keV	0.6 keV/°C

By using the range-energy loss tables mentioned above, the correspondence between the pulse height analyzer channel thresholds and incident proton energy can be determined. This is shown in figure II-4. An important facet of the correspondence shown in this figure is that for channel numbers greater than 29 (and less than 72) two incident proton energies can be associated with each channel threshold. Below channel 29, the availability of the range information provided by D_2 makes the association between incident proton energy and channel threshold unique. The effect of these *double-valued* pulse height analyzer channels on the analysis of the data will be discussed in Section IV.

The proton response of the vertical telescope was determined by exposing the assembled telescope to a series of proton beams using the Caltech Tandem Van de Graff accelerator [31].

The electron response of the detectors in the vertical telescope was determined by exposing nearly identical detectors to the beam of a magnetic spectrometer [32]. Electron geometrical factors as a function of energy for D_1 and D_2 determined in this manner are given in figure II-5. It is clear from these results that the electron sensitivity of the $V_1V_2\sqrt{V_3}$ rate is negligible. The thin depletion depth and high electronic threshold of the H_1 detector insure that the electron sensitivity of the H_1 rate is $< 10^{-4}$ [33].

The incident energy ranges corresponding to the rates measured by this experiment are summarized in table II-3. In addition to the average geometrical factors included in table II-3, energy dependent proton

Figure II-4

Correspondence between pulse height analyzer channel thresholds and incident proton energy (incident in mylar window). The D_1 discriminator level is indicated, along with the energies corresponding to the triggering of D_2 and D_3 . The alpha particle response is also shown. Note the set of channels for which there is no one-to-one correspondence between channel threshold and incident proton energy. These channels are referred to as *double-valued*.

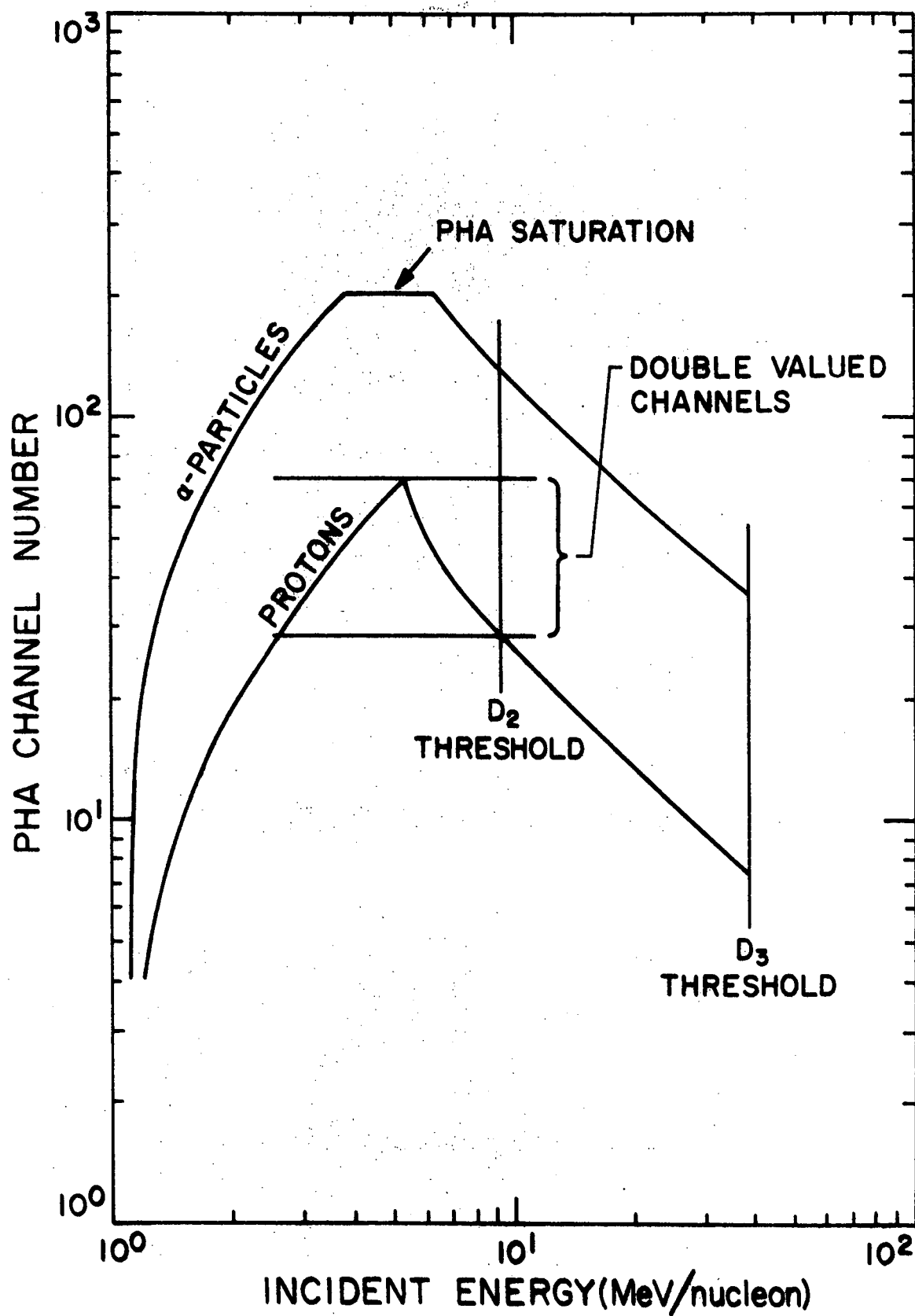


Figure II-5

Electron geometrical factors for $V_1\overline{V_3}$ and $V_2\overline{V_3}$ rates.

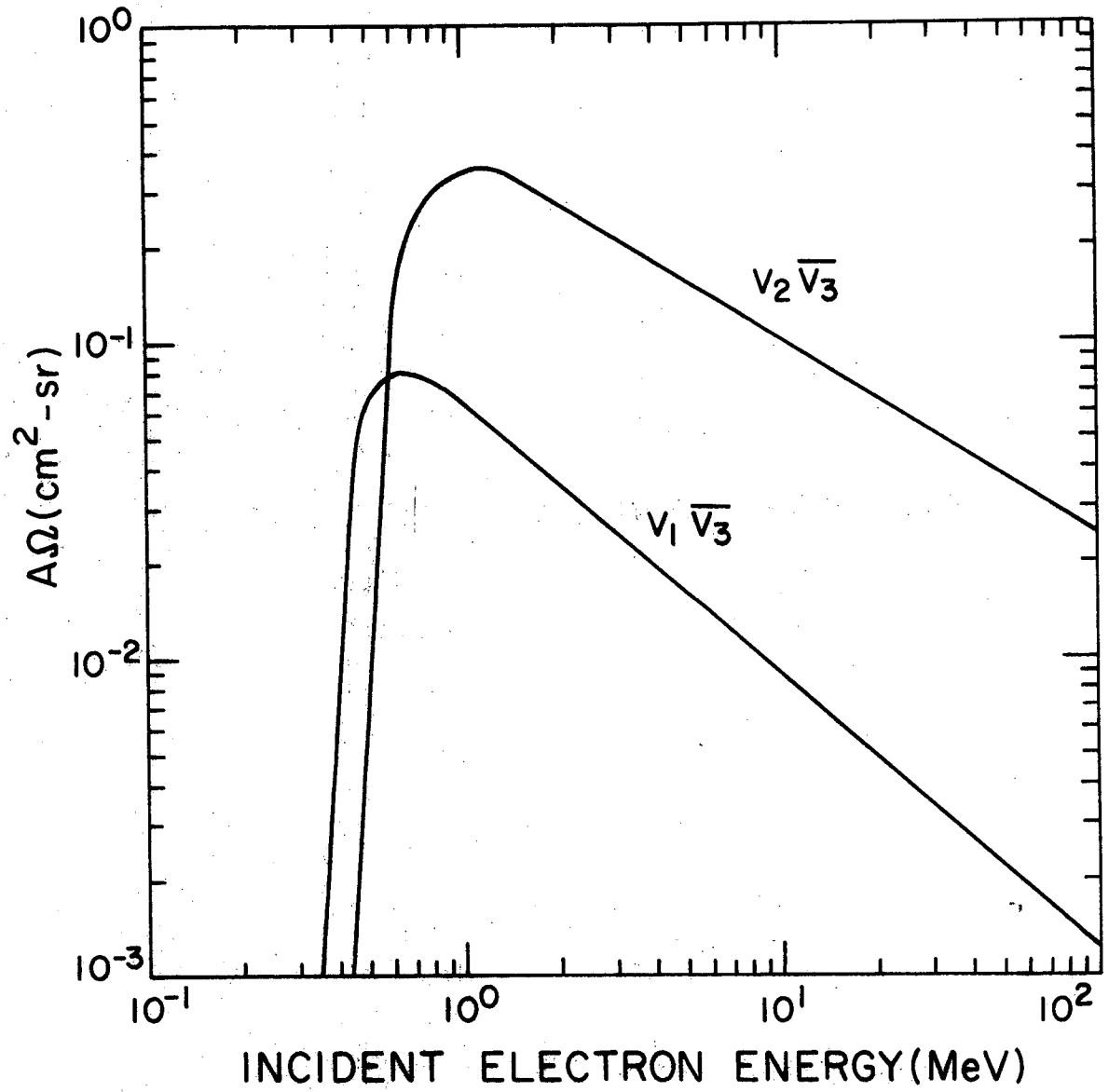


Table II-3

Incident Energy Ranges Corresponding to
Electronic Rate Configurations

Rate Configuration	Incident Energy Range		Approximate Geometrical Factors (A_Ω) ($\text{cm}^2\text{-sr}$)	
	Electrons (MeV)	Nuclei (MeV/nucleon)	Electrons	Nuclei
$V_1\overline{V}_3$	0.45-1.8	1.24-40.4	0.08	1.06
$V_2\overline{V}_3$	0.67-2.5	9.3-40.4	0.36	1.42
$V_1V_2\overline{V}_3$	0.67-1.8	9.3-40.4	10^{-3}	1.16
H_1	---	0.88-~4.5	10^{-4}	0.013
V_3	0.53	37.	?	?

geometrical factors have been calculated for all rates but V_3 using a Monte Carlo technique. These are shown in figures II-6 and II-7. Comparing these two figures, the effect of the passive collimation in the horizontal telescope is clear: the high energy response of the H_1 rate is quite complex.

Figure II-6

Energy dependent geometrical factors for the $V_1\overline{V}_3$, $V_2\overline{V}_3$, and $V_1V_2\overline{V}_3$ rates.

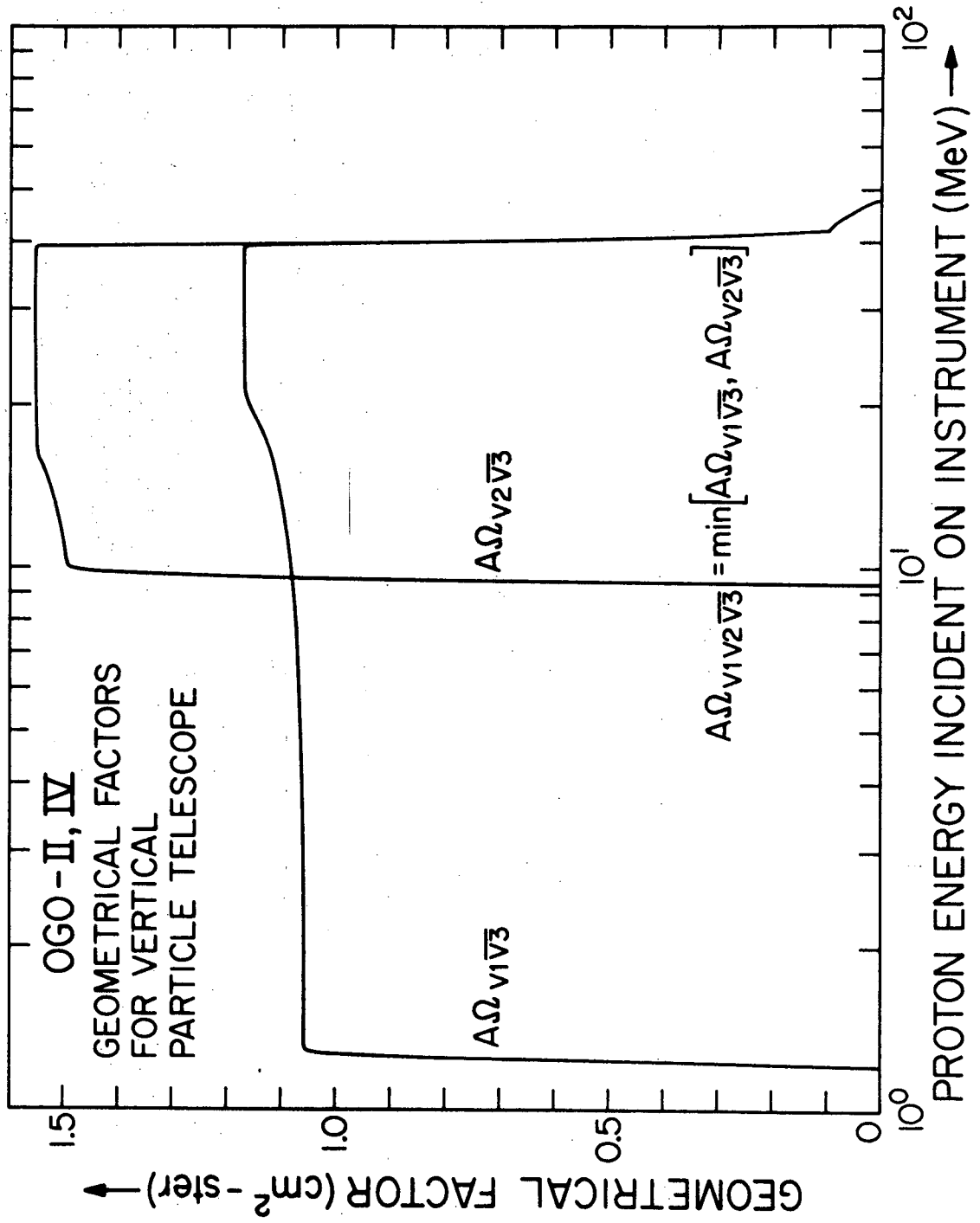
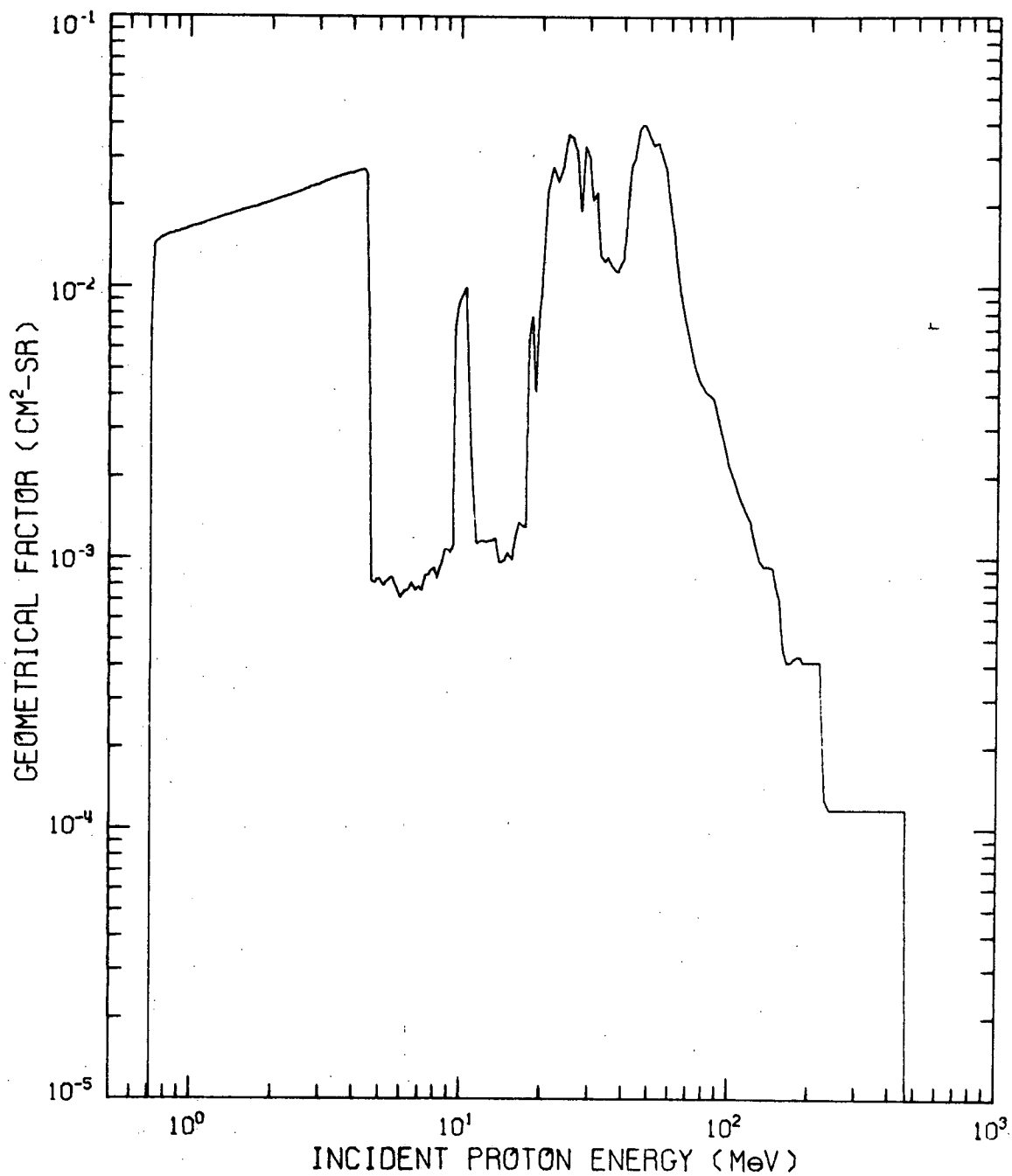


Figure II-7

Energy dependent geometrical factor for the H_1 rate.

OGO-IV HORIZONTAL TELESCOPE
GEOMETRICAL FACTOR



III. SATELLITE

OGO-4 is the fourth in the series of six Orbiting Geophysical Observatory satellites sponsored by the National Aeronautics and Space Administration. This satellite was launched from the Pacific Missile Range on 28 July 1967 into an orbit with an initial inclination of 86° , apogee of 908 kilometers, perigee of 412 kilometers, and orbital period of 98 minutes [34].

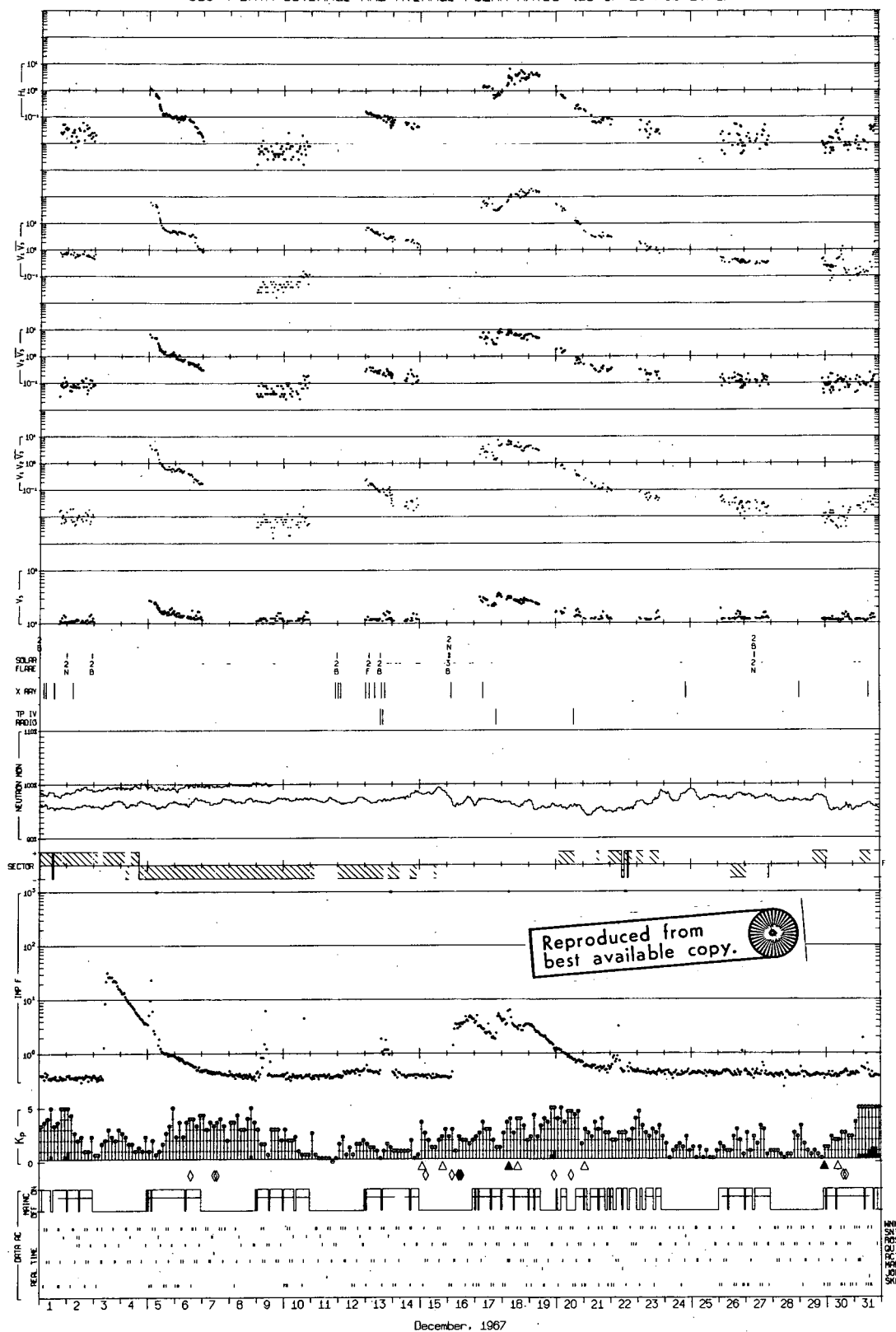
The instrument described in Section II was mounted on the spacecraft so that only particles incident on the vertical telescope from directions within 30° of the zenith do not trigger the anti-coincidence counter, D_3 , prior to passing through the solid state detectors, D_1 and D_2 (see figure II-1). Similarly, the horizontal telescope was mounted so that collimated particles represent particles incident from directions nearly perpendicular to the zenith.

Because of a need to time-share the spacecraft telemetry facilities between two sets of experiments, the data collected by this experiment were only available about 50% of the time: often in two day periods separated by two day gaps in the data. The effect of this telemetry configuration on the data from this experiment is illustrated in the OGO-4 Data Coverage Plots [35]; figure III-1 is a typical example of these plots.

Figure III-1

A typical example of the OGO-4 Data Coverage Plots. An explanation of the information displayed on this figure is given by Evans [35], where a complete set of these plots covering the entire period during which at least one of the OGO-4 tape recorders was operable will also be found. These plots are designed to fulfill the dual purpose of indicating the availability of the data from this experiment and of comparing these data to other geophysical, interplanetary, and solar data of interest.

OGO-4 DATA COVERAGE AND AVERAGE POLAR RATES (as of 28 Feb 1971)



The spacecraft was deactivated on 23 October 1969, but the failure of the second of the two on-board tape recorders on 19 January 1969 represented, at least for this study, the practical limit of the period for which useful data are available.

The trajectories of OGO-4 during several typical orbits mapped onto a polar representation of geocentric latitude *vs.* geocentric longitude are shown in figure III-2. As the plane of the satellite orbit remains relatively stationary in space, the earth rotates under the satellite, causing the apparent shift in the trajectories. Contours of constant invariant latitude (Λ) [36] are also projected into this coordinate system for reference; it should be noted that some of the orbits reach a much lower maximum invariant latitude than others, especially in the south.

Since many of the charged particle effects which can be measured by this experiment are closely related to the geomagnetic field and the sun-earth-satellite orientation, the data observed with OGO-4 can be more efficiently organized in a coordinate system reflecting the position of the satellite in the geomagnetic field and the sun-earth-satellite orientation. Of several coordinate systems reflecting these parameters, one of the most effective and widely used is that consisting of invariant geomagnetic latitude (Λ) *vs.* magnetic local time (MLT) [37]. The trajectories shown in figure III-2, mapped into this system, are shown in figure III-3. It is clear that in this coordinate system the effects of the rotation of the earth are minimized, and the differences in maximum

Figure III-2

A projection of typical OG0-4 trajectories onto a polar representation of geocentric latitude *vs.* geocentric longitude. Projections of these trajectories onto both geographic poles are shown for comparison, and contours of constant invariant geomagnetic latitude (Λ) are indicated.

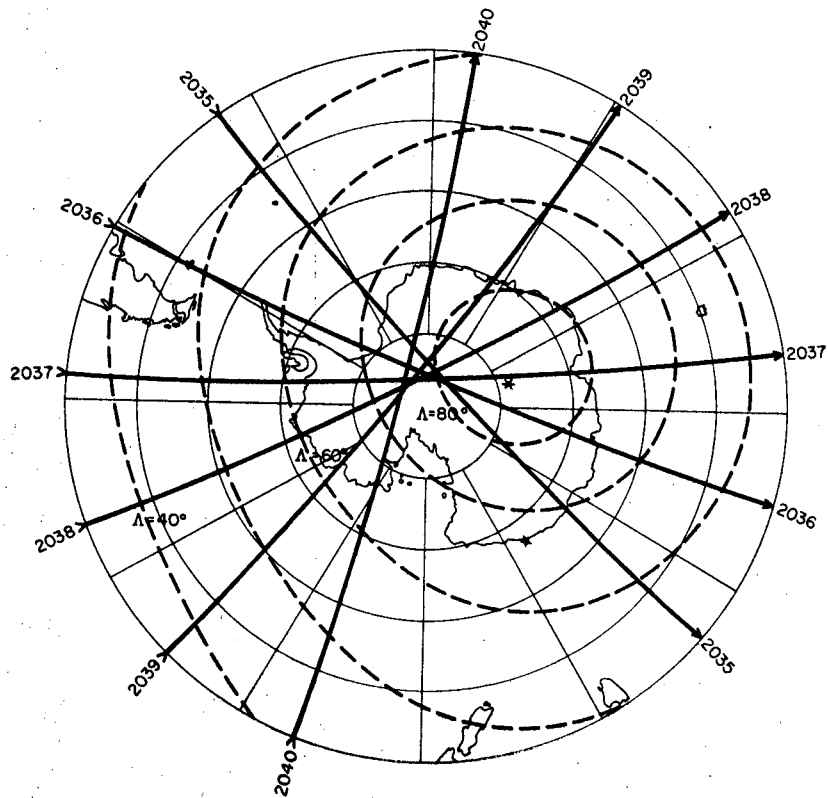
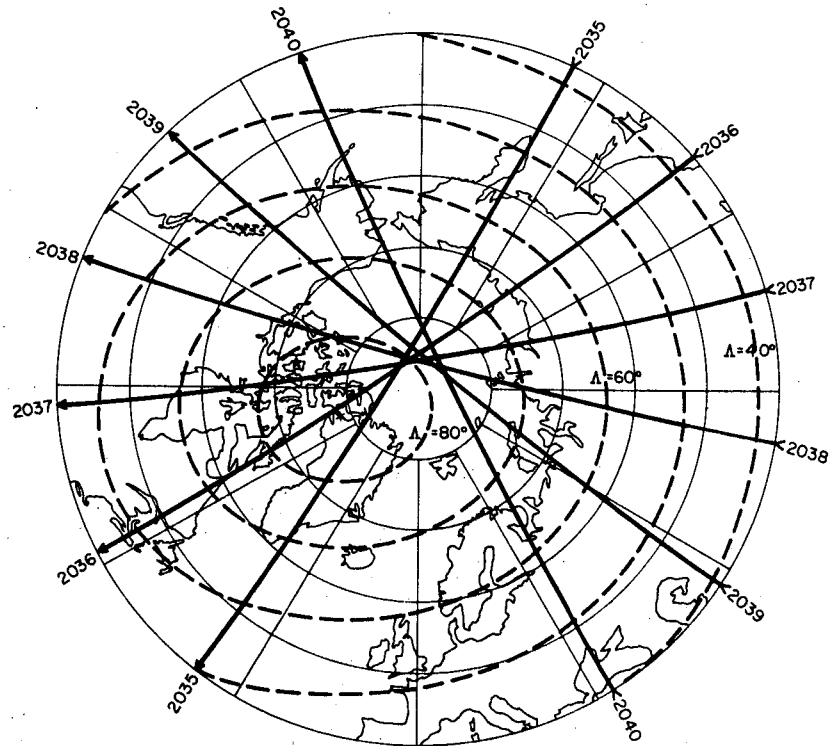
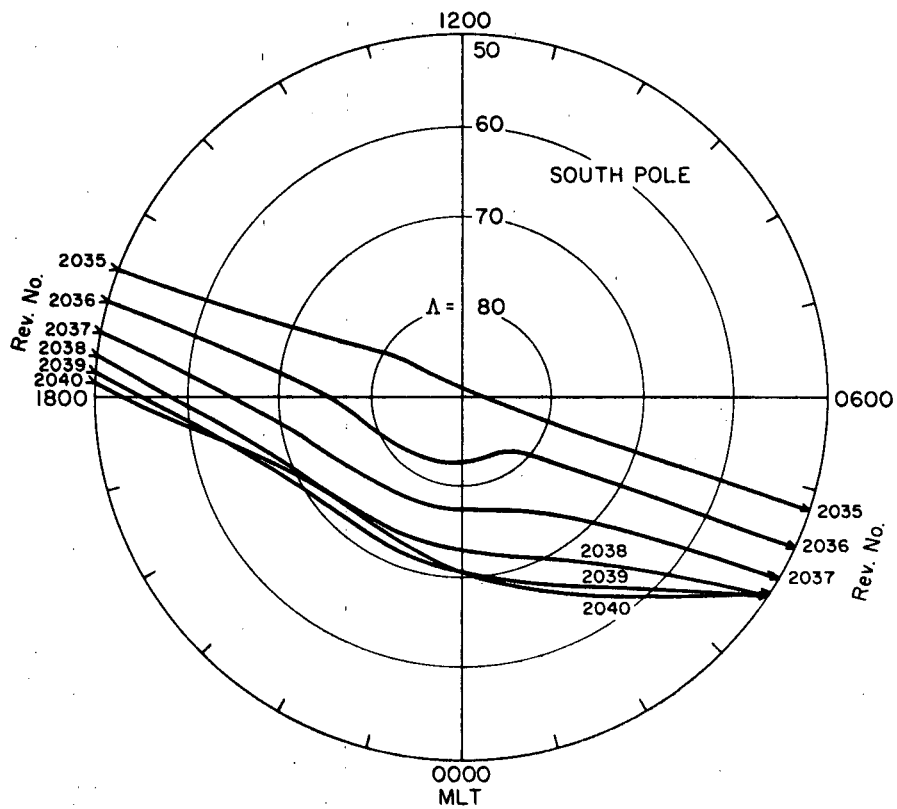
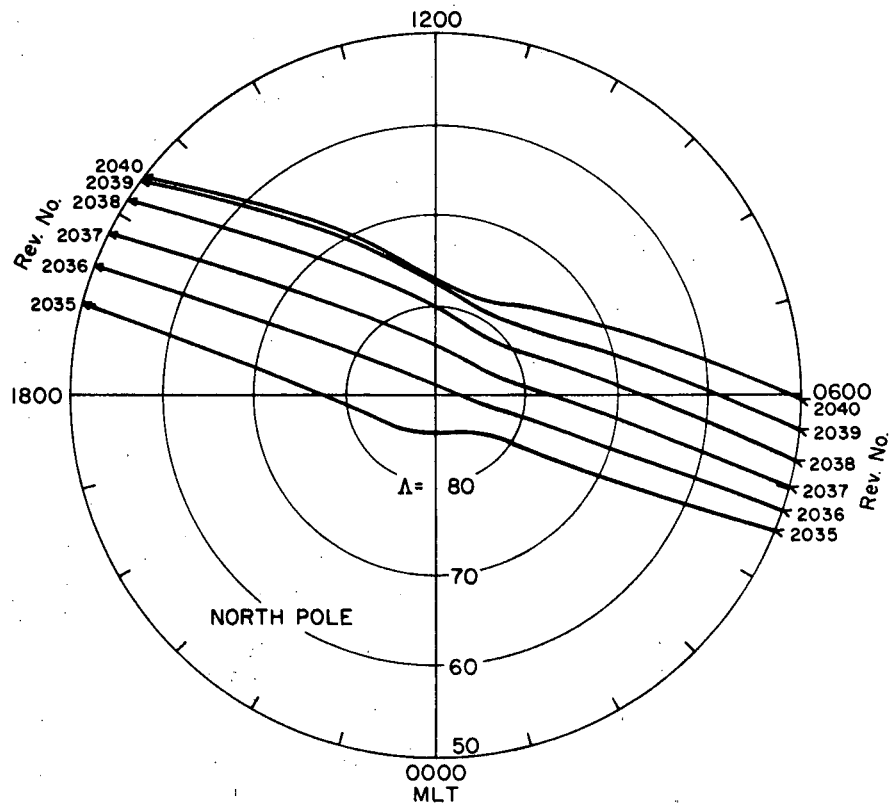


Figure III-3

A projection of the same OGO-4 trajectories shown in figure III-2 into a geomagnetic coordinate system: invariant latitude (Λ) vs. magnetic local time (MLT). The field coefficients given by Cain, *et al.* [38] were used to calculate Λ .



invariant latitude are depicted more explicitly.

Since for the bulk of the observations reported here a critical distinction will be made between data collected at low and high polar geomagnetic latitudes (see section V), the data collected during polar passes such as 2039 and 2040 in the north and 2038, 2039 and 2040 in the south may be seriously degraded due to the limited degree to which the satellite penetrates to high geomagnetic latitudes.

IV. DATA ANALYSIS

The processing scheme used for the data from this experiment is illustrated by the block diagram shown in figure IV-1. The data came to Caltech stored on two classes of magnetic tapes: experimenter tapes and attitude-orbit tapes. The former contained the decommutated data for this experiment, while the latter provided the position and orientation of the spacecraft as a function of time (one point per minute) calculated from data collected by tracking stations. The information from these two classes of tapes was interleaved, time ordered and stored on a third class of magnetic tape, referred to as an abstract tape. The study being reported here has involved the processing of data from a total of 931 magnetic tapes, representing almost 300,000 minutes ($\sim 62 \times 10^6$ read-outs) of playback data. The format of the data on these tapes is described elsewhere [39].

A complete collection of plots showing the detector rates as a function of time [28] serve as a catalogue of these data from which one can evaluate the performance of the experiment and specify the periods of data most suitable for a particular study. With this information any of the other programs indicated on figure IV-1 can be employed.

The calculation of rates for the output of the solid state detectors is complicated somewhat by the fact that only the 2^0 , 2^4 and 2^9

Figure IV-1

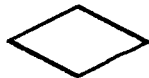
Block diagram representation of the procedure developed to process OGO-4 data at Caltech. The symbolism used is as follows:



= magnetic tape



= computer program (program names are given in capital letters.)



= branch (decision)

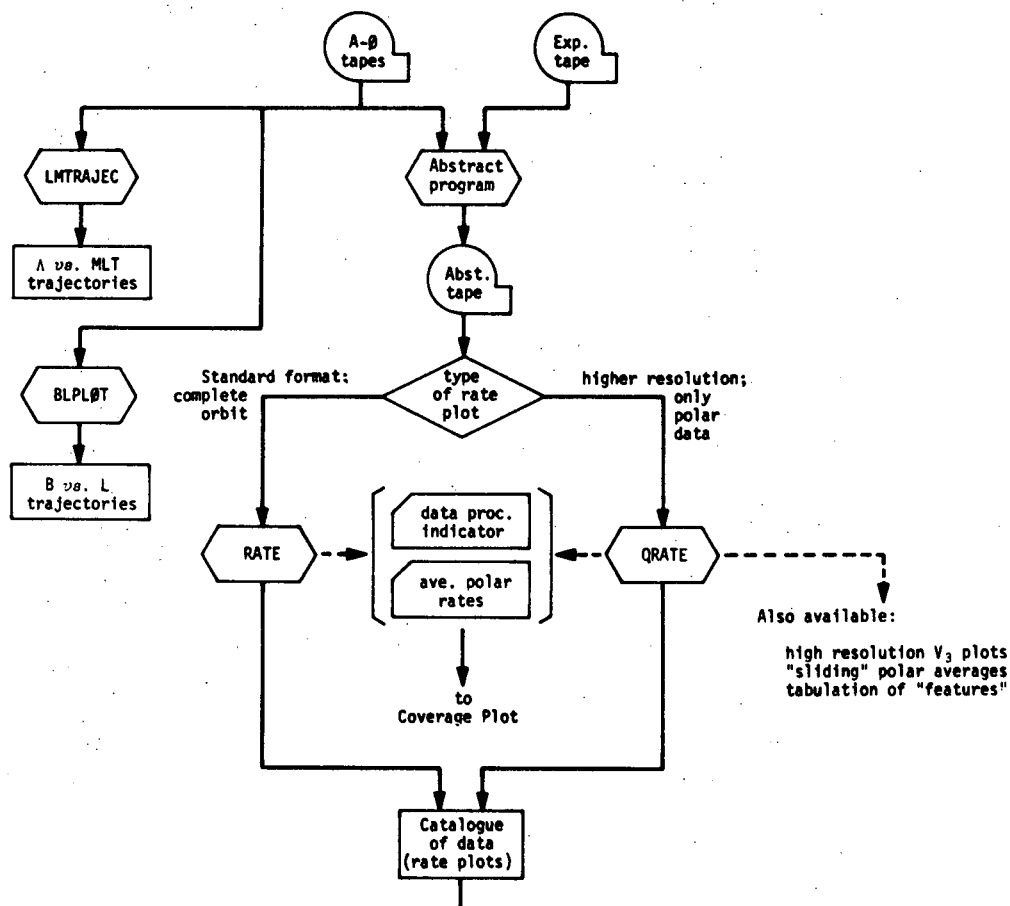


= cards punched



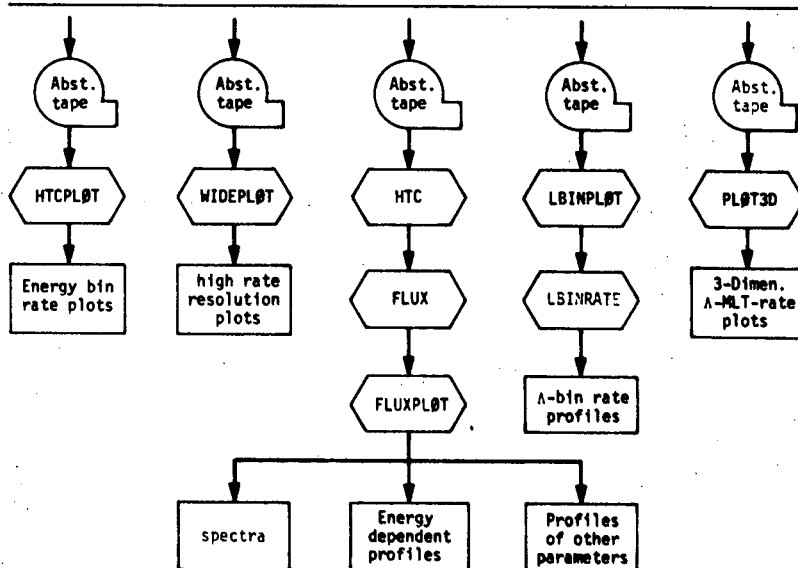
= results (only the resultant plots are shown on this diagram; each program has the option of tabulating results as well.)

The rate plots, which constitute the data catalogue, are discussed by Evans, *et al.* [28].



The decision at this point depends on the type of problem being studied and the available data as indicated on the rate plots and OGO-4 Data Coverage Plots.

Some of the choices currently available are indicated.



bits of the rate scalers are recorded. Figure IV-2 illustrates that special care must be exercised in the calculation of rates in some ranges, and that for detection rates above ~ 500 counts per read-out (~ 1740 counts per second for playback data) an unambiguous determination of these rates can be made only in special circumstances.

Using the accumulation of many pulse height analyzed events along with the response curve shown in figure II-4 and the energy dependent geometrical factor illustrated in figure II-6, differential flux spectra can be calculated. However, as pointed out in connection with the D_1 response curve (figure II-4), for a range of pulse height analyzer channels the correspondence between channel threshold and incident proton energy is not one-to-one. As a consequence, the spectra presented in Section V have been calculated using the iterative technique illustrated in figure IV-3.

Figure IV-2

Probabilities of a change occurring in the 2^0 , 2^4 and 2^9 -bits of a detector scaler during one read-out as a function of the event rate expressed in counts/read-out.

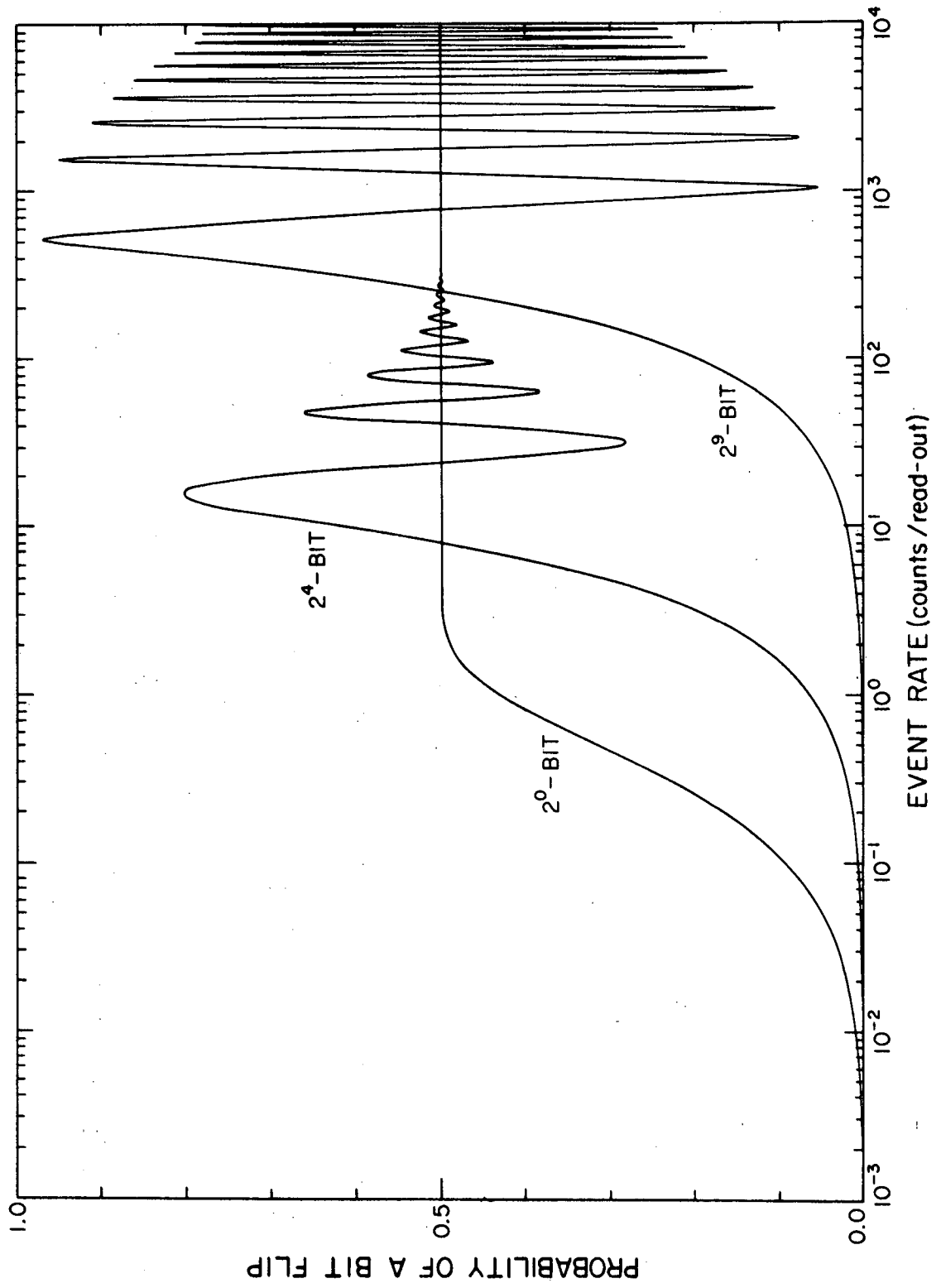


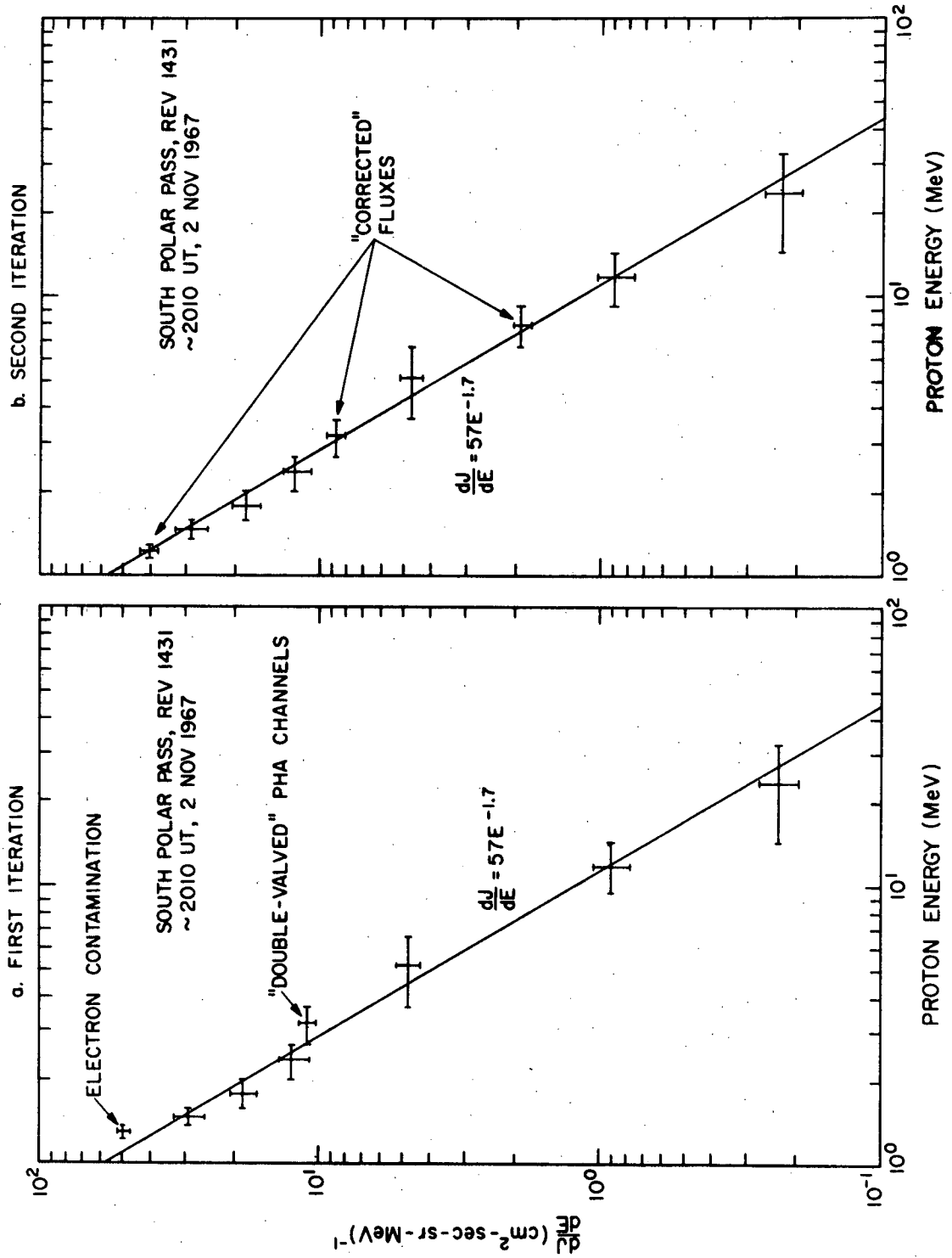
Figure IV-3

Iterative technique used to calculate differential energy spectra.

A spectrum is first calculated in a straightforward manner, and standard regression techniques are used to determine the "best" fit to

$$\frac{dJ}{dE} = AE^{-\gamma}$$

using only the points for which the energy identification is unique (figure IV-3a). This function is then used to determine the proportion of events in a double valued energy bin to be assigned to each energy interval corresponding to the group of pulse height analyzer channels involved. The flux for this group of channels is then recalculated. The results of this procedure (figure IV-3b) are valid (for the affected points) only to the extent that the actual spectrum agrees with the function used to approximate it.



V. OBSERVATIONS

Utilizing the data processing procedure outlined in Section IV, many of the available data from OGO-4 have been processed. The OGO-4 Data Coverage Plots [35] indicate the periods during which data were available, and also indicate for which of these periods the data have been processed. These data are particularly appropriate to the study of the entry of solar particles into the earth's magnetosphere, and several periods have proven to be instructive. In addition to electron observations, two examples of proton observations will be presented as illustrative of the type of observations available. A more complete compilation of pertinent data, including those events presented here, is given in Appendix A.

Electron Observations

Although the instrument described in Section II was not designed primarily to detect electrons, several periods of high electron fluxes were observed in the polar cap regions on board OGO-4. Some of the characteristics of electron polar cap observations have previously been reported [27,40,41], but the data presented here provide, for the first time, a comprehensive mapping of the boundary of the electron polar cap region. As discussed in Section VII, this boundary represents the boundary between open and closed geomagnetic field lines.

As mentioned in Section II, the $V_1\overline{V_3}$ and $V_2\overline{V_3}$ rates are much less sensitive to electrons than to protons. Although the contribution of electrons to the observed rates varies considerably, it is typically $\leq 15\%$ for the $V_1\overline{V_3}$ rate and $\leq 35\%$ for the $V_2\overline{V_3}$ rate. In addition, we recall that the OGO-4 anti-coincidence scintillator, V_3 , is sensitive to electrons above a threshold energy of ~ 530 keV. Normally, then, electrons constitute a rather minor constituent of the observed rates. There are periods, however, when the electron flux is sufficiently high relative to the proton flux that electrons become an identifiable constituent of the $V_1\overline{V_3}$, $V_2\overline{V_3}$ and V_3 rates. The identification of these periods and the identification of the rates as predominantly due to electrons is illustrated in figure V-1. The rates from this polar pass show a uniform electron polar cap flux between 1750:40 UT and 1805:40 UT; beyond 1806:00 the spacecraft had moved to invariant latitudes where the electrons did not have free access. That this enhancement can be associated strictly with electrons can be seen clearly by comparing the $V_2\overline{V_3}$ rate (electrons and protons) with the $V_1V_2\overline{V_3}$ rate (protons only). In order to improve the precision with which the electron polar cap boundary could be specified, the V_3 rate was plotted on an expanded scale, shown in figure V-2a.

Figure V-2b illustrates that the edge of the electron polar cap was normally associated with an electron spike near magnetic local midnight (MLT \approx 2100-0211). Figure V-2c is an example of an electron polar cap observation showing a particularly striking feature (i.e. the sharp depression at 0233:40 UT). These features were rarely observed and normally occurred only late during the recovery phase of a magnetic

Figure V-1

Rates observed during a typical OGO-4 polar pass ($\Lambda \geq 50^\circ$) illustrating an enhanced electron polar cap flux. These data are from the north polar pass of Rev. 6291 on 26 September 1968.

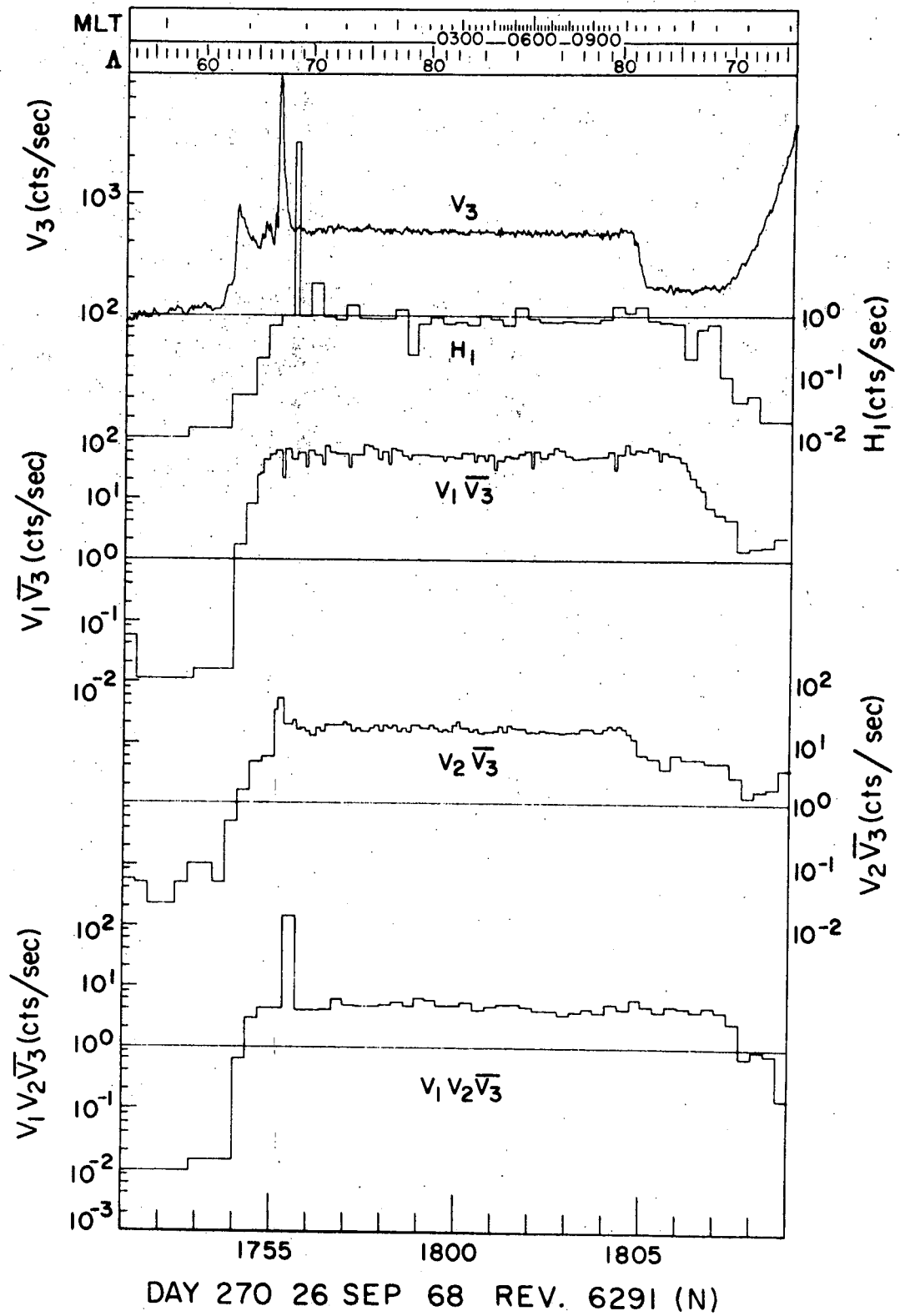


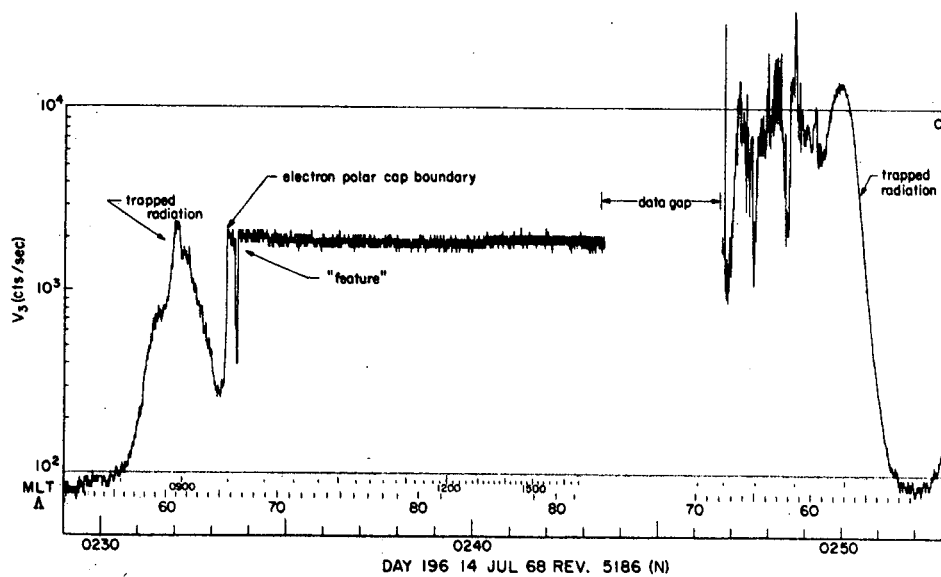
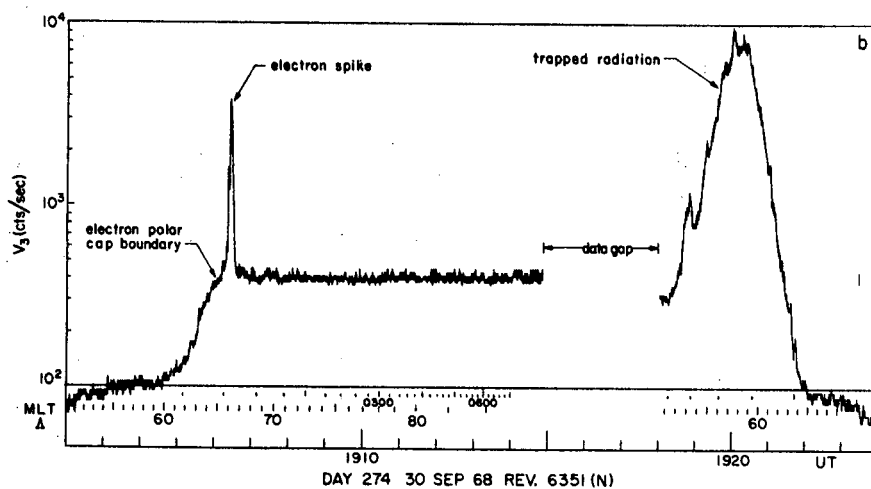
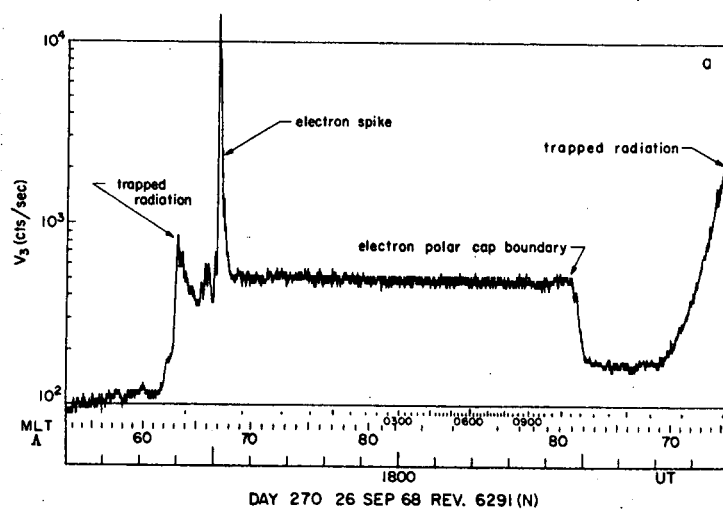
Figure V-2

High resolution plots of the V_3 rate, showing characteristic electron polar cap observations:

V-2a: V_3 rate shown in figure V-1.

V-2b: An example of the type of electron spike associated with the edge of the electron polar cap between MLT \sim 2100 and MLT \sim 0200.

V-2c: An example of a well-defined feature in the electron polar cap flux. Such features were rarely observed.



storm.

A total of 333 such observations were made during magnetically quiet periods, and the resultant map of the electron polar cap boundary is shown in figure V-3. Here the geomagnetic coordinates (invariant latitude and magnetic local time) of each observation of the boundary are indicated by a symbol. The apparent dependence on geomagnetic activity will not be discussed here. The values reported by Vampola [27], which he extrapolated to magnetically quiet conditions, are shown for comparison.

We can now define the following terms with respect to the electron results from this experiment: *high polar latitudes (HPL)* and *low polar latitudes (LPL)*. High polar latitudes will refer to the invariant latitudes between the electron polar cap boundary and the geomagnetic pole; low polar latitudes will refer to the invariant latitudes between geomagnetic cutoff for 1.2-40 MeV protons (below which polar proton fluxes cannot be observed due to the Earth's magnetic field) and the electron polar cap boundary. These definitions will be useful in organizing the proton observations.

Proton Observations

Most of the data collected by this instrument are by design dominated by proton fluxes. Since we are interested in studying those periods during which the proton counting rate changes significantly during a time scale of several hours, the proton data can be effectively

Figure V-3

Observed electron polar cap boundary data in an invariant latitude-magnetic local time coordinate system.

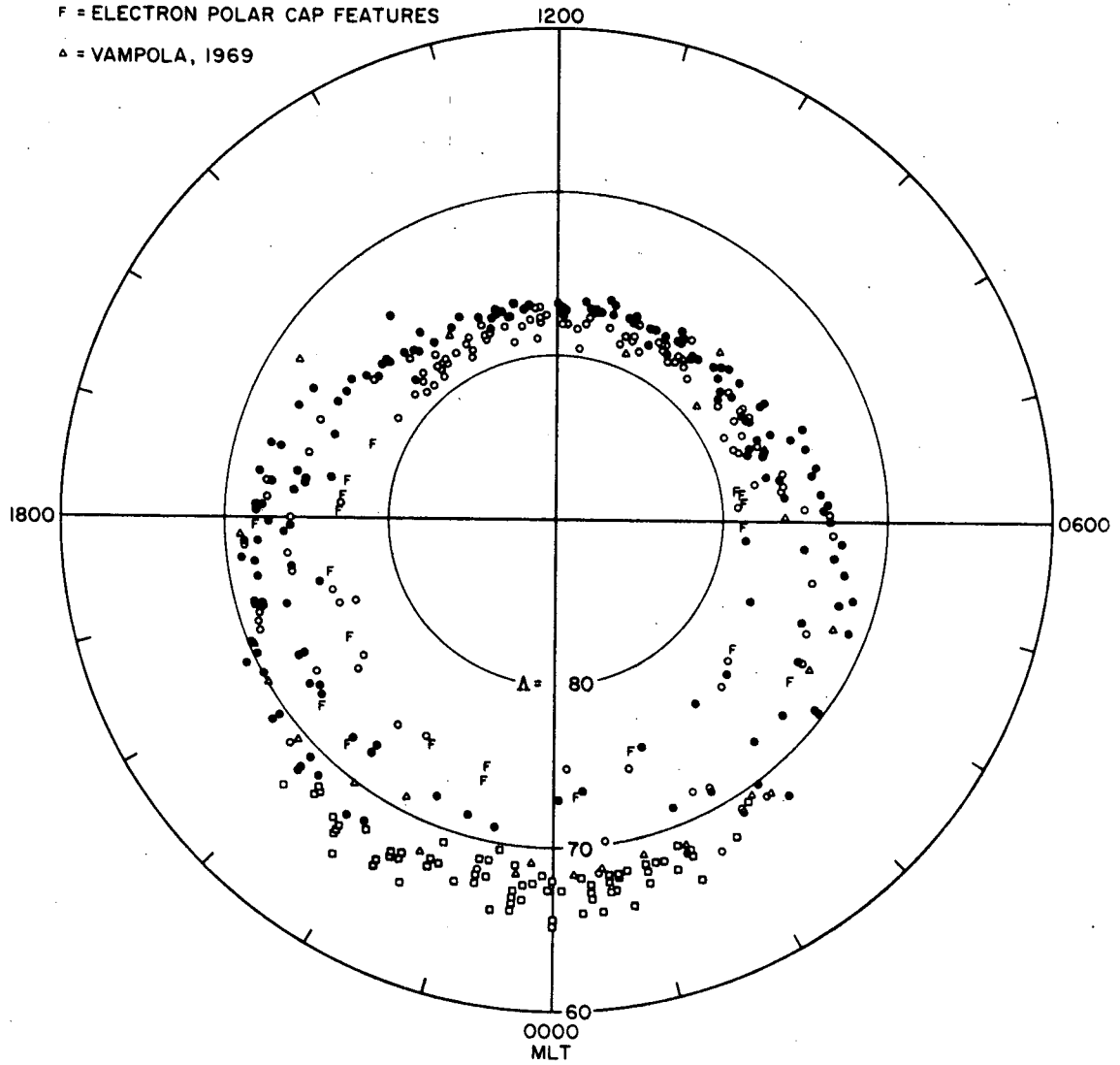
○ = $K_p < 2^-$

● = $2^- \leq K_p < 4^-$

□ = ELECTRON SPIKES

F = ELECTRON POLAR CAP FEATURES

△ = VAMPOLA, 1969



displayed on a plot of proton counting rate (or flux) as a function of time, which is referred to as a *profile*. In particular, we will be interested in comparing the profiles of fluxes measured at low polar latitudes and at high polar latitudes. As discussed in Section VII, the north and south low polar latitude regions are most likely connected by closed field lines, while the north and south high polar latitudes are not. Therefore, no distinction will be made between data collected in the north and south low polar latitude regions, whereas the data from the two high polar latitude regions will be kept separate.

The temporal variations observed in the proton flux can normally be divided into two main types: those events associated with and having the characteristics of solar flare events, and those events which have been variously referred to as Energetic Storm Particles (Bryant, *et al.* [42,43] and Rao, *et al.* [44]), Delayed Particle Events (Lin and Anderson [45]), and Protons Associated with Centers of Solar Activity (Fan, *et al.* [46]). We will follow the lead of Anderson [47] and try to avoid any semantics problem by referring to these events as *EDP* (Energetic Delayed Particles) events. Although treated in more detail in Section VI, a brief description of the essential differences between these two classes of events may indicate why the distinction between them is made. Flare events are characterized by impulsive ejection of particles by the sun followed by their propagation through interplanetary space. This typically results in a rapid rise (~few hours) to a maximum proton flux, followed by a long, nearly exponential decay with a time constant of about one day. EDP events, on the other hand, are characterized by a region of

limited radial extent and enhanced low energy particle flux being convected outward by the solar wind plasma (expanding solar corona). For our purposes here, EDP events are phenomenologically characterized by the following (after Anderson [47]):


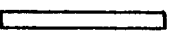
1. Fluxes occur predominately at low energies.
2. Profiles show much more rapid rise and fall than flare event profiles and often exhibit large fluctuations during the event.
3. The duration of the event is normally between $O(1 \text{ hour})$ and $O(1 \text{ day})$.
4. Events are often associated with a "weak depression" in the sea level neutron monitor rates.
5. Events are sometimes associated with one or more geomagnetic sudden commencements or sudden impulses.

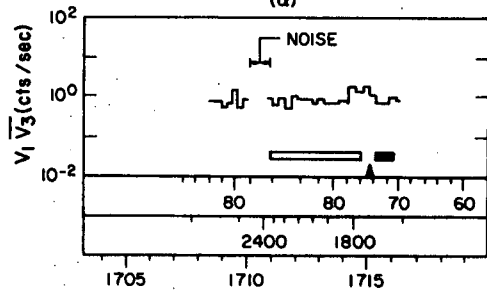
Presented below are typical examples of the observations of both of these classes of particle events.

EDP event of 1 December 1967

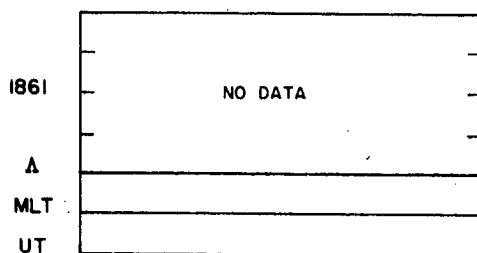
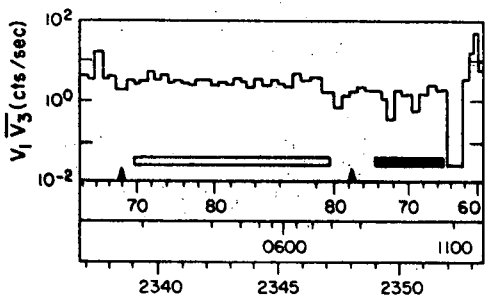
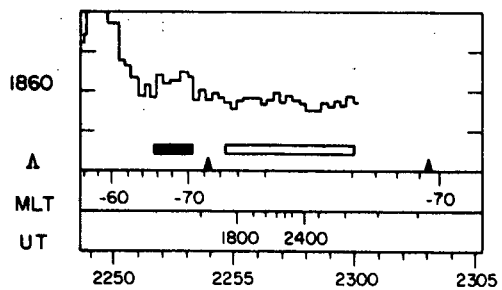
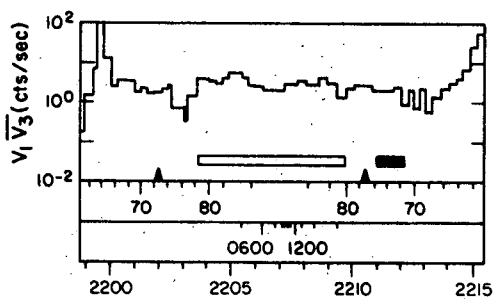
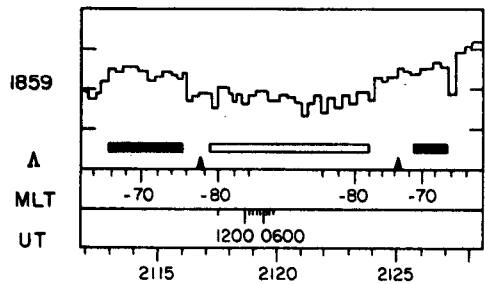
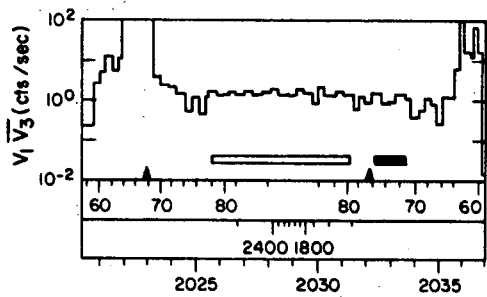
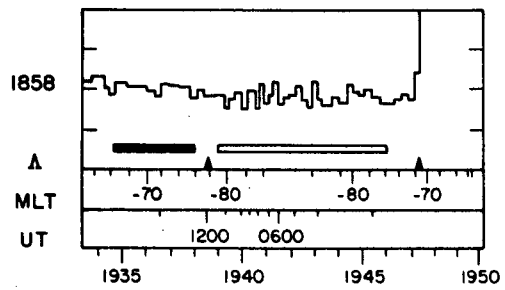
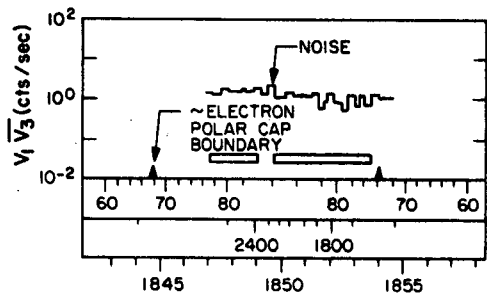
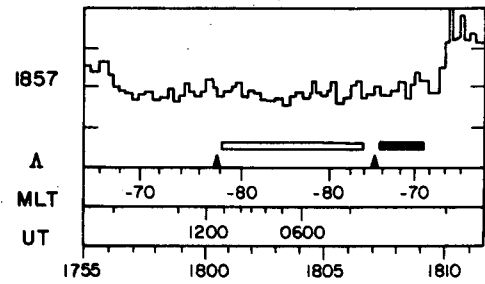
Figure V-4 shows the $V_1 \overline{V_3}$ rate as a function of time for each available polar pass from 1700 UT on 1 December 1967 to 0700 UT on 2 December. This figure illustrates the averaging intervals used to obtain average counting rates for each of the polar cap regions (LPL and HPL), and the relation between these averaging intervals and the electron polar cap boundary data presented in figure V-3. The profiles of the flux measured in the low polar latitude (LPL) region and in the

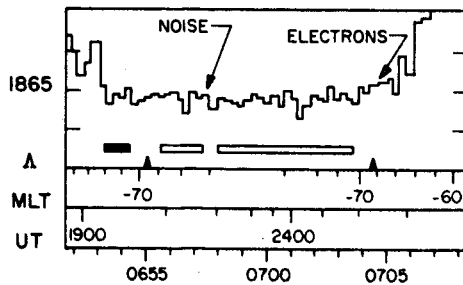
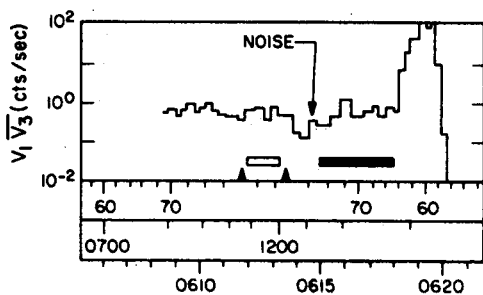
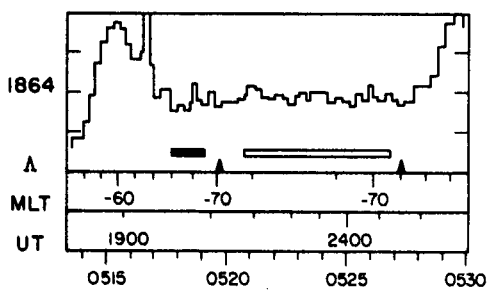
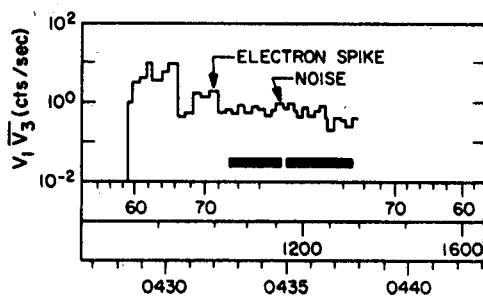
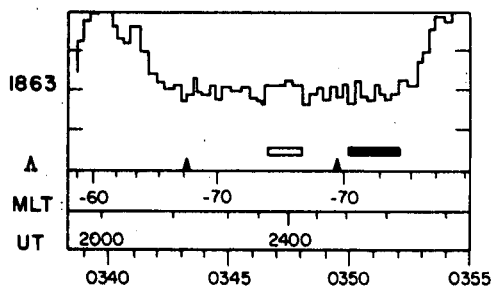
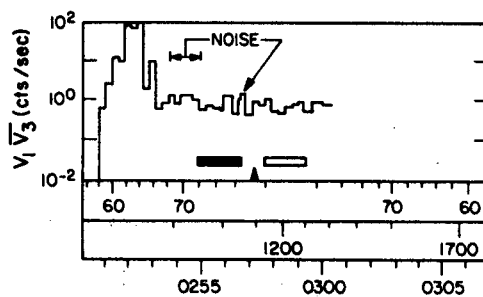
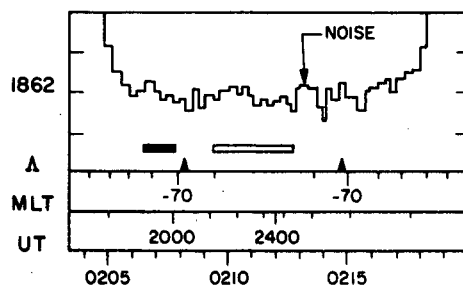
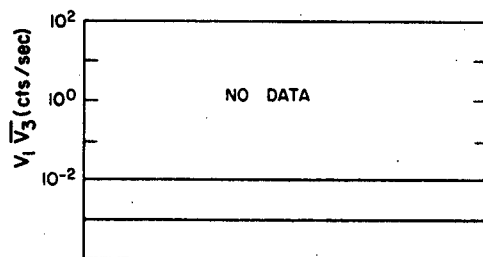
Figure V-4

$V_1 V_3$ counting rate (~ 15 second averages) during all of the available polar passes from 1700 on 1 December 1967 to 0700 on 2 December. The averaging intervals used to obtain average rates for low polar latitude () and high polar latitudes () are shown and compared to the approximate location of the electron polar cap boundary (Δ) as shown in figure V-3. In addition to universal time, geomagnetic coordinates (Λ and MLT) are also indicated.

NORTH POLE
(a)

REV. NO.

SOUTH POLE
(β)



north and south high polar latitude (HPL) regions are in figure V-5. All data points shown in this figure have errors comparable to those of the four points with explicit error bars. The arrows near the top of the figure indicate a gap in the data, which included both a south and a north polar pass (see Section III). The time resolution of the LPL profile is twice that of the other two profiles because the north and south LPL regions are considered equivalent.

The identification of this event as an EDP event is supported by the extremely fast "decay" of the flux, the predominantly low energy nature of the event (see discussion of spectra below), and the presence of a weak depression in the Alert Neutron Monitor [48]. In addition, figure V-6 shows a direct comparison between the data in figure V-5 and the interplanetary flux of 0.79-9.6 MeV protons and 0.17-1.00 MeV electrons measured by the University of Chicago experiment on board IMP-F [49]. The correlation between these interplanetary data and the LPL profile is notable.

The most obvious features of these profiles are that (1) all three profiles are different (a peak occurs first at LPL, next at northern HPL, and last at southern HPL) and (2) only the LPL peak occurs at the same time as the peak seen in the IMP-F data.

In order to determine the relationship among these peaks, spectra were calculated at eight times during this event; the data for which spectra were calculated are indicated by the circled points on figure V-5. These spectra are shown in figure V-7. The data upon which the spectra

Figure V-5

Flux profiles for EDP event of 1 December 1967. The profile for each region is distinguished from the other profiles according to the following code:

- low polar latitudes
- north high polar latitudes
-● south high polar latitudes

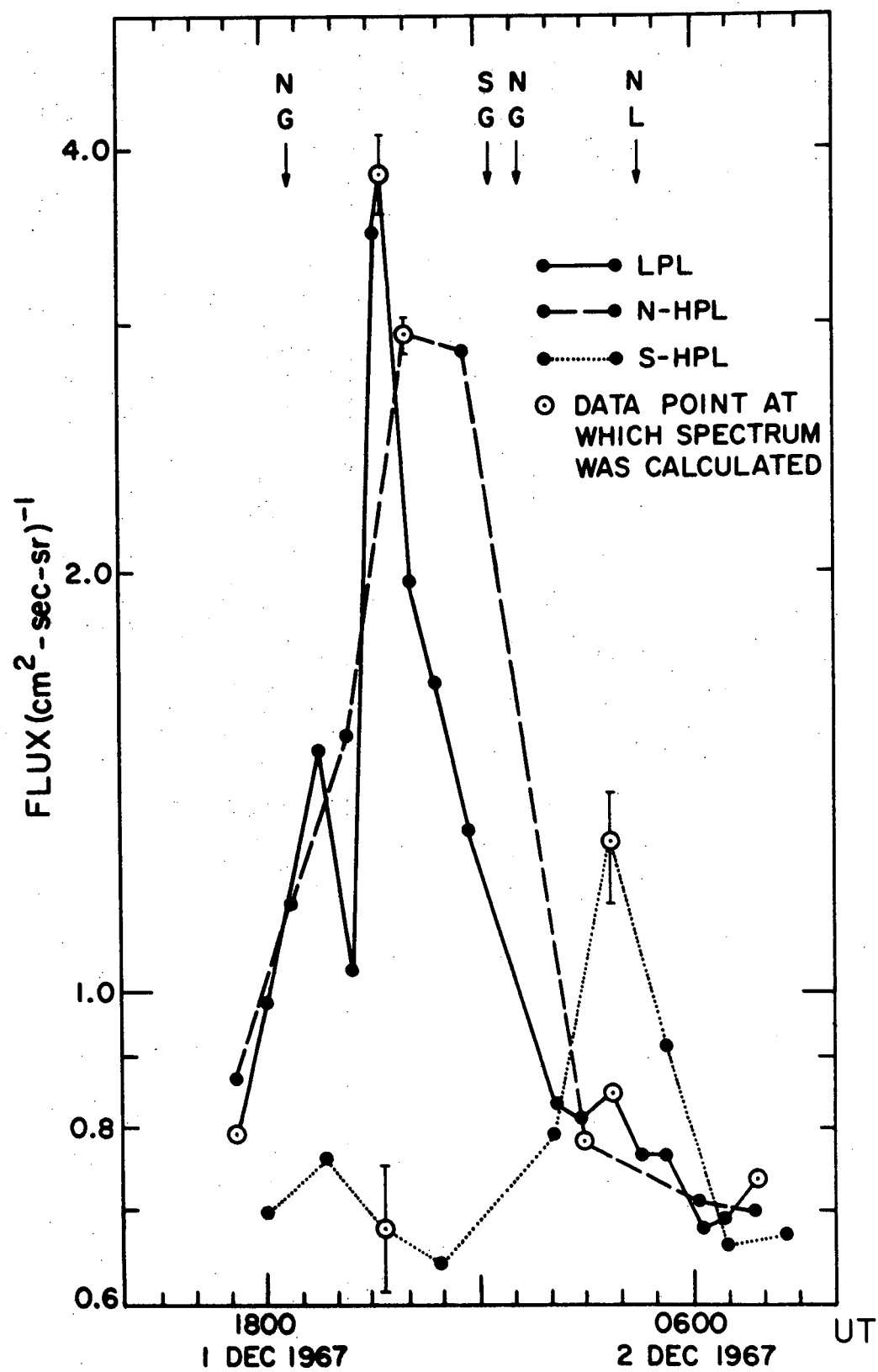


Figure V-6

A direct comparison between interplanetary and polar cap particle observations for the EDP event of 1 December 1967. Interplanetary data are the flux of 0.79-9.6 MeV protons and 0.17-1.00 MeV electrons measured by the University of Chicago experiment on board IMP-F [49]. Polar cap data are the flux of 1.2-40 MeV protons and 0.4-1.0 MeV electrons measured by $V_1\overline{V_3}$ on board OGO-4. The interplanetary data have been multiplied by 0.32 to normalize them to the OGO-4 flux at the EDP peak.

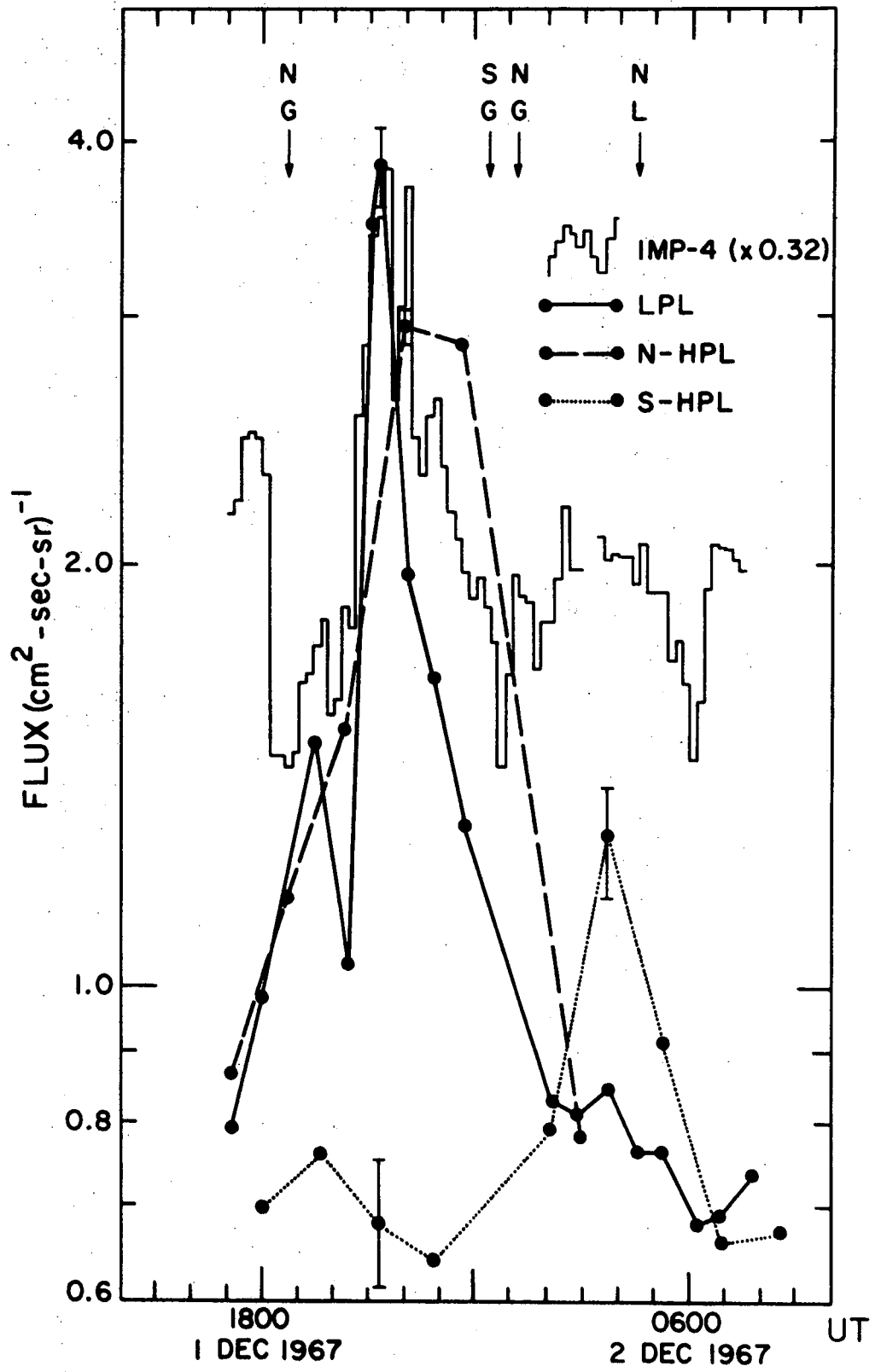
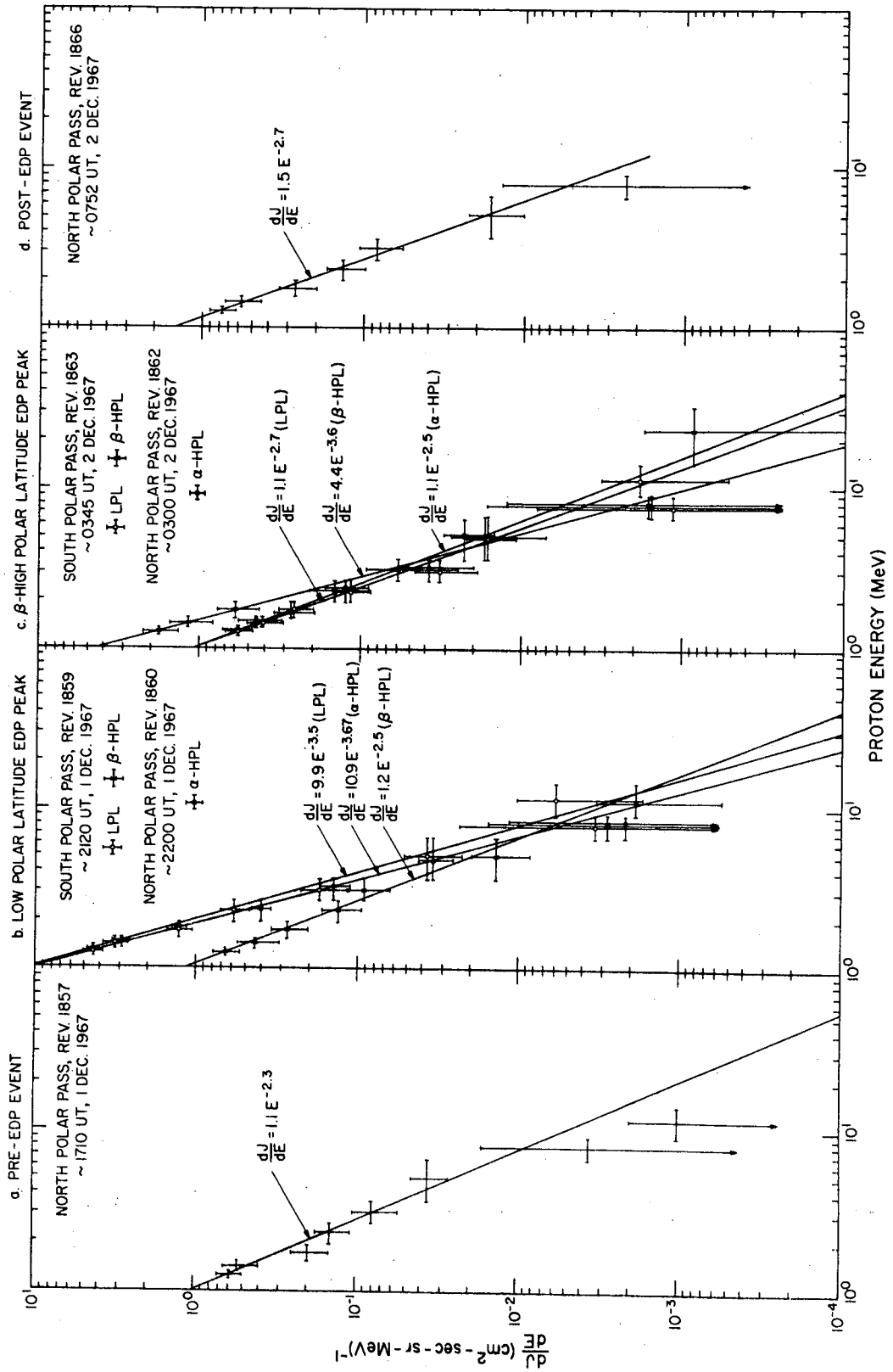


Figure V-7

Differential energy spectra of the following fluxes calculated from data collected during the 1 December 1967 EDP event:

- V-7a: Low polar latitudes prior to the beginning of the event.
- V-7b: Low polar latitude peak, northern high polar latitude peak, and southern high polar latitude data from the same time.
- V-7c: Flux from each of the three regions collected at or near the southern high polar latitude peak.
- V-7d: Low polar latitudes after the end of the event.

In all four cases, LPL data points are indicated by an open circle (o), northern HPL by a closed circle (•) and southern HPL by a cross (×).



in figure V-7b were based were collected during consecutive polar passes in order to minimize any differences due to temporal effects; the same is true of the data in figure V-7c. We note the striking interchange in rôles from figure V-7b to figure V-7c between the southern HPL region and the LPL and northern HPL regions.

These eight spectra are summarized in table V-1, which gives the coefficient and exponent of the best fit for each spectrum to an equation of the form

$$\frac{dJ}{dE} = AE^{-\gamma}$$

where J is the flux in particles/cm²-sec-sr, and γ is referred to as the spectral index. One standard deviation errors for A and γ , as well as the χ^2 "goodness of fit" parameter, are also indicated on this table.

The spectra observed at each of the peaks indicate the following:

(a) compared to the spectra observed before and after the event, each of the peaks consisted of a larger proportion of low energy protons and exhibited spectral indices typical of those observed for EDP events in interplanetary space [50], and (b) the spectral index of the flux was essentially the same at each peak. The first point supports the identification of these peaks as due to EDP fluxes, while point (b) is consistent with the interpretation that all of the peaks represent a sampling of the same particle population. This interpretation is aided by the observations that the magnitude and spectrum of the ambient flux change very little throughout the event and that the spectral indices for the peak fluxes are significantly different than the index for the ambient flux.

TABLE V-1

1 Dec. 1967 EDP Event Spectra (see figure V-7)

Best Fit to $\frac{dJ}{dE} = AE^{-\gamma}$

Relationship to Event	Coefficient "A" (cm ² -sec-sr-MeV) ⁻¹	Spectral Index "γ"	χ ²	P(>χ ²)
Pre-event LPL	1.07 ± 0.18	2.31 ± 0.23	9.33	0.316
LPL peak	9.90 ± 0.15	3.52 ± 0.22	0.96	0.995
Northern HPL peak	10.90 ± 0.11	3.67 ± 0.17	2.52	0.961
Southern HPL at LPL peak	1.21 ± 0.21	2.53 ± 0.29	1.47	0.983
LPL at Southern HPL peak	1.13 ± 0.19	2.66 ± 0.24	2.19	0.974
North. HPL at S. HPL peak	1.10 ± 0.23	2.52 ± 0.32	1.95	0.962
Southern HPL peak	4.43 ± 0.26	3.62 ± 0.41	1.28	0.989
Post-event LPL	1.47 ± 0.21	2.69 ± 0.29	1.08	0.993

These observations lead to the following description of the 1 December 1967 event. The interplanetary region of enhanced flux arrives at the earth and is observed almost simultaneously by IMP-F and at LPL. About 1.2 hours later, by which time the LPL flux has decreased significantly, this flux is observed to reach a maximum at northern HPL. Finally, after these two fluxes have definitely returned to ambient flux levels, the EDP flux is observed at southern HPL.

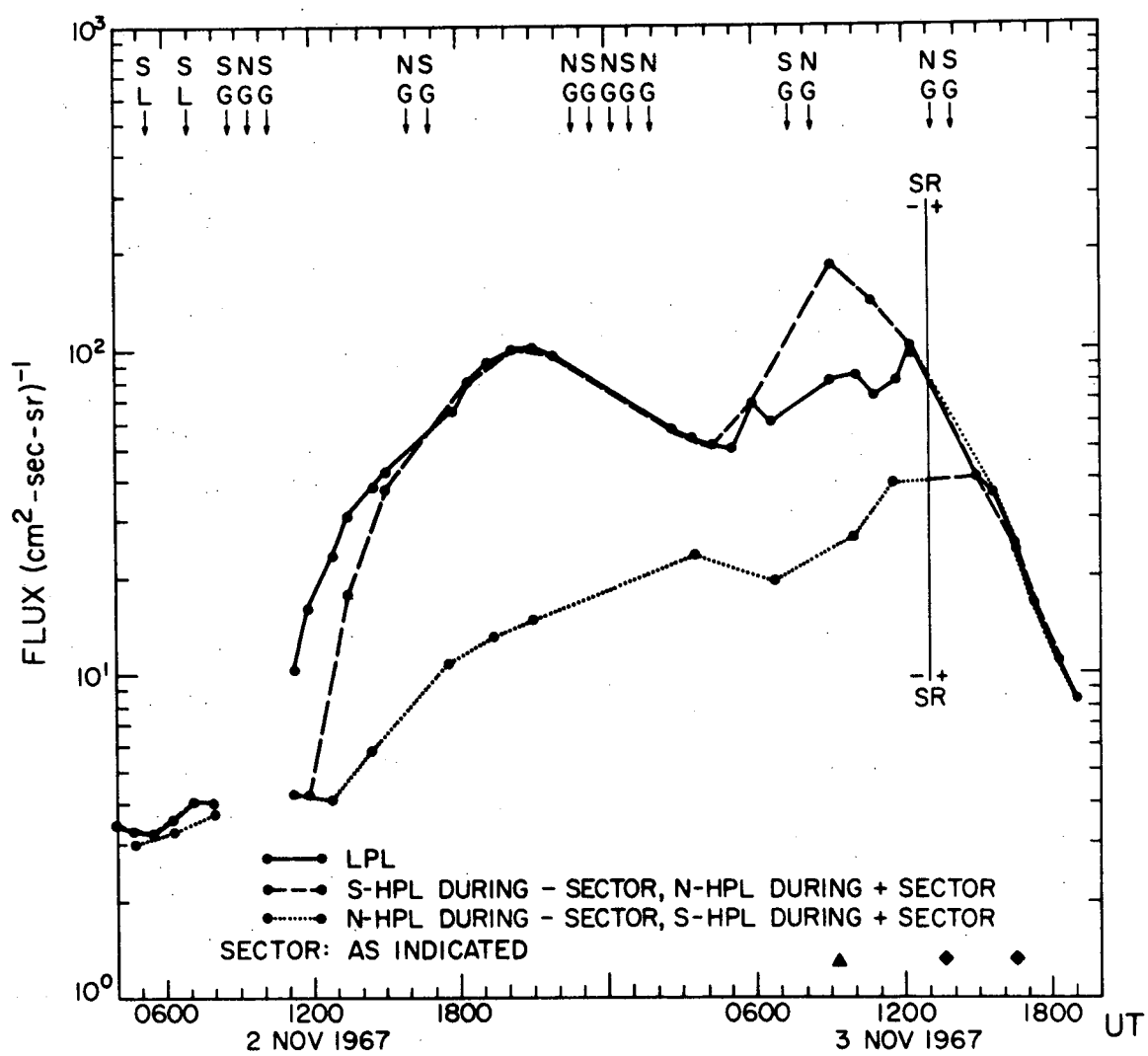
Solar Flare Event of 2 November 1967

The second of the two classes of solar particle events of interest here consists of those events associated with solar flares. As with EDP events, we will compare the profiles of the flux at low polar latitudes and the flux at north and south high polar latitudes. Many flare events have been used in this study; most of these are subject to the limitation imposed by the time-sharing nature of the OGO-4 telemetry: in general, data are available for two day periods separated by two day gaps. This limitation is more critical for flare events, which might last 6-8 days, than for EDP events, which have typical durations between one hour and one day.

Typical of the observations which, in spite of this limitation, have features of interest are the profiles of the 2 November 1967 flare event in figure V-8. Preliminary results of the study of this event have been previously reported [11]. Typical errors are indicated for arbitrarily selected data points.

Figure V-8

Profiles of the 2 November 1967 solar flare event. The symbols in this figure are explained in Appendix A (see table A-3). A 2B flare occurred on the sun at 0852 UT on 2 November 1967, accompanied by 2-12 Å X-ray emission that peaked at 0858 UT.



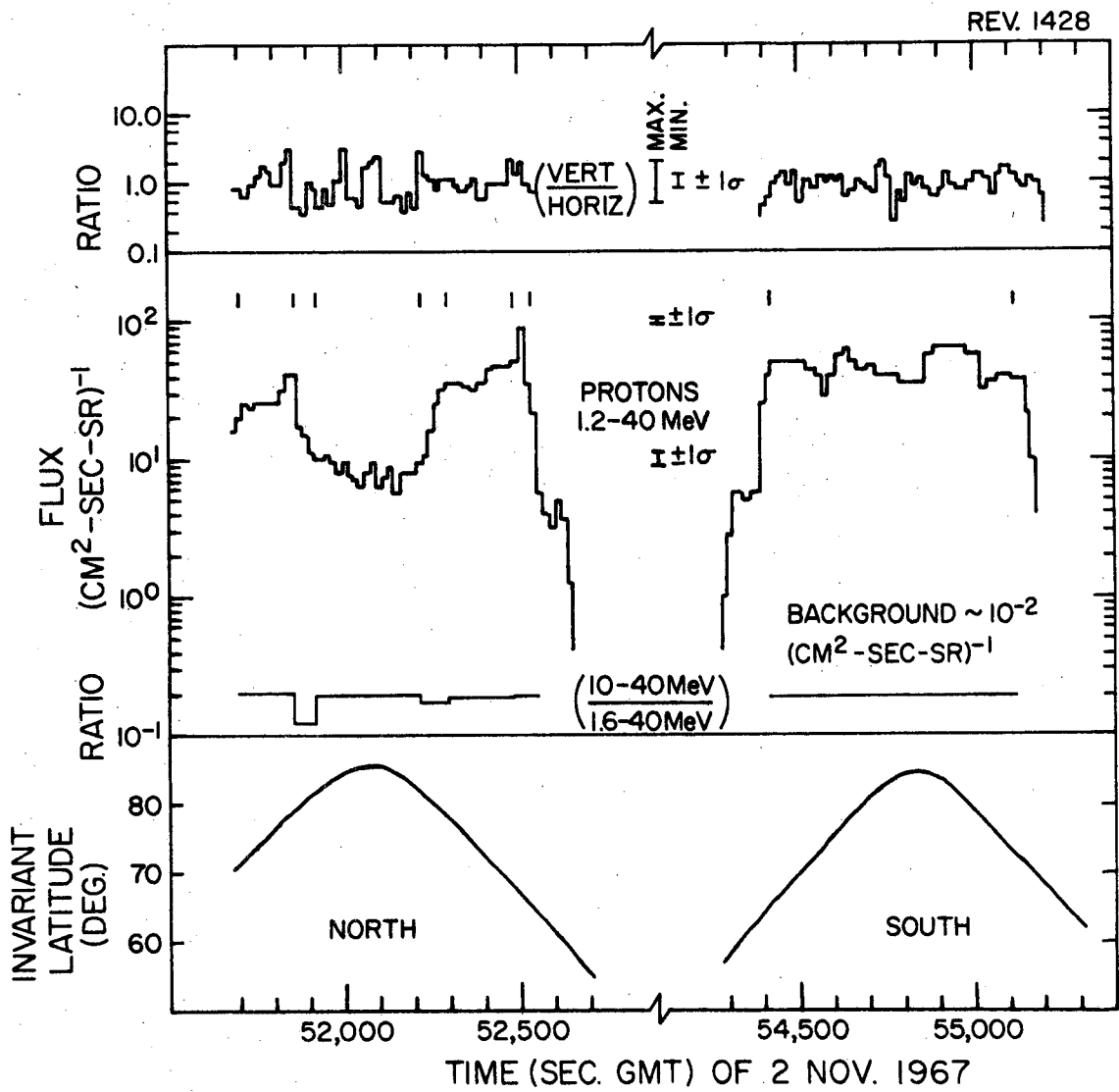
This is a particularly good example of a prolonged difference between the flux observed in one high polar latitude region and the flux observed in the other two polar regions. The north high polar latitude flux is consistently lower than the other two fluxes for a period of ~25 hours. This type of profile configuration, where one high polar latitude profile is markedly different than the other high polar latitude profile has been referred to as a North-South (N/S) asymmetry [11,25].

The appearance of such a N/S asymmetry during a single polar pass is illustrated by figure V-9. This figure shows the $V_1\overline{V}_3$ rate for the north and south polar passes of one orbit early during the 2 November 1967 event. Southern polar passes from later in the event show even less structure. The ratio of the flux of 10-40 MeV protons to the flux of 1.6-40 MeV protons is an indication that the same ratio of minimum to maximum flux occurred over the entire measured energy range from 1.2 to 40 MeV. As is discussed below, pulse height analysis gives the same indication. Figure V-9 also contains the ratio of the vertically incident to the horizontally incident flux, normalized so that unity corresponds to an isotropic flux. There is no evidence of a large anisotropy in conjunction with the intensity variations, ruling out a pitch-angle dependent cut-off effect.

The manner in which the feature in the north polar proton flux illustrated in figure V-9 is repeated consistently for a long period as shown in figure V-8 suggests the possibility of referring to these observations as persistent features. A feature in the proton polar cap flux will be termed *persistent* if it is observed during two or more

Figure V-9

Selected north and south polar passes observed early during the 2 November 1967 solar flare event. Isotropy is indicated by a vertical/horizontal ratio of unity. Any spectral change would be indicated by a change in the 10-40 MeV/1.6-40 MeV proton ratio, which has a statistical error of $\leq 1\%$. Invariant latitude is included for reference.



consecutive orbits (excluding orbits for which appropriate data are unavailable).

The mapping of the regions of maximum and minimum intensity into the invariant latitude-magnetic local time (Λ -MLT) coordinate system is shown in figure V-10, along with the low latitude rigidity cutoff previously determined for 1.5 MeV protons during a magnetically quiet period in 1961 [51].

Spectra were calculated throughout this event, and figure V-11 shows a typical example of the spectrum from the northern high polar latitude region compared to the spectrum from the low polar latitude region observed at the same time. The shapes of these spectra are remarkably similar and differ only by a constant multiplicative factor. Although there are some variations early in the event, as shown on figure V-12, no prolonged energy dependent effects can be observed.

Comparison of Electron and Proton Observations

During the 28 September 1968 event, a comparison between electron polar cap observations and the features which occur in the polar proton intensities was possible, and it is shown in figure V-13. During this event the persistent proton feature took the form of a depression. The observations of the electron polar cap boundary are mapped into an invariant latitude-magnetic local time coordinant system and represented by solid circles; the high latitude limits of the enhanced flux region associated with low polar latitudes appear as open circles. It is clear that the

Figure V-10

A mapping of the north polar passes of OGO-4 into invariant latitude-magnetic local time coordinates for the period of the 2 November 1967 flare event. The locations of the regions of maximum and minimum proton fluxes are shown. Observed geomagnetic cutoffs are indicated and compared to cutoffs reported for a quiet geomagnetic field in September, 1961 [51]. The extent of data coverage is indicated where it is less than a complete polar pass.

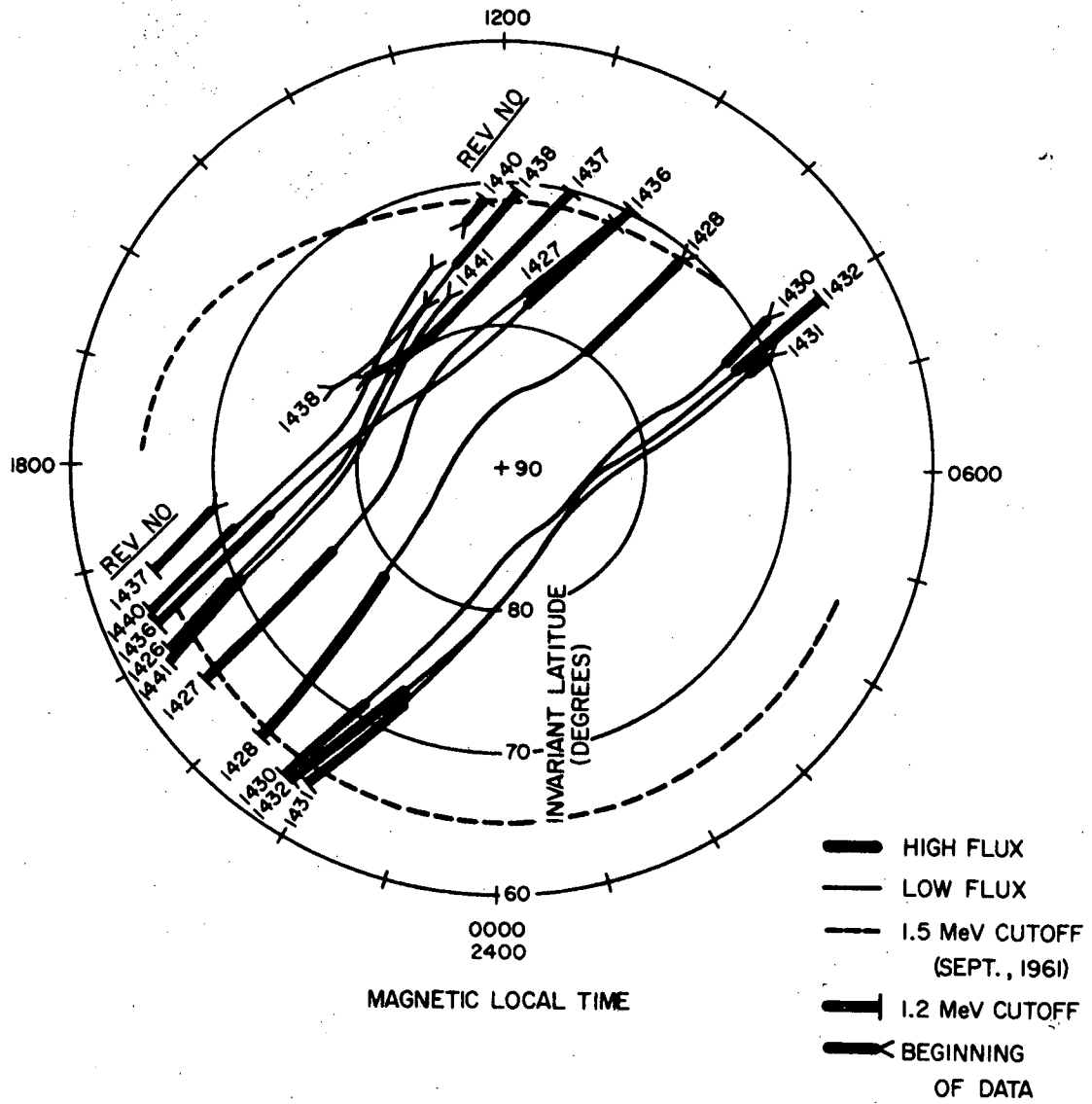


Figure V-11

Typical proton differential energy spectra observed during the 2 November 1967 solar flare event. Open circles represent the spectrum observed at low polar latitudes, and crosses represent the spectrum observed at the same time at northern polar latitudes.

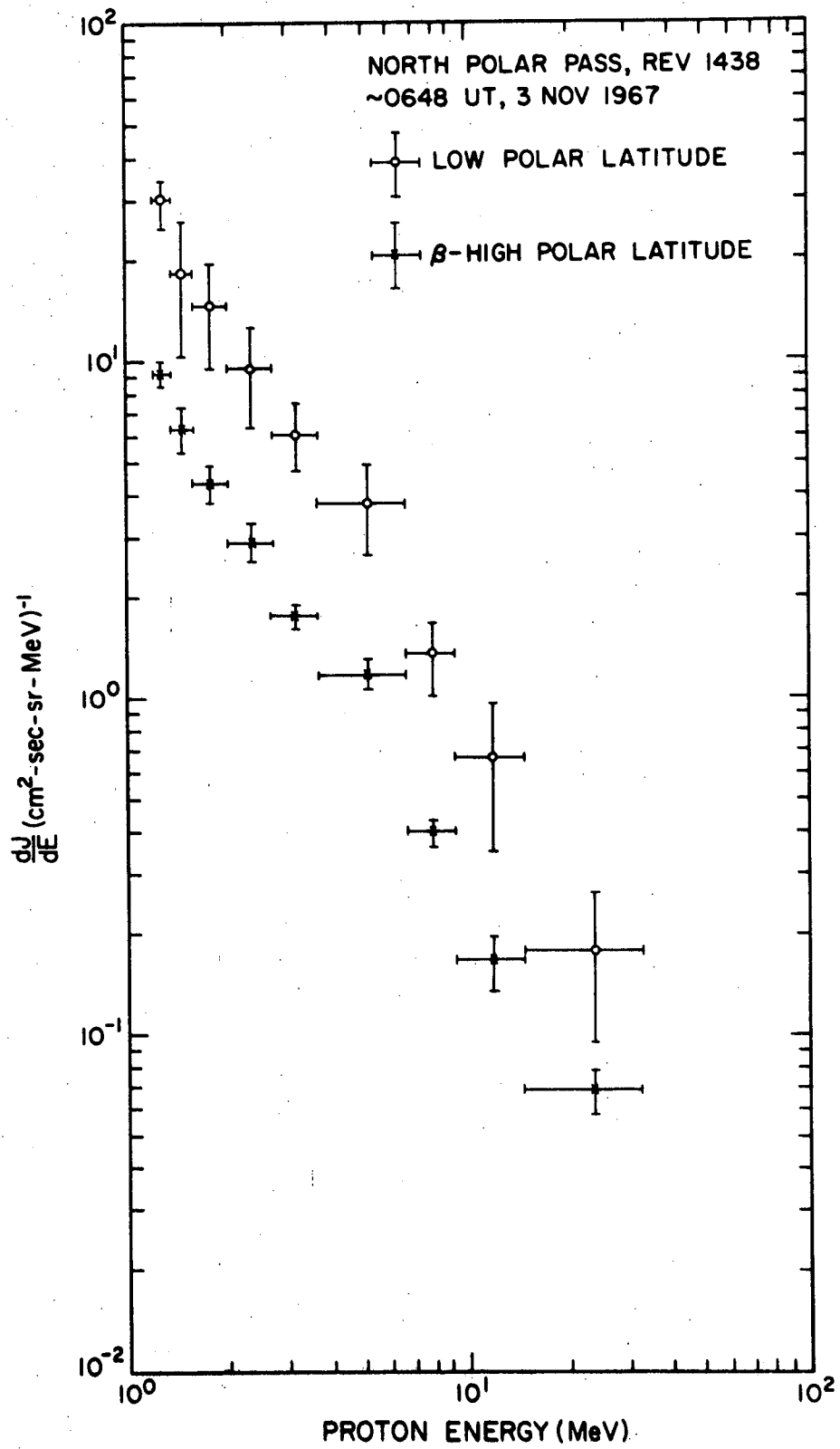
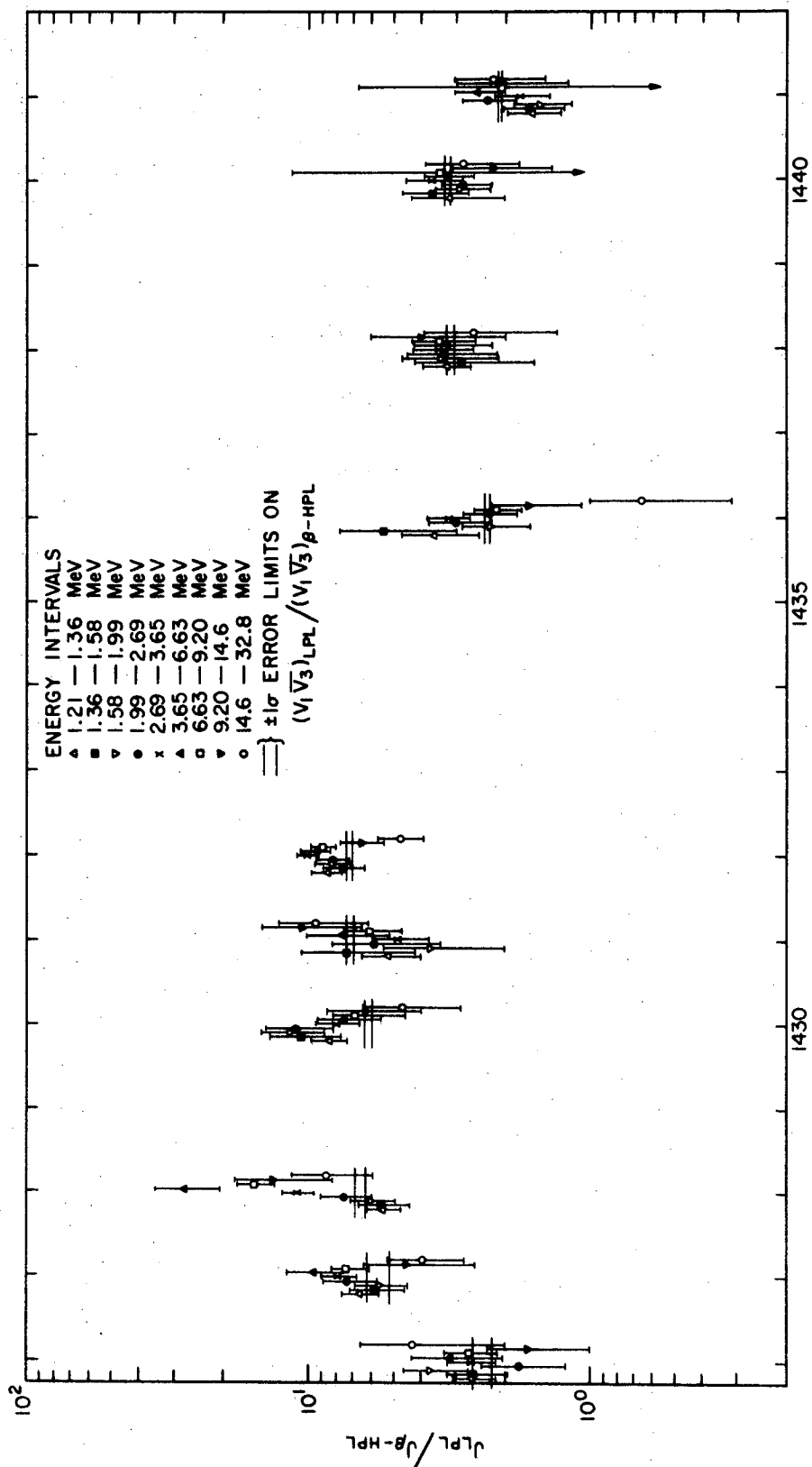


Figure V-12

Ratio of low polar latitude flux to northern high polar latitude flux as a function of energy for the period of the 2 November 1967 solar flare event. Each symbol consistently represents the ratio for a specific range of energies. The longer horizontal lines indicate the $\pm 1\sigma$ limits of the ratio of the low polar latitude $V_1\overline{V_3}$ rate (1.2-40 MeV protons) to the northern high polar latitude $V_1\overline{V_3}$ rate.



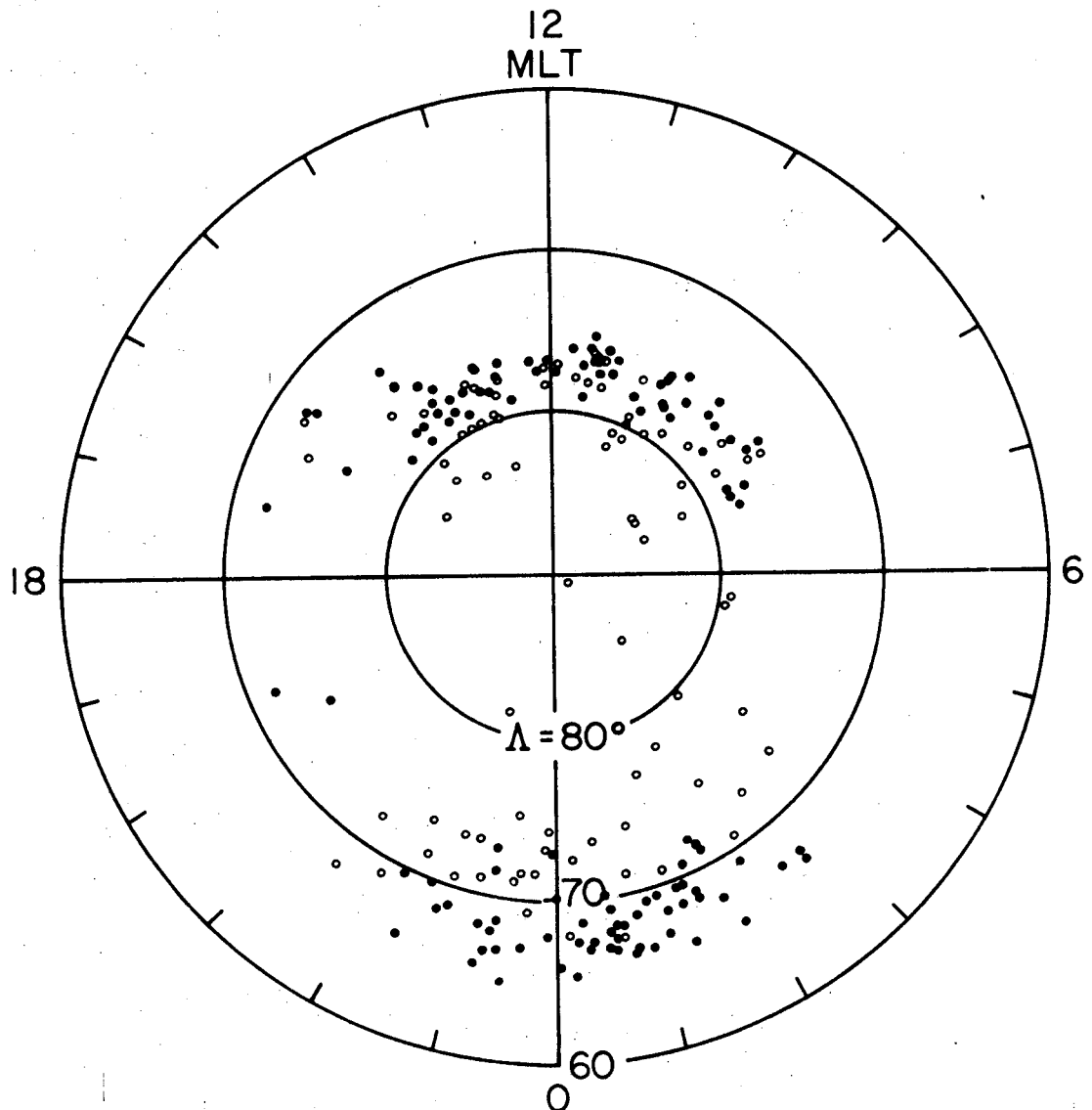
REV. NO. DURING 2 NOVEMBER 1967 EVENT

Figure V-13

Comparison in invariant latitude-magnetic local time coordinates of observed electron polar cap boundaries with observed high latitude limits of regions with enhanced proton fluxes. During the event shown, these enhanced fluxes were observed at low polar latitudes.

SEPT. 28, 1968

- ELECTRON
- PROTON



latitudes of the proton limits are \geq the latitudes of the electron polar cap boundary. This comparison indicates that the region where electrons have rapid access is the region where the proton access is delayed.

VI. BACKGROUND

The significance of the data presented in Section V can be most effectively investigated in the proper context. As will be pointed out in Section VII, these data are particularly relevant to questions concerning the configuration of the distant geomagnetic field. Since charged particles observed in the polar regions propagate through interplanetary space, a brief description of this environment and the behavior of energetic solar particles therein is appropriate. In order to establish the context for the discussions to follow, the distorted configuration of the near-earth geomagnetic field will be presented, along with the significance and difficulties of studying the distant geomagnetic field.

Interplanetary Environment

The model which we will use here is the one which was first proposed by Parker [52]. In this model the solar corona plasma continues to expand radially outward from the sun to form a super-Alfvenic solar wind. The solar magnetic field is "frozen into" the solar wind plasma [53] and is thus convected outward from the sun. In the presence of a homogeneous, uniform solar wind flow, the combination of the radial solar wind flow and the rotation of the sun would cause the solar magnetic field to be pulled into an Archimedian spiral configuration, such that near the earth

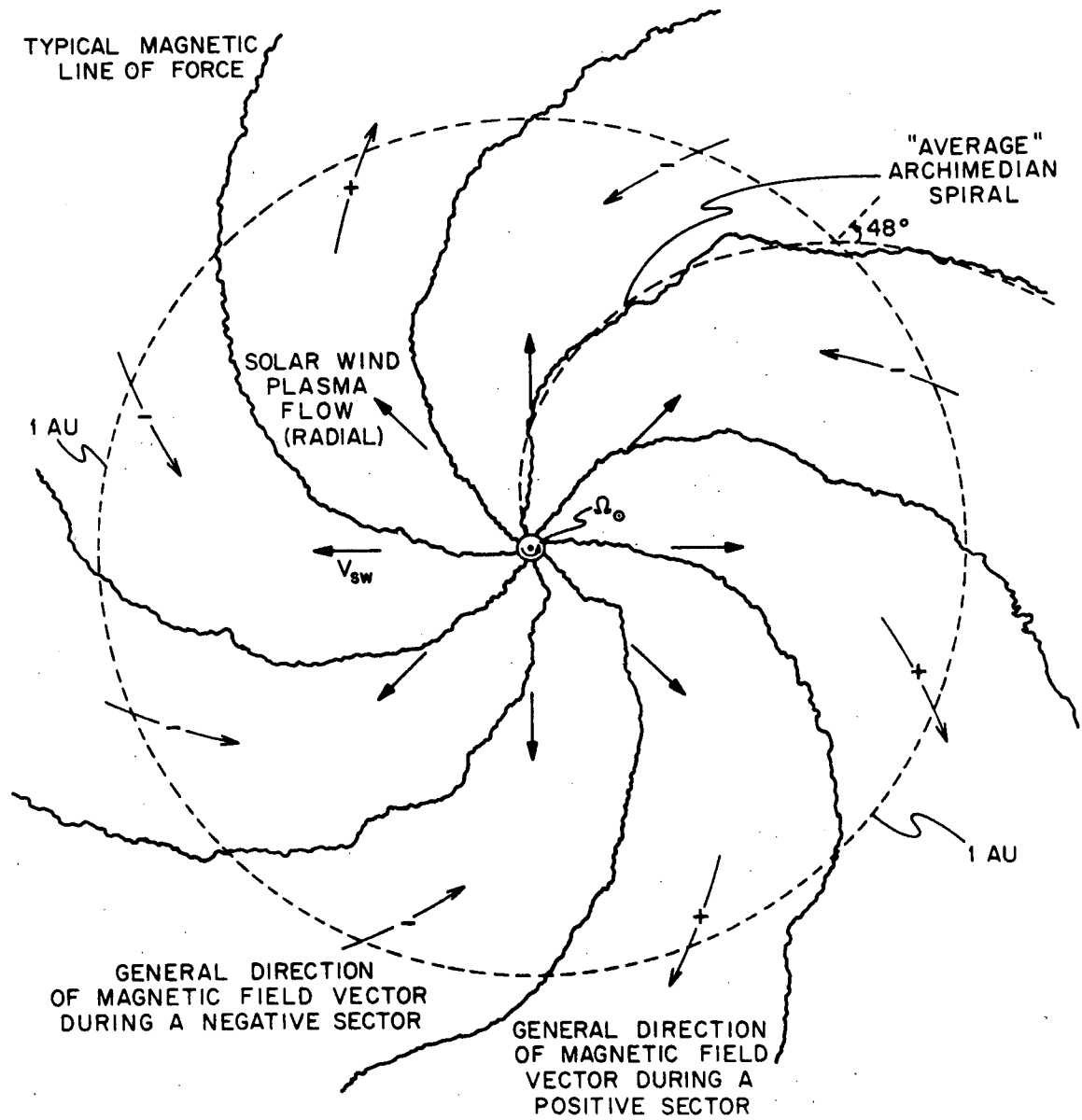
the angle between the magnetic field and a radial vector would be about 48° , measured in the ecliptic plane [54]. Neither the source of the magnetic field nor the medium in which it is being convected is either homogeneous or uniform, however. As a consequence, the configuration of the interplanetary magnetic field fluctuates considerably from this ideal position (*Cf.* [55]), and the actual configuration is more like that depicted schematically in figure VI-1. An important parameter of the solar magnetic field is the mean direction of the field, designated as positive (negative) if the field direction is predominately away from (toward) the sun along the average spiral direction. Most of the time this mean direction is observed to be divided into sectors [56], also shown in figure VI-1. The history of this sector structure during the lifetime of the OGO-4 data acquisition [57,58] is indicated on the OGO-4 Data Coverage Plots (an example is shown in figure IV-1; the complete set is given by Evans [35]).

As indicated in Section V, solar cosmic ray events can be divided into two different phenomenological classes: (a) the prompt event, or solar flare event, in which particles arrive within a few hours of the parent flare, and (b) delayed events, or EDP (Energetic Delayed Particle) events, in which particles arrive a day or more after the parent flare [59]. Since each of these classes of events has been observed with OGO-4, it is appropriate to briefly discuss some of the phenomenological aspects of each.

Solar flare particles are thought to be injected into interplanetary space impulsively at the sun more or less coincident with a relatively

Figure VI-1

Schematic representation of the configuration of the solar magnetic field near the ecliptic plane.



NOT TO SCALE

large release of energy (e.g. optical, X-rays, synchrotron radiation from energetic electrons). After injection, the propagation of these particles from the sun to the point of observation is determined by the characteristics of interplanetary space. The results of this propagation are normally an increase in the interplanetary flux to a maximum over a time scale of about five to fifteen hours [59], followed by a decay which becomes more or less exponential after a few hours with a decay time constant on the order of a day. The radial gradient in the flare flux is normally negative at 1 AU early in the event, but may become positive during the decay phase. Such a positive gradient has been observed by O'Gallagher $\left(\frac{1}{J} \frac{dJ}{dR} \approx 2.0 \times 10^{-3} \% / R_{\oplus} \right)$ [60]. Current models for the propagation of solar flare protons in interplanetary space [61,33] give $\frac{1}{J} \frac{dJ}{dR} \approx 1.5-11.0 \times 10^{-3} \% / R_{\oplus}$ as typical for gradients near 1 AU for late times ($t > 140$ hours). Early during the decay phase, interplanetary gradients could be as high as $40-50 \times 10^{-3} \% / R_{\oplus}$, depending on the position of the flare on the sun [33].

Anisotropies in the interplanetary proton fluxes associated with prompt events are observed throughout most events [59,62]. The degree and direction of the anisotropy varies greatly, however, during each event and also from one event to another. During the early phase of a prompt event, particles are normally observed streaming out from the sun along the direction of the interplanetary magnetic field [63,64]. This field aligned anisotropy decays rapidly and is usually not dominant shortly after the maximum flux is observed (5 to 15 hours after onset) [59,63]. After this time the anisotropy direction is independent of the magnetic

field direction and is inferred to be parallel to the solar wind velocity for a period of a few days [59]. The magnitude of the anisotropy during this phase is energy dependent and is normally between 5% and 20% [63]. Late in the decay phase of the event (more than four days after onset) the anisotropy is directed more or less perpendicularly to the magnetic field direction and its magnitude is $\leq 5\%$ [65]. The general duration and magnitude of interplanetary anisotropies during these three phases will be referred to in Section VII when the effect of these anisotropies on polar cap observations is discussed.

Another aspect of interplanetary anisotropies which will be of significance in Section VII is that, in general, the magnitude of the maximum anisotropy is inversely dependent upon the solar longitudinal separation between the parent flare and the foot of the interplanetary line of force passing through the point of observation [59]. Although this is generally true, large ($\geq 3:1$) anisotropies have been observed at lower proton energies during the initial phases of some flare events which are time correlated to east limb optical flares [66].

The other class of solar particle events consists of the delayed events, or EDP events, which have been observed many times in interplanetary space (e.g., as cited in Section V, [42-47,50]). Most of the phenomenological aspects of these events are mentioned in Section V, so we will confine our attention here to their source, with one exception: these events are usually associated with large field directed anisotropies in interplanetary space [44]. These EDP phenomena are normally associated

with the so-called "active" regions of the sun; the enhanced flow of plasma from such a region sets up an interplanetary configuration such as that illustrated in figure VI-2 [cf. 42,46,47], which co-rotates with the sun. The effect of simultaneous observations at radially separated points in space would be to observe an abrupt and short-lived enhancement at the most sunward observation point first and at the point furthest from the sun last. The importance of this class of events to our study is that such events are associated with spatially well-defined interplanetary features which sweep past the earth and down the geomagnetic tail (see below) at a nearly constant velocity, that of the solar wind. Polar cap observations of EDP events will provide the basis for determining approximately where the particles observed in a given region of the polar cap gained access to the geomagnetic field.

Geomagnetic Field and Magnetic Merging

An important consequence of the existence of the solar wind is the resultant configuration of the earth's magnetic field. The result of this plasma-magnetic field interaction is the confinement of the geomagnetic field to a cavity, called the magnetosphere, whose size and shape are determined by a balancing of the various magnetic and plasma pressures involved [67-70]. The current picture of the near-earth configuration of the magnetosphere is illustrated in figure VI-3 (cf. [71]). As a matter of definition, those geomagnetic field lines on which some charged particles are capable of completing at least one bounce period (i.e., mirroring in both hemispheres) will be termed *closed* field lines. Those on

Figure VI-2

Schematic representation of an interplanetary region of enhanced low energy flux co-rotating with the sun [42,46,47]. As the region co-rotates past the earth, radially separated observation points would record different event "arrival" and "departure" times. The difference between these times would depend only upon the solar wind velocity and the radial separation between the points.

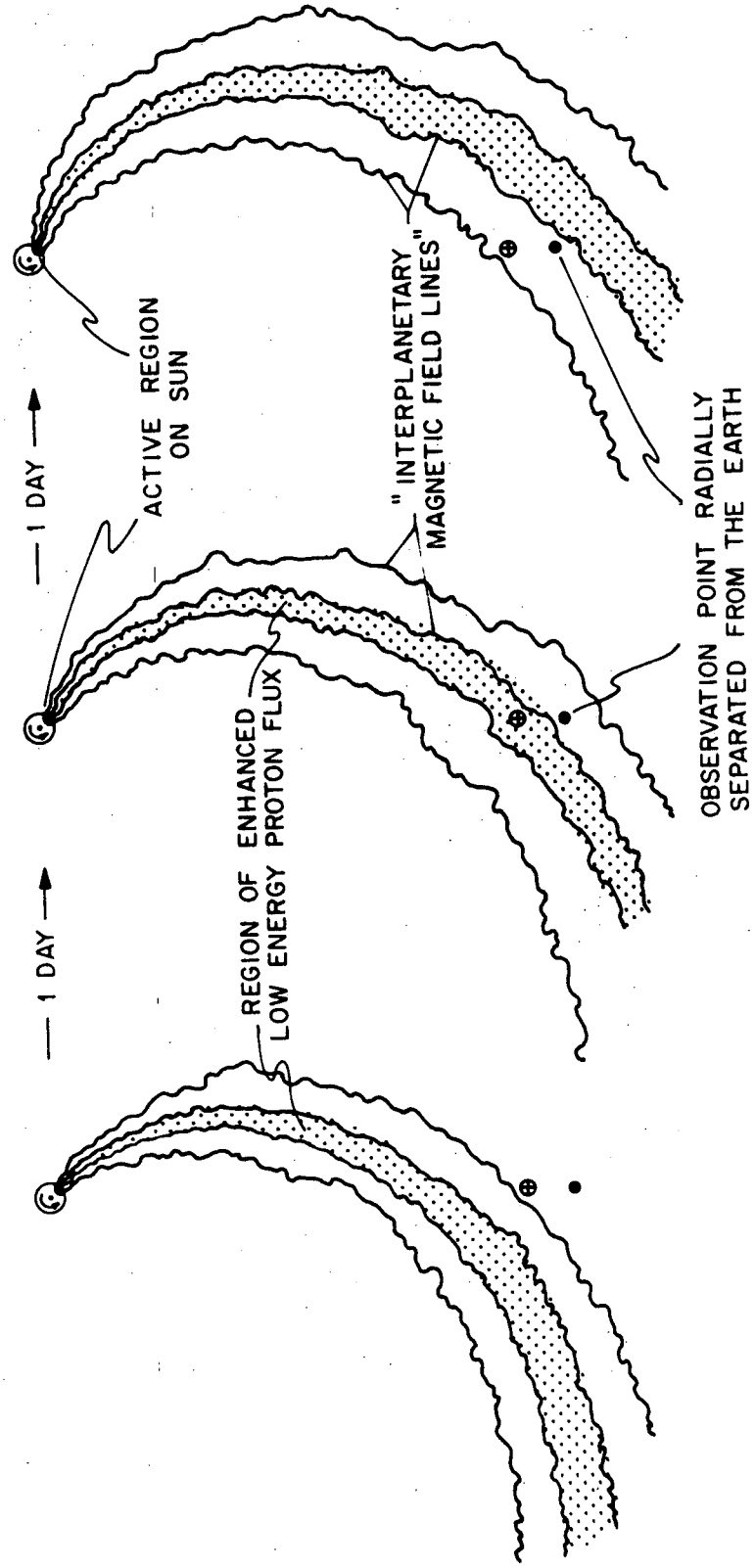
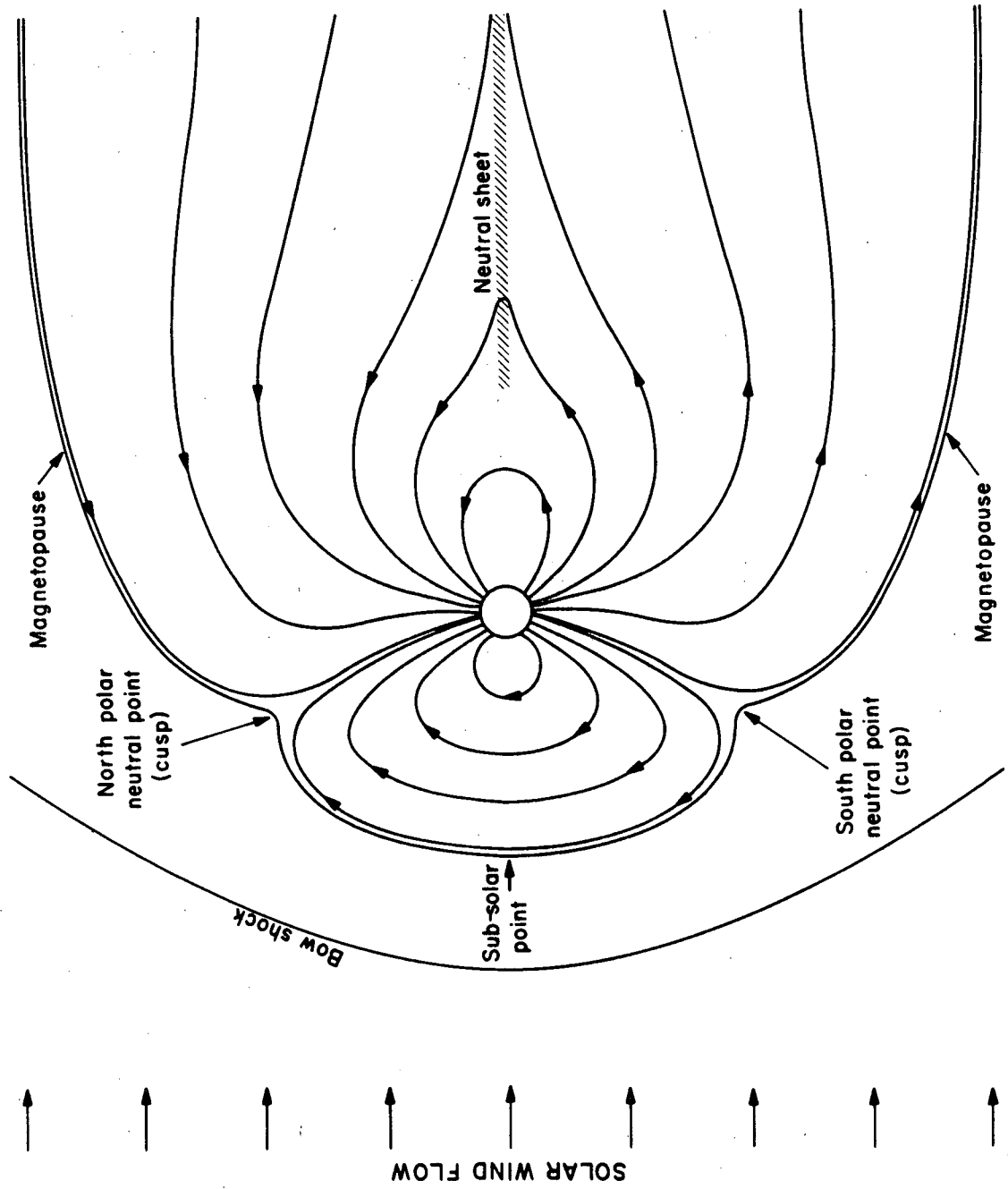


Figure VI-3

Schematic representation of the near-earth configuration of the earth's magnetosphere.



which such trajectories are impossible for any charged particles will be termed *open* field lines. In general, the open field lines constitute the field in the distant geomagnetic tail (see, for instance, [72,73]). The configuration of the geomagnetic tail has been mapped rather completely at least as far behind the earth as about $80 R_{\oplus}$ (somewhat beyond the orbit of the moon) [71,72,74-76]. There is some indication that at least a geomagnetic wake may extend as far as $500 R_{\oplus}$ [77,78] or $1000 R_{\oplus}$ [79-81] behind the earth. These observations are, however, complicated by the motion of the tail [80], and the detailed structure at these distances has not been measured directly.

A concept which will be of importance later should be defined at this time: that of an *access window* for the entry of particles into the magnetosphere. For a given location in the interior of the magnetosphere, the access window for particles of a given rigidity will be defined as the set of all points on the "surface" of the magnetosphere where particles of that rigidity can gain access to the interior and be subsequently observed at the given location. Since a surface *per se* may be well-defined neither in the distant tail nor in a region where the two fields are directly connected, the use of the term "surface" is meant to imply (a) the interface between the geomagnetic field and the interplanetary magnetic field and/or (b) the extension of this interface through a region where the fields are directly connected, if such a region exists. This definition is similar to, but more formal than, that given by Gall, *et al.* for what they refer to variously as "penetration regions" [82] and "windows" [83].

In the absence of direct measurements of the distant geomagnetic tail (beyond $80 R_{\oplus}$), one of the currently unresolved questions concerning the geomagnetic field is whether or not this field merges (i.e. reconnects) with the interplanetary magnetic field. The rôle of charged particle observations in the resolution of this question is that they can act as "probes" of a magnetic field where direct measurements of the field are infeasible. Assuming either the presence or absence of magnetic field merging between the solar and terrestrial fields, it is possible to postulate what the resultant magnetic field configuration might be. An analysis of a configuration so obtained will then yield implications concerning the characteristics of charged particle access from interplanetary space to the interior of the magnetosphere and the relationship between interplanetary particle fluxes and fluxes observed in the polar cap regions. Comparisons of polar cap observations with the predictions concerning these observations arising from such a magnetic field configuration will yield constraints to be incorporated in the model.

The implications of merging between the solar and terrestrial magnetic fields are not, however, restricted to questions of particle access into the magnetosphere. It is generally thought, for instance, that magnetic field merging may play a rôle in the formation of solar flares [5], and might even be involved in galactic phenomena [6]. An investigation of these possibilities is hampered, though, by the lack of concrete evidence concerning the conditions under which merging could take place.

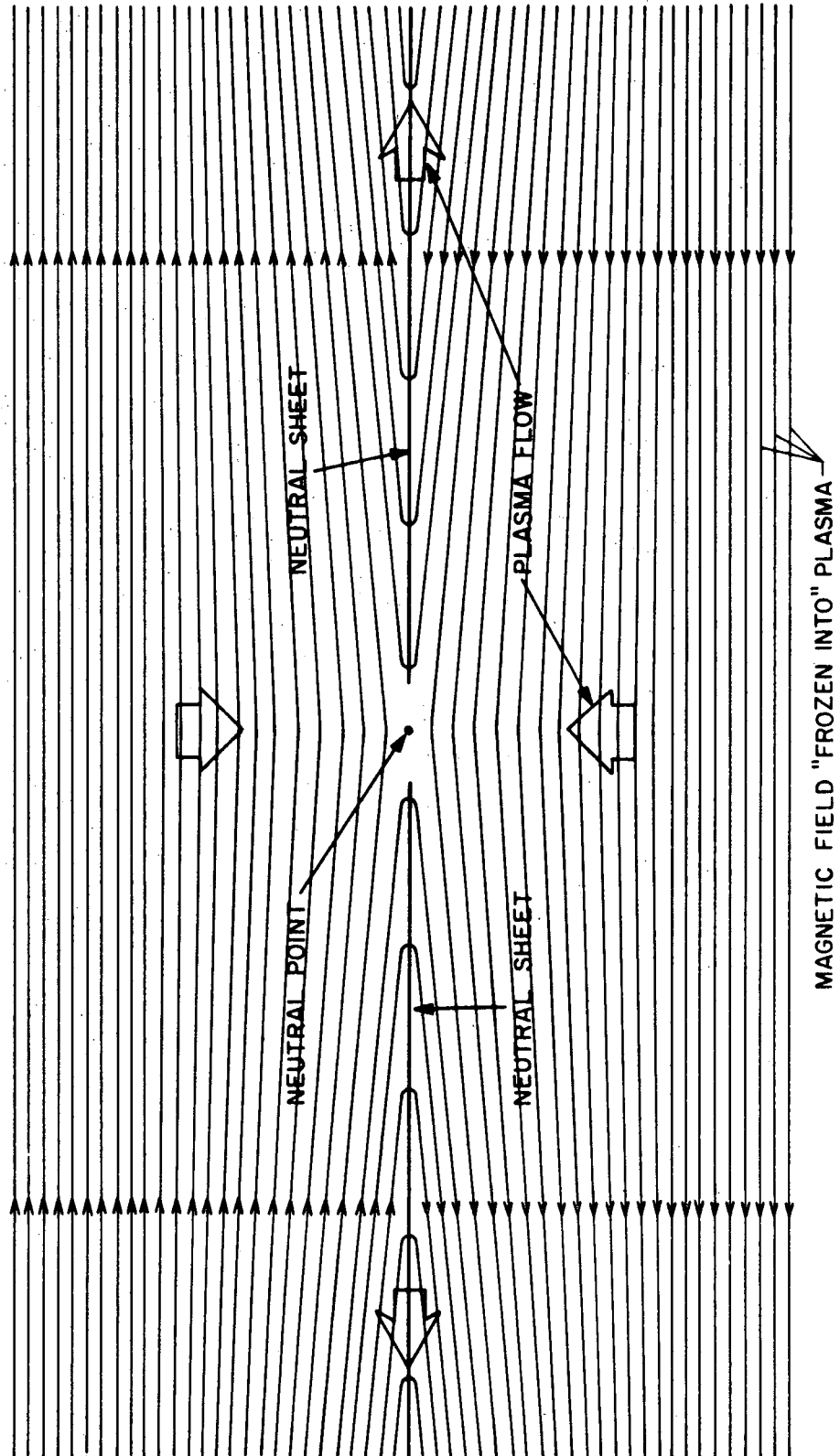
The basic mechanism for the reconnection of magnetic fields is

provided by the finite conductivity of the plasma. In 1956, Sweet [84] pointed out that the diffusion rate for magnetic fields in the vicinity of a *neutral point* (at which \vec{B} vanishes) will be much faster than in other regions of a plasma. Since the magnetic forces vanish at such a point, the magnetic field will tend to form a sheet near which \vec{B} reverses direction on a relatively small length scale; such a sheet is termed a *neutral sheet*. A neutral point also tends to be a stagnation point of the plasma flow, in which case the magnetic field is convected toward the neutral point, where the field lines are "broken" and "reconnected" as the direction of the plasma flow changes by 90° . Since the field vanishes at the neutral point, however, the process is more accurately thought of as one in which the field being carried to the neutral point disappears and reappears in a different configuration, as determined by the fluid flow. Figure VI-4 illustrates this process, which is referred to as Sweet's mechanism; its astrophysical implications have been investigated by Parker [85].

In order to provide a mechanism whereby higher merging rates than those associated with Sweet's mechanism could be attained, Petschek [86] has suggested that while diffusion may be presumed to dominate the magnetic merging in the immediate vicinity of the neutral point, the plasma which is convecting the field away from the neutral point (after merging) may be moving at the Alfvén velocity, V_A . Petschek finds that the maximum incoming plasma velocity which can be supported by such a scheme is given by the following recursive relation:

Figure VI-4

Schematic depiction of a neutral point, at which the magnetic field is shown undergoing merging *via* Sweet's mechanism. The angle between the two fields near the neutral sheet has been exaggerated.



$$U_m = \frac{\pi V_A}{4 \ln \left(\frac{16 U_m^2 \pi \sigma L}{V_A c^2} \right)} \quad (6.1)$$

where σ is the conductivity of the plasma at the neutral point, and L is the scale size of the diffusion region. Sonnerup [87] has recently refined this approach somewhat, and has reported the following relationship for determining the maximum plasma velocity at which the fields may merge:

$$U_m = V_A (1 + \sqrt{2}) \quad (6.2)$$

By treating the basic field equations involved, Yeh and Axford [88] conclude that in general there is no maximum merging velocity, although they show that Sonnerup's solution is a special case of their solution -- the only non-singular case, according to Sonnerup. Considering the scarcity of observational information concerning magnetic merging, it is virtually impossible to determine which, if any, of these solutions is more nearly correct. Even establishing the absence of merging between the solar and terrestrial magnetic fields would be significant.

As a matter of terminology, geomagnetic field configurations arising from the assumption of the absence of magnetic merging between the solar and terrestrial fields are referred to as *closed* magnetospheric models, while those configurations based on the presence of merging are termed *open* magnetospheric models. In the next Section, after a discussion of

the general implications of the electron and proton observations, examples of each of these types of magnetospheric models will be presented and compared to the OGO-4 results presented in Section V and Appendix A.

VII. DISCUSSION

The information in Section VI provides the basic framework into which the data presented in Section V can be placed. The OGO-4 electron observations provide a comprehensive determination of the boundary between low polar latitudes (closed field lines) and high polar latitudes (open field lines). After this interpretation of the electron data has been established, the proton observations can be used to investigate the characteristics of the "windows" where these charged particles can gain access to the geomagnetic field. The observations of EDP events will be of particular interest in this regard, especially with respect to characterizing the positions and extents of these access windows. These EDP data represent the first reported observations of clearly identifiable interplanetary features, which are propagating down the tail, appearing at different times in different regions of the polar cap. With the particle access configuration established, the three major models of the distant geomagnetic field will be presented, noting the relationship of each to the fundamental question of magnetic merging. The pertinent predictions and extrapolations of the field configuration resulting from each model will be compared with the OGO-4 data with the result that severe constraints can be placed on each model.

Electron Polar Cap

The low magnetic rigidity and high velocity of the 0.4-1.0 MeV electrons observed by this experiment make these electron observations of particular importance in defining the transition between the region of open field lines and the region of closed field lines in the magnetosphere [7-9,27,41,89,90]. The identification of the electron polar cap with open geomagnetic field lines can be established as follows. The origin of 50 keV polar cap electrons has been shown to be beyond about $64 R_E$ behind the earth by moon shadowing experiments conducted with a lunar orbiter by Van Allen and Ness [89], Van Allen [7,8], Anderson and Lin [9], and Anderson [90]. In addition, Van Allen and Ness [89] observe a diffusion rate perpendicular to the magnetic field less than 100 km/sec between the moon and the earth. These observations, coupled with the low rigidity of the electrons, imply that the edge of the electron polar cap plateau should reflect the boundary of open field lines closely. The high electron velocities mean that differences in mode or position of access which might cause large variations in proton fluxes are not significant in electron observations. For instance, Van Allen [8] reports transit times for electrons travelling from interplanetary space to inside the magnetotail of ≤ 100 seconds, which were interpreted by Van Allen as indicating that electrons can gain direct access to the geomagnetic tail. As a result of the high velocities and rapid access, the electron flux over the polar caps is relatively homogeneous above the electron polar cap boundary (see figures V-1 and V-2, also Vampola [27] and West and Vampola [41]). The relative uniformity of the electron flux

inside the boundary makes the specification of the location of this boundary rather unambiguous. We therefore interpret the data presented in figure V-3 as a definition of the region of the polar cap which is associated with open field lines in the geomagnetic tail. Whereas Vampola [27] has reported 25 observations of this boundary which he has extrapolated to geomagnetically quiet conditions (indicated on figure V-3), the 333 boundary observations made withOGO-4 during magnetically quiet periods constitute a much more comprehensive mapping of the open field line region than has previously been possible.

For the purpose of clarifying the proton observations, it is clear that the region defined as the high polar latitude (HPL) region in Section V is associated with the geomagnetic field lines which constitute the geomagnetic tail. Likewise, the low polar latitude (LPL) region is associated with closed geomagnetic field lines, which never extend far from the earth ($< 30 R_E$). In order to avoid the complications associated with any transition region, data associated with high polar latitudes have been collected at invariant latitudes well above the boundary indicated on figure V-3. Low polar latitude data similarly avoid the region close to the boundary of open field lines. As shown by figure V-18, persistent proton features can be identified consistently with the region of open field lines. With this in mind, we turn now to the proton observations.

Access of 1.2-40 MeV Protons

While electrons are able to define the edge of the open field line region with some precision, the much lower velocities and higher rigidities of the 1.2-40 MeV protons make them more sensitive to the effects of interplanetary gradients and anisotropies, different access modes and access window positions. Consequently, they can be used as "probes" to investigate the characteristics of the access windows.

Prior to the report of preliminary results from this experiment for the 2 November 1967 event [11], some evidence of polar cap features was available [12-20], but the observations were too sparse to lead to comprehensive analysis. Although since the report of the persistent feature observed during the 2 November 1967 event several observations of persistent features have been reported [21-26], the conclusions drawn from these observations still suffer from a paucity of data: only Bostrom [21] and Morfill and Quenby [26] have reported observations from more than one event (two events in both cases).

A summary of all of the proton events observed to date in the OGO-4 data is presented in figure VII-1. As indicated in this figure, there is a strong correlation between the pole in which a persistent feature was observed on OGO-4 and the interplanetary sector structure. With notable exceptions, the persistent features were observed in the north pole during negative sectors and in the south pole during positive sectors. This correlation is consistent with other reported studies in which the interplanetary sector structure has been considered [13,24-26,91-93 (the

Figure VII-1

Summary of OGO-4 observations of solar events. The information indicated on this figure is as follows:


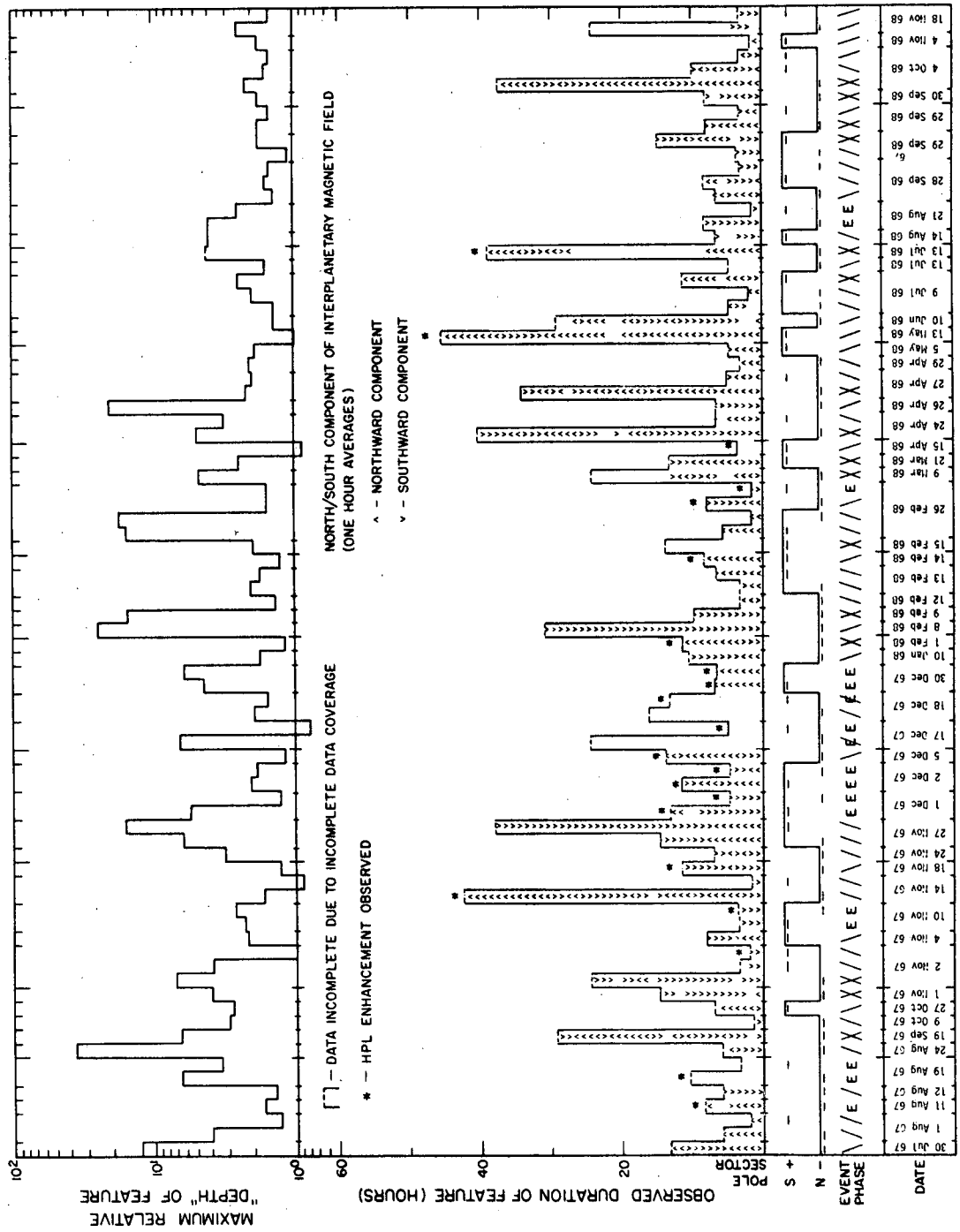
1. Each event is identified by date.
2. The phase of the flare during which a persistent feature was observed is indicated:
 / = observation during the rise of flare
 \ = observation during the decay of flare
 E = EDP event observation
3. The pole in which the persistent feature was observed is indicated (_ _) and compared to the interplanetary magnetic field sector ().
4. The duration (in hours) of the feature is indicated. In 75% of these observations the actual duration of the event was not measurable due to incomplete data coverage.
5. The history of the north/south component of the solar magnetic field is represented by a vertical sequence of "▲"s (northward component) and "▼"s (southward component). Each symbol represents the average sense of this component during one hour [94]; the lowest symbol indicates the status of this component at the beginning of the observations.

Figure VII-1 (continued)

6. Those events during which an enhancement was observed at high polar latitudes are indicated (*).
7. For each polar pass of the indicated pole during the event, the ratio of the LPL $V_1\overline{V_3}$ rate to the HPL $V_1\overline{V_3}$ rate was calculated. The maximum of these ratios is plotted as the "maximum relative 'depth' of the feature."



last three do not involve satellite proton polar cap observations)]. In accordance with this correlation and for the sake of clarity, the following terms will now be introduced: α -pole and β -pole. These terms have been carefully selected in an attempt to avoid any terms which might connote any feature of any model. The correspondence between the north and south geomagnetic poles and the α -pole and β -pole is dependent upon the interplanetary sector and is given in table VII-1. With this definition, the field lines in the geomagnetic tail associated with the α -pole are usually more nearly antiparallel to the interplanetary magnetic field lines than those field lines in the geomagnetic tail associated with the β -pole. We can now restate the sector correlation noted above as: "With notable exceptions, the persistent features were observed in the β -pole." The persistent flare event features were correlated with the interplanetary sector structure in this manner 91% of the time, while they appeared to be completely uncorrelated with the north-south component of the interplanetary field. The interplanetary field had a southward component only 54% of the time, and figure VII-1 shows that during several events this component changed direction several times with no notable effects.

The data in table VII-2 tend to strengthen the correlation between the interplanetary sector structure and the observations of persistent features considerably. This table lists all of the instances when a sector reversal was observed in interplanetary space [94] while a persistent polar cap feature was being observed. Within the constraints imposed by the inherent time resolution of the observations and the frequent gaps in the data, the following is implied by these data: persistent features

TABLE VII-1

Correspondence Between α -pole/ β -pole
North/South Geomagnetic Poles

	North Pole	South Pole
Positive Interplanetary Sector	α -pole	β -pole
Negative Interplanetary Sector	β -pole	α -pole

TABLE VII-2

Time Correlation of Sector Reversals [94] with Persistent Features

Date	Last Feature Obs.			Sector Reversal Univ. Time (HHMM)	1st Pass after SR in Same HPL		Figure Showing Profile
	Hours Before SR	$\sqrt{V_1 V_3}$ (cts/sec) LPL	$\sqrt{V_1 V_3}$ (cts/sec) HPL		Hours after SR	$\sqrt{V_1 V_3}$ (cts/sec)	
11 Aug 67	0.2	28.	40.	1600	1.5	26.	
28 Oct 67	0.6	0.8	0.4	1200	1.0	0.55	
3 Nov 67	1.3	89.	28.	1300	1.8	45.	E-3
10 Nov 67	0.9	3.4	2.2	2300	4.0	2.8	E-4
10 Feb 68	3.9	2.45	1.09	0500	0.9	2.3	E-10
10 Feb 68	1.4	4.3	11.6	1300	0.3	3.3	
12 Feb 68	1.9	0.94	0.65	1100	0.6	1.85	E-11
10 Jun 68	1.2	525.	398.	1230	0.3	501.	
10 Jul 68	0.8	141.	252.	0300	0.8	112.	
2 Sep 68	0.6	3.84	1.26	1200	1.0	3.02	
28 Sep 68	0.8	67.	57.	0800	0.8	75.	
28 Sep 68	0.6	162.	119.	2000	1.0	163.	
30 Sep 68	1.2	350.	305.	2100	0.3	316.	
30 Sep 68	1.2	285.	213.	1400	0.4	282.	
30 Sep 68	0.8	390.	253.	1600	0.8	385.	

observed prior to a reversal in the interplanetary magnetic field are not present in the data within $O(1 \text{ hour})$ after the reversal. Additionally, there appears to be no distinction in this regard between persistent HPL depressions and persistent HPL enhancements.

This strong correlation between the interplanetary sector and the persistent features, embodied in the α -pole/ β -pole terminology, can now be used to help organize and interpret additional aspects of the proton observations.

EDP Events

The observations of EDP events are of particular interest because these events can be associated with an interplanetary region of limited spatial extent which is propagating radially away from the sun (and thus down the length of the geomagnetic tail) at a reasonably constant and well defined velocity: that of the solar wind. As a consequence, time delays between the appearance of the event in different polar cap regions must be directly related to the time required for the region of enhanced flux in interplanetary space to propagate from one access window to the next.

A total of eleven EDP events and possible EDP events have been observed with this experiment. These are tabulated in table VII-3, which includes an indication of some of the factors leading to the identification of each event as an EDP event. In every case the event was observed first at low polar latitudes, which recent work [26,95] involving the

TABLE VII-3

OGO-4 Observations of EDP Events

Date	Univ. Time of LPL Peak (HHMM)	Delay (hrs. UT) between LPL Peak and: α -HPL Peak β -HPL Peak		Alert Neutron Monitor Indi- cation? ^a	SC/SI within 4 hrs. of LPL Peak?	Unam- biguous Ident. as EDP Event? ^b	Figure Showing Profile
11 Aug 67	0400	0.0	2.0	FD	YES	NO ^b	A-1
19 Aug 67	0548	1.2	13.9 ^c	WD	YES	YES	A-2
10 Nov 67	2145	1.1	--- ^d	NO	NO	YES	A-4
15 Nov 67	0400	--- ^e	6.0	NO	NO	YES	
15 Nov 67	0830	--- ^e	5.1	NO	NO	NO	
1 Dec 67	2130	1.2	7.0	WD	NO	YES	A-5
2 Dec 67	1300	1.3 ^c	3.8 ^c	NO	NO	YES	A-6
17 Dec 67	0600	0.0	21.2	NO	NO	NO	
30 Dec 67	1135	1.4	5.9	FD	YES	YES	A-7
30 Dec 67	1420	2.2	--- ^e	FD	YES	YES	A-7
27 Aug 68	1515	0.4	1.3	NO	NO	NO	
1 Oct 68	0130	--- ^e	5.0	FD	YES	YES	
Average delays:		1.4±0.4	6.9±3.3				

a. FD = Forbush Decrease; WD = weak depression

b. All events in this table exhibit most of the phenomenological characteristics of EDP events (e.g. only observed at low energies, rapid variations in counting rate, short duration), but those indicated by "NO" in this column have some facet which is not completely consistent with EDP observations (cf. discussion in Appendix A concerning the 11 August 1967 event).

c. Observation is uncertain or impossible due to a data gap.

d. Sector reversal occurs before β -HPL EDP peak would be expected.

e. Observation impossible due to orbit which did not penetrate to HPL.

calculation of proton trajectories in a model magnetosphere has indicated corresponds to an access window in the vicinity of the earth (within about $20 R_{\oplus}$). After a short delay, which averaged 1.4 ± 0.4 hours, the event was observed at α -high polar latitudes. After a much longer time delay (6.9 ± 3.3 hours) the event was observed at β -high polar latitudes. The following conclusions can be made and are illustrated in figure VII-2 (an average solar wind velocity of 400 km/sec is assumed in calculating the access window "positions"):

1. THE ACCESS WINDOW FOR 1.2-40 MeV PROTONS OBSERVED AT α -HIGH POLAR LATITUDES IS SOMEWHAT FURTHER FROM THE SUN THAN THE ACCESS WINDOW FOR THOSE PROTONS OBSERVED AT LOW POLAR LATITUDES. (α -high polar latitude access window is located approximately $320 \pm 90 R_{\oplus}$ behind the earth.)

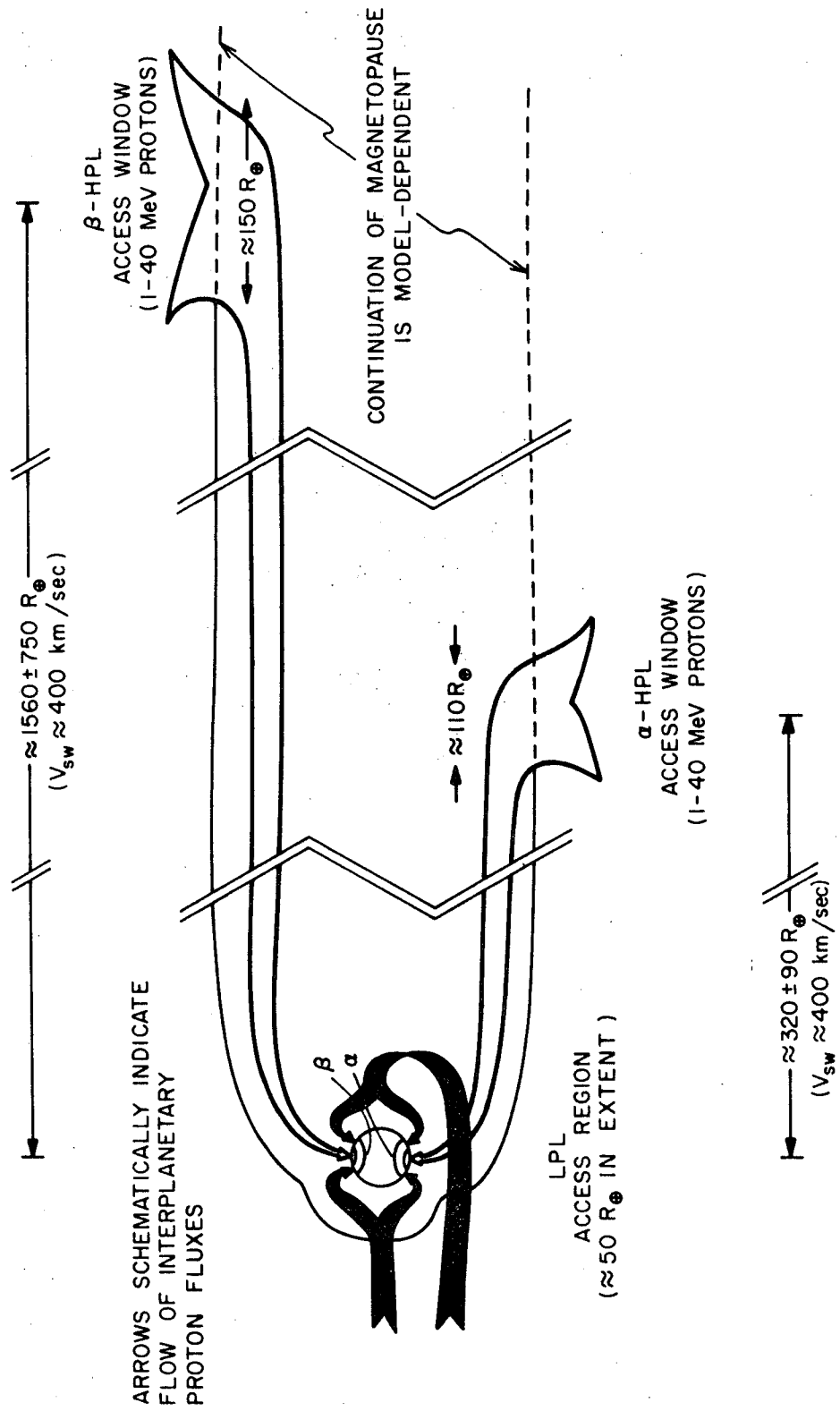
2. THE ACCESS WINDOW FOR 1.2-40 MeV PROTONS OBSERVED AT β -HIGH POLAR LATITUDES IS SIGNIFICANTLY FURTHER FROM THE SUN THAN THE ACCESS WINDOW FOR THOSE PROTONS OBSERVED AT LOW POLAR LATITUDES. (β -high polar latitude access window is located approximately $1560 \pm 750 R_{\oplus}$ behind the earth.)

Examples of these EDP observations are given in figures A-1, A-2, A-4 through A-7, and V-4.

In addition to the location of the access windows, estimates of the extent of the windows can also be inferred from these data. Although in general the polar cap flux is related to the interplanetary flux by a

Figure VII-2

Schematic representation of the configuration of the magnetospheric access windows for 1.2-40 MeV protons. This configuration is referred to as the $L_{\alpha\beta}$ configuration in the text. This diagram is intended to be completely model-independent; magnetic fields are not indicated, nor are details concerning the method by which protons gain access.



convolution integral, all that is needed at this point is an estimate. For this purpose, the "width" of the feature, ΔT , as shown on a profile, may be related to the spatial extent of the feature in interplanetary space, L_{ip} , and the spatial extent of the access window, L_w , by the approximation

$$\frac{L_{ip} + L_{w,reg}}{V_{sw}} \approx \Delta T_{reg} \quad (7.1)$$

where V_{sw} is the solar wind velocity, and "reg" represents one of "LPL", " α -HPL", or " β -HPL". Using ~ 1 hr. as a typical value for L_{ip} (indicated by the data presented by McCracken, *et al.* [66] and Anderson [47]), the OGO-4 EDP observations give the following estimates for the extent of the access windows:

$$\begin{aligned} L_{LPL} &\sim 50 R_{\oplus} \\ L_{\alpha-HPL} &\sim 110 R_{\oplus} \\ L_{\beta-HPL} &\sim 140 R_{\oplus} \end{aligned} \quad (7.2)$$

These numbers are very rough estimates due to the sparcity of well defined data and the assumptions made above, but the ratio between any two of these values can be considered accurate to within a factor of 2.

Questions relating to the details of the magnetic field configuration in the vicinity of the access windows and the method by which this access is achieved will be discussed below, after considering the extent to which the solar flare event observations support the $L_{\alpha\beta}$ access window configuration illustrated in figure VII-2.

Flare Events

The interpretation of the EDP event observations was aided in no small degree by the availability of several events for which the data coverage was virtually continuous and almost uninterrupted. Because of the much longer duration of solar flare particle events, conclusions drawn from observations of flare events are, in contrast, subject to the following two limitations: (1) the time-sharing nature of the OGO-4 telemetry made it virtually impossible to obtain a profile of a complete flare event (see Section III), and (2) the interplanetary configuration of proton fluxes during solar flare events is highly dependent on non-uniform interplanetary parameters and parameters related to the parent flare. The first point implies that several flare events must be observed to construct a comprehensive picture of particle access. The second point, on the other hand, implies that this is a limitation not confined to data from OGO-4. Indeed, any conclusions drawn from observations of a single flare event are subject to the limitation that only one set of solar flare and interplanetary parameters are represented. As the basis for the conclusions presented here, though, more than twenty-five solar flare events were investigated, representing a wide range of these parameters; these observations are summarized in table A-1.

Although interpretations of the proton flare event observations are complicated by the effects of interplanetary propagation, at least four aspects of these observations imply an $L\alpha\beta$ configuration for the access regions:

1. Flare onsets consistently occur later at β -high polar latitudes than at either low polar latitudes or α -high polar latitudes. The 2 November 1967 event (figures V-7 and A-3) is a particularly good example of this: there are two β -pole observations after the beginning of the flare is seen at LPL, showing a flux comparable to the pre-event flux at β -HPL. The 13 July 1968 event, shown in figure A-12, is another example of this delayed onset phenomenon.

2. Flare onsets are sometimes observed to occur later at α -HPL than at LPL. Once again, the 2 November 1967 event (figures V-7 and A-3) is a good example of this type of observation.

3. The "shape" of the β -HPL profile relative to the LPL profile consistently exhibits the characteristics expected in observations taken further from the sun: in all cases the β -HPL peak (a) is broader, (b) represents a smaller maximum flux, and (c) occurs at a later time. The 13 July 1968 event (figure A-12) is a perfect example of this phenomenon. Note that the β -HPL peak is clearly broader, lower, and later than the LPL peak. Other complete examples are scarce due to the data acquisition problem, but the 1 February 1968 event (figure A-8) is notable.

4. Occasionally the peak β -HPL flux is greater than the LPL flux measured at the same time. This results in the persistent feature being an enhancement, normally during the decay phase of the event. The 1 February 1968 (figure A-8) and 13 July 1968 (figure A-12) events

are graphic examples of this type of observation, but the 13 May 1968 event (figure A-11) is particularly notable: a significant β -HPL enhancement lasting for more than forty hours. An access window configuration of the $L_{\alpha\beta}$ type discussed above would mean that a β -HPL enhancement should be observed whenever the interplanetary flux gradient is positive and large enough:

$$\frac{1}{J} \frac{dJ}{dR} \geq 5 \times 10^{-3} \%/R_{\oplus} \text{ for a } V_1 \overline{V_3} \text{ rate of } \sim 10 \text{ cts/sec.}$$

The consistency with which all four of these phenomena are observed is strong evidence for the existence of the $L_{\alpha\beta}$ access window configuration illustrated in figure VII-2.

Thus, the OGO-4 proton observations consistently imply that the 1.2-40 MeV proton access windows are often related in the manner illustrated in figure VII-2, which we are referring to as the $L_{\alpha\beta}$ configuration. This configuration and other aspects of these data are quite relevant to the problem of placing constraints on the possible configurations of the distant geomagnetic tail.

Models of the Distant Geomagnetic Field Configuration

As mentioned above, one of the important and currently unresolved questions concerning the geomagnetic field is the degree to which the solar and terrestrial magnetic fields merge. Although charged particle observations cannot answer this question directly, a great deal of insight can be gained by analyzing the implications of such observations in the context of possible configurations of the geomagnetic field. Several such

configurations can be postulated, of course, but we will deal here with three fundamentally different models: a closed configuration (i.e., no merging), referred to as *model A*, an open configuration involving merging near the sub-solar point on the front of the magnetosphere (*model B*), and an open configuration involving merging at the polar neutral points (*model C*). Each of these models will be dealt with in turn: after a brief description of the major facets of a model, some of the consequences with respect to charged particle observations in the polar caps will be investigated. Following the discussion of the model, the pertinent OGO-4 data will be compared to these predictions. The results of this comparison between the model predictions and the OGO-4 results are listed in table VII-4. In this table, the predictions which are not attributable to one or more of the proponents of a given model and are thus the responsibility of this paper are indicated by italics; these extrapolations will be discussed below.

Closed Magnetospheric Configuration -- MODEL A

In the absence of merging, there will be no direct link between the geomagnetic field and the interplanetary magnetic field. Michel and Dessler have dealt with this picture extensively [3,10,96-100]. The most striking characteristic of this model is a very long tail, extending as far as an astronomical unit or more behind the earth [3]. As one moves away from the earth along the tail, the tail is pictured as being gradually flattened by the anisotropic pressure of the interplanetary magnetic field looping over the tail. It is postulated that somewhere between 1.1 and

TABLE VII-4

Correlation of Magnetic Field Configuration Predictions with OGO-4 Data

	Conse- quence of model A? ¹	Conse- quence of model B? ²	Conse- quence of model C? ³	Conclu- sion from OGO-4 Data?	References to OGO-4 Data
1. Persistent features are correlated with interplanetary sector measured at 1 AU.	NO	YES	YES	YES	Tables VII-2 and A-1 Figures VII-1, A-3, A-4, and A-9
2. Persistent features are correlated with N/S component of solar magnetic field.	NO	YES	NO	NO	Table A-1 Figure VII-1
3. Disappearance of persistent feature correlated with sector reversal at 1 AU within 0(1 hour).	NO	?	YES ⁴	YES	Table VII-2 Figures A-1, A-3, A-4, and A-9
4. Delay between LPL EDP peak and α -HPL EDP peak is 0(1 hr).	NO	YES	YES ⁴	YES	Table VII-3 Figures A-1, A-2, A-4 thru A-7, and V-4
5. Delay between LPL EDP peak and β -HPL EDP peak is 0(7 hrs).	?	NO	YES ⁴	YES	Table VII-3 Figures A-1, A-2, A-5 thru A-7, and V-4
6. β -HPL flux should always be \leq α -HPL flux.	YES	NO	NO ⁴	NO ⁵	Figures A-8, A-11, and A-12

TABLE VII-4 (continued)

(Correlation of Magnetic Field Configuration Predictions with OG0-4 Data)

	Conse- quence of model A? ¹	Conse- quence of model B? ²	Conse- quence of model C? ³	Conclu- sion from OG0-4 Data?	References to OG0-4 Data
7. Interplanetary flux gradients contribute to persistent features and N/S asymmetries.	YES	NO	YES	YES	Consequence of $L\alpha\beta$ access window configuration
8. Interplanetary anisotropies contribute to persistent features and N/S asymmetries.	?	YES	YES	YES?	Discussed in text
9. Persistent features or N/S asymmetries in the absence of interplanetary anisotropies.	YES	NO	YES	YES	Indirect evidence: east limb flares, flare decays, & long duration features
10. Persistent β -HPL > α -HPL in absence of interplanetary solar-directed anisotropies.	NO	NO	YES	YES	EDP events
11. β -HPL access window is about five times further behind the earth than α -HPL access window.	NO	NO	YES	YES	Consequence of $L\alpha\beta$ access window configuration

TABLE VII-4 (notes)

¹Michel and Dessler [10]: Extended geomagnetic tail, flattened by interplanetary magnetic field, becoming filamentary beyond 1.1-1.5 AU. Diffusive access from the earth to the filamentary region; rapid access to filaments for α -pole.

²Dungey [2], Axford, *et al.* [104], Reid and Sauer [13], Van Allen, *et al.* [25], and others: merging near the subsolar point on the magnetopause; implies north and south geomagnetic tails are both of the same length. Rapid access along field lines; interplanetary anisotropies may cause different HPL fluxes in the two poles.

³Frank [4]: Merging at the polar neutral points; implies north and south geomagnetic tails may be of different lengths. Rapid access along field lines; interplanetary gradients as well as anisotropies may affect polar cap observations.

⁴Answer depends upon the satisfaction of the constraints specified in the text. See also Appendix C.

⁵ β -HPL flux to α -HPL flux ratios as great as 2 have been observed during the decay phase of solar flare events; figure A-11 is a good example of a period during which the β -HPL flux was about 30-40% higher than the α -HPL flux; this implies a gradient of $\sim 2 \times 10^{-3} \%/R_{\odot}$. See also figures A-8 and A-12. This degree of enhancement is greater than would be expected from a solar-directed interplanetary anisotropy, the magnitude of which is typically between 5% and 20%.

1.5 AU the tail has become so drastically flattened ($\sim 10^3 R_\oplus$ wide by $\sim 10 R_\oplus$ thick at about $10^4 R_\oplus$ behind the earth) that the field becomes filamentary [10]. It is questionable, however, whether such a degree of flattening is supportable [101].

The primary mode of access for charged particles is by diffusion through the sides of the tail [10,97-99]. Michel and Dessler also postulate that charged particles may be able to rapidly gain access to the geomagnetic field in the filaments (i.e., beyond 1.1-1.5 AU) [10]. Michel and Dessler further point out that such a mechanism will probably be more effective for one pole than the other, depending on the orientation of the interplanetary field near the pertinent filaments in such a way that particles should be able to enter the filaments of the α -tail (defined in terms of the sector at 1.1-1.5 AU) more readily than those of the β -tail. This could lead to north/south differences in the fluxes observed at high polar latitudes, which would be correlated with the configuration of the interplanetary field at 1.1-1.5 AU (*cf.* A1 and A3 in table VII-4). The north/south component of the field does not appear to be pertinent to these access mechanisms (*cf.* A2). Although these mechanisms appear to be independent of the presence of interplanetary anisotropies (*cf.* A8, A9 and A10), it would seem that interplanetary flux gradients between 1 AU (LPL access window) and 1.1-1.5 AU could result in the observation of persistent features in the polar caps (*cf.* A7).

It is instructive to cast these access mechanisms in the framework of access windows. Both poles are said to have a window for slow, diffusive

access extending from ≥ 1 AU to $\leq 1.1-1.5$ AU, in which the rate of access is postulated to be independent of the orientation of the interplanetary field, and hence the same in both windows. Beyond these access windows, in the filamentary portion of the tail (*cf.* A11), is the rapid access window, which is postulated to be effective only for the α -pole. This access window configuration implies that the β -HPL flux can never exceed the α -HPL flux, since any flux gaining access to the β -tail would gain access to the α -tail at the same rate through the diffusive windows (*cf.* A6). The predictions of this model with respect to the observation of EDP events also follow from this picture of the access windows. The EDP peak would, of course, be observed at LPL coincident with the arrival at 1 AU of the interplanetary region of enhanced flux. After a delay of 10-50 hours (approximate solar wind propagation time for 0.1-0.5 AU), a peak would be observed at α -HPL. If the diffusion rate in the diffusive access windows were sufficiently rapid, an additional α -HPL EDP peak might be observed, coincident with a β -HPL peak and before the α -HPL peak due to access through the rapid access window. Whether or not the diffusion rate is rapid, however, it is clear that in either case the EDP observations would be phenomenologically quite different than those observed with OGO-4 (*cf.* A4 and A5).

As indicated in table VII-4 these predictions are inconsistent with the OGO-4 data. With the severe constraints which these data place on this model, it is questionable whether it can remain supportable in its present form. This does not imply, however, that no other closed magnetospheric configuration could be developed which would meet these constraints.

Magnetic Merging at the Sub-solar Point -- MODEL B

In contrast to the situation in model A, significant merging between the geomagnetic field and the interplanetary magnetic field will result in a configuration in which the high polar latitude regions are directly connected to interplanetary space. In 1961, Dungey [2] pointed out that in the presence of a southward component in the interplanetary magnetic field there might be two magnetic neutral points in the geomagnetic-interplanetary magnetic field system: one on the solar side of the magnetosphere, perhaps near the sub-solar point on the magnetopause, and the other behind the earth. As he and others have pointed out [102-107], if conditions at the neutral points were such as to allow magnetic field merging, then a configuration could be postulated wherein geomagnetic field lines merge with interplanetary field lines on the solar side of the magnetosphere, are pulled back across the polar caps as the solar field continues to propagate with the solar wind, and eventually reconnect at the anti-solar neutral point, after which the lines migrate back around the polar caps to the front of the magnetosphere again. Since the length of the tail in this configuration would be the product of the "age" of the tail (average time from merging at the neutral point on the solar side of the magnetopause to reconnection at the anti-solar neutral point) and the average propagation velocity, near the magnetopause, of the plasma in which the interplanetary field line is imbedded, the north and south geomagnetic tails would necessarily be the same length. Although both are the same length, as Dungey [106], Reid and Sauer [13], Van Allen, *et al.* [25], and others have pointed out, one tail may be connected to portions of the

interplanetary field which are solar-directed, while the other is connected to an anti-solar-directed field. This effect depends on the orientation of the solar field in the ecliptic plane (e.g. the sector of the solar field) near the earth (*cf.* B1 and B3 in table VII-4), and the entire process is dependent on the presence of a southward component in the solar field (*cf.* B2).

The access mechanism for low rigidity particles in this model is rather simple: the direct connection between the polar cap magnetic field and the interplanetary magnetic field allows interplanetary fluxes to gain access to the polar cap regions directly, although the trajectories involved may be non-adiabatic. Reid and Sauer [13], Van Allen, *et al.* [25], and others [24,26,108] have pointed out that interplanetary anisotropies may contribute to features observed in the polar cap regions (*cf.* B8), especially if adiabatic motion is invoked to imply that the only particles seen at α -HPL will be those having interplanetary pitch angle within a few degrees of zero, while the only particles seen at β -HPL will be those having interplanetary pitch angles within a few degrees of 180° . The validity of this assumption is discussed below and in Appendix B.

Several consequences for polar cap charged particle observations can be extrapolated from this model; most of these are consequences of the implied access window configuration: both HPL access windows located the same distance (the most recent estimates being a few hundred earth radii [25]) behind the LPL access window, which is, again, within $\sim 20 R_\oplus$ of the earth (*cf.* B11). Although interplanetary flux gradients could not, of course,

cause north/south asymmetries, they might cause persistent features if large enough $\left(\left| \frac{1}{J} \frac{dJ}{dR} \right| \geq 3 \times 10^{-2} \% / R_{\oplus} \right)$ to cause discernible differences between the LPL flux and the HPL flux (cf. B7). Clearly, then, with that one possible exception, persistent features and north/south asymmetries would not be expected except in the presence of interplanetary anisotropies (cf. B9 and B10). Also, if the interplanetary anisotropy were solar-directed, one would expect to observe a larger flux at β -HPL than at α -HPL (cf. B6). This access window configuration also implies that during EDP events both HPL peaks would be observed at the same time: on the order of an hour after the LPL peak (cf. B4 and B5).

The disappearance of persistent features may or may not be correlated to sector reversals, depending on the effect a given reversal has on the magnitude of the interplanetary anisotropy. If the anisotropy disappears coincident with the sector reversal, then so also will the persistent feature. If the anisotropy is unaffected by the sector reversal, then the feature should be seen to change from one pole to the other, staying in the β -pole (or α -pole) (cf. B3).

The extent to which the OGO-4 data agree with these predictions is illustrated in table VII-4. The net result of the observations is the implication that although interplanetary anisotropies may contribute to the features observed at the polar caps, other causes are clearly important as well. In particular, the EDP event observations are somewhat difficult to interpret in the context of an open field configuration in which the north and south HPL access windows are the same distance from the earth.

Magnetic Merging at the Polar Neutral Points -- MODEL C

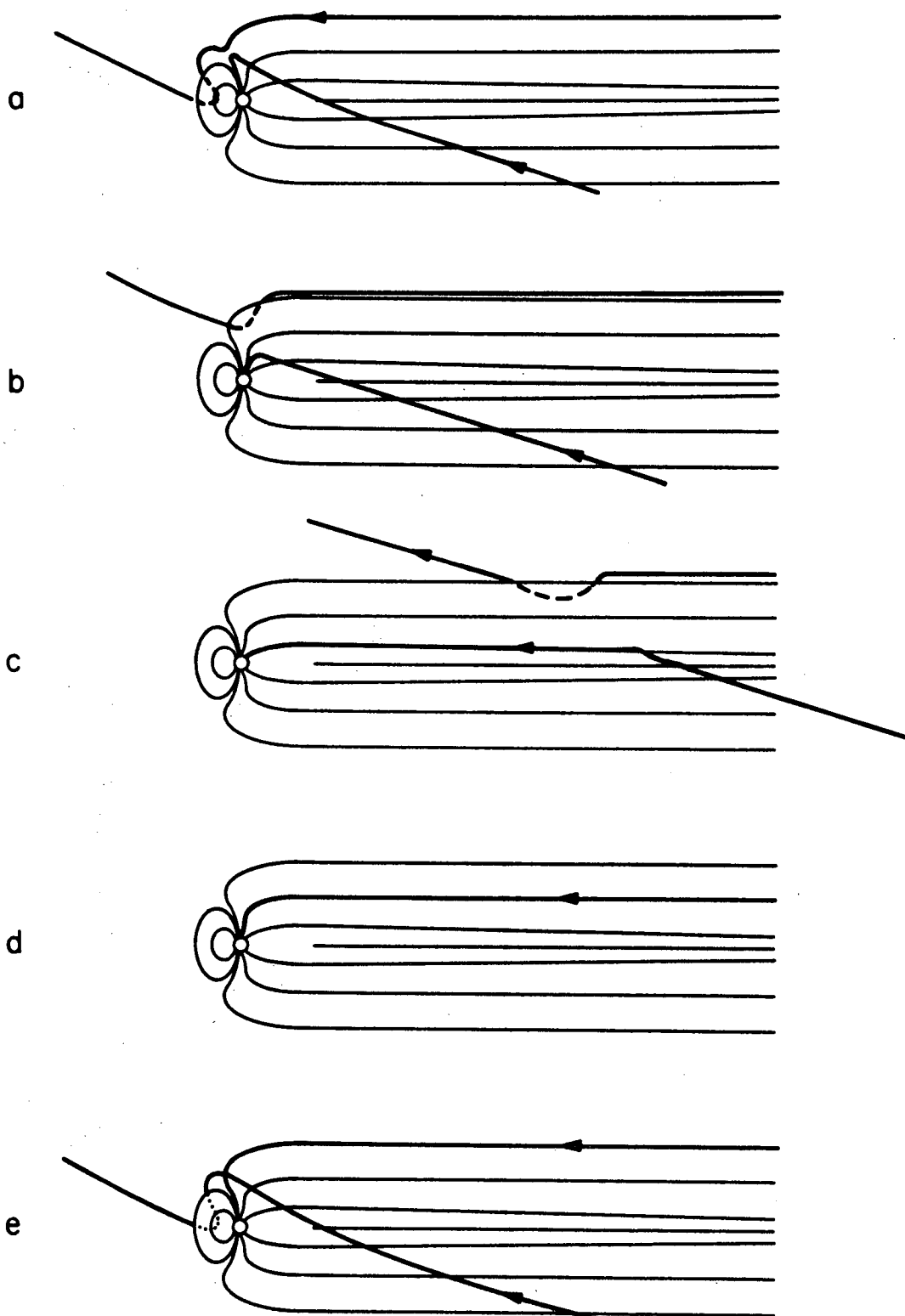
Frank has recently proposed a new variation of the open geomagnetic field configuration in connection with his studies of the relationship among the polar cusp region, the neutral sheet region, and auroras [4,109, 110]. Although this model was originally intended to explain other phenomena, its relevance to the problem of particle access into the magnetosphere is unique: it is an open configuration in which widely separated access windows might be a natural consequence. It is important, therefore, to investigate what constraints must be placed on the model to yield the sector-dependent $L\alpha\beta$ access window configuration prior to discussing the consequences of the model with respect to charged particle access. First, though, a brief description of the model is necessary.

All merging which takes place between the geomagnetic field and the interplanetary field is assumed to take place only at the polar neutral points (see figures VI-3 and VII-3). After a geomagnetic line of force merges with an interplanetary line of force, the foot of the line of force is pulled back along the boundary of the high polar latitude region. The intersection of the line of force and the magnetopause travels along an extension of the polar "cusp" region along the flank of the magnetosphere until the neutral sheet region is reached. At this point one of two things occurs, depending on the pre-merging configuration of the geomagnetic field line:

- A. The geomagnetic field line was originally a closed field line. The other end of the original line, which connects to the other

Figure VII-3

Schematic representation of the "history" of an open geomagnetic field line which merges with an interplanetary magnetic field line at the northern polar neutral point. The geomagnetic line of force merges at the neutral point (a), is pulled back along the cusp region (b) and into the neutral sheet region (c). The line eventually begins to migrate across the polar cap (d), until it once again passes near the polar neutral point (e).



pole, has been following a similar path along the "cusp" region in the other hemisphere. In the neutral sheet the lines again merge, re-connecting the two ends of the original interplanetary field line. The reconnected geomagnetic field line is eventually convected back to the front of the magnetosphere to undergo the process again.

B. The geomagnetic field line was originally an open field line. The other end of the original geomagnetic field line is no longer connected to the earth, and consequently appears to play no further part in the process of particle access. The line of force connected to the earth eventually begins to migrate across the tail until it is passing near the neutral point again, at which time the process can start again. The migration takes place to replenish open field lines which are being removed from the neutral point by the merging process (see figure VII-3).

Since only the open field lines are involved in the definition of access into the high polar latitude regions, we will confine our attention to the second process.

Since the interplanetary lines of force continue to be convected away from the earth by the solar wind, the length of the geomagnetic tail would be proportional to its "age": i.e., the time required for a line to complete an entire cycle, from merging to merging again. This time, in turn, is in some sense inversely proportional to the rate at which open field lines merge at the neutral point. It is immediately obvious, of course, that if the open field line merging rate were different at the two neutral points,

then the north and south geomagnetic tails would be of different lengths. There is, therefore, a mechanism whereby an $L_{\alpha\beta}$ configuration could be established. It remains, however, to investigate what conditions must be met to achieve the configuration of figure VII-2, which theOGO-4 data have established. There are at least three features which are pertinent in this regard:

- (1) the relative locations of the access windows,
- (2) the extent of the access windows, and
- (3) the time correlation between the disappearance of persistent features and sector reversals in the interplanetary field.

(1). The observational evidence which was discussed in relation to the $L_{\alpha\beta}$ access window configuration illustrated in figure VII-2 indicates that the position of the β -HPL access window can be between 3 and 10 times as far behind the earth as the α -HPL access window. For this to occur, the rate at which open field lines merge at the α -polar neutral point must be 3-10 times the rate at the β -polar neutral point. The theoretical investigation of this point is rather complex and is considered in detail in Appendix C. One of the major difficulties encountered in trying to deal with magnetic merging in this configuration is the applicability of earlier studies, all of which have concentrated on a configuration like that shown in figure VI-4: two exactly antiparallel fields considered in a plane parallel to the fields and perpendicular to the interface between them. The work of Sweet [84], Petschek [86], Sonnerup [87], and Yeh and Axford [88], discussed above, can be generalized to treat two non-antiparallel fields by the superposition of a constant field perpendicular

to the plane in which they analyze the antiparallel field configuration and by making the suitable minor readjustments of their results (see (6.1) and (6.2)). The configuration of the fields at the geomagnetic neutral points, however, involves, as shown in figure C-2, the interaction between a region where the field is homogeneous and a region where the orientation of the field is a strong function of position. Assumptions must consequently be made concerning the merging likelihood for two fields as a function of the angle between them in the presence of fields at all such angles. The implications of three such assumptions, chosen as representative of a wide range of possible assumptions, are investigated in Appendix C.

The main conclusions to be drawn from the results of Appendix C are that (a) such differences in polar merging rates are well within the limits of reasonable parameters if certain assumptions are made concerning the angular dependence of the merging rate, and (b) if the sector is redefined in terms of the earth-sun line and the interplanetary field direction near the polar neutral point instead of the average spiral angle and the field direction far from the earth, the correct sector correlation follows.

That the critical interplanetary field configuration is that of the portion of the field near the polar neutral points complicates matters considerably. It is not clear how this configuration depends in detail on the field configuration in interplanetary space and on the solar wind parameters [cf. 111,112]. Nor is it clear that for a given set of interplanetary parameters the interplanetary field will make the same angle with the

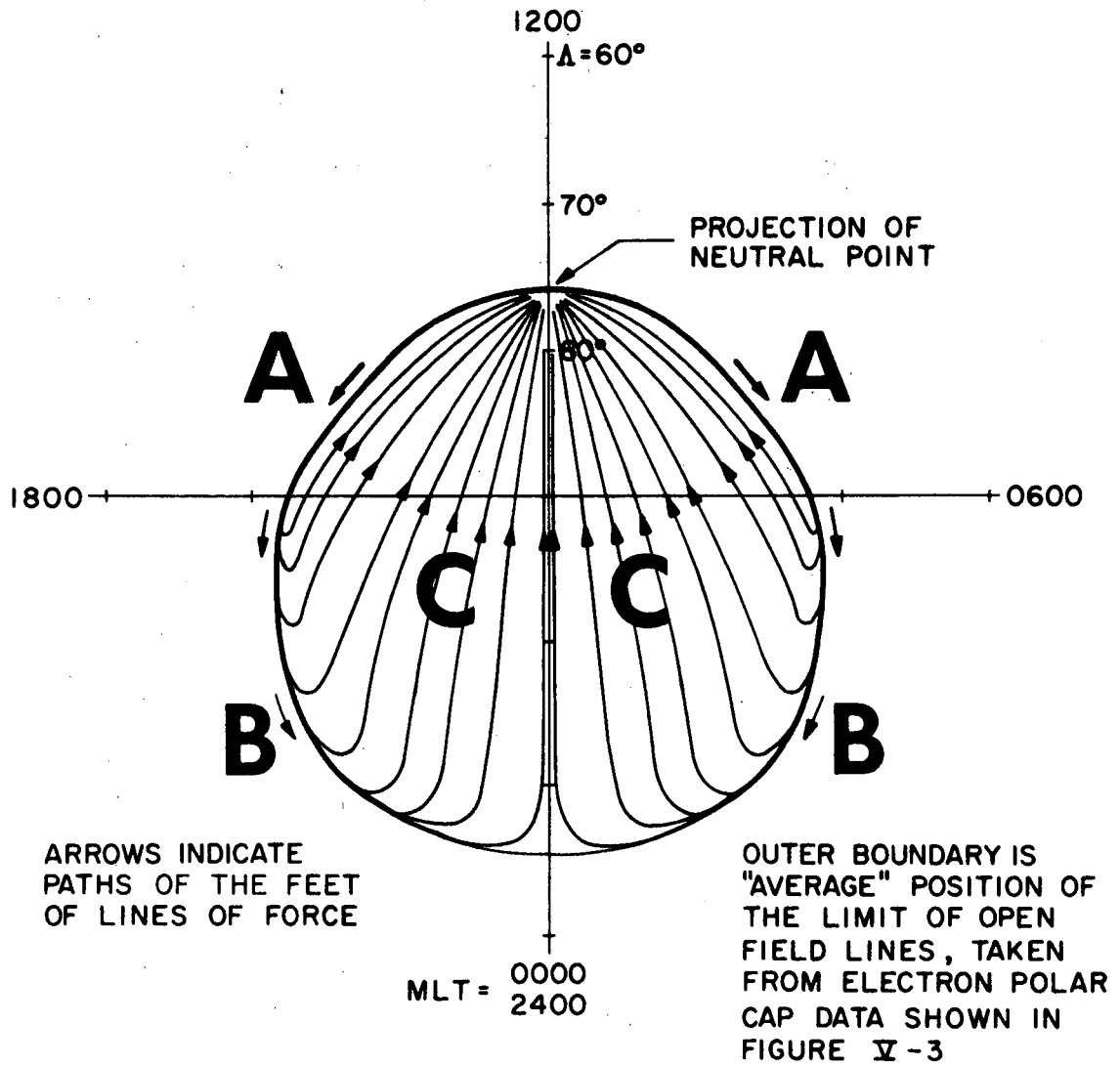
earth-sun line at one neutral point as it does at the other. Until this question is resolved, it will not be possible to determine whether there is an exact, detailed correlation between the access window positions inferred from the data and those inferred from this model.

(2). The size of the HPL access windows relative to their positions places constraints on the way in which the geomagnetic field lines migrate from the neutral point to the neutral sheet region and back to the neutral point. Figure VII-4 shows a tentative migration pattern, wherein the paths followed by the feet of the open lines of force are shown projected into an invariant latitude-magnetic local time coordinate system. After merging at the neutral point a line is pulled down the cusp region (paths A), into the neutral sheet region (paths B), and finally migrates back to the neutral point (one of paths C). As soon as the foot of a line of force enters the central region of the polar cap (C), the intersection of that line with the magnetopause becomes part of the HPL access window for that pole. It remains part of the access region until the magnetopause intersection is no longer connected to the polar region (i.e., until the line merges again at the neutral point). The length of the access window (measured parallel to the axis of the tail) is therefore proportional to the time required for the lines to migrate from the neutral sheet region (B) across the polar cap (C) to the neutral point.

The data presented in Section V indicate the parameters given in (7.2) as "typical" for the $L\alpha\beta$ access window configuration. In contrast to the case for the positions of the access windows, the length of the windows does not seem to depend heavily on the interplanetary sector. This

Figure VII-4

Tentative sketch of the migration pattern for polar geomagnetic field lines in Frank's magnetospheric model (model C). Examples of the "paths" followed by the feet of the polar field lines are projected into a Λ -MLT coordinate system.



would imply that the time spent by a line migrating across region C would need to be more or less independent of the total migration time for a complete cycle. This is a clear constraint which the experimental data place on this configuration.

(3). The data shown in table VII-2 indicate that persistent β -HPL features disappear within about one hour after a reversal in the interplanetary sector. This means that within one hour after a sector reversal from, for instance, negative to positive the northern high polar latitude access region has changed from a β -HPL configuration to an α -HPL configuration. This establishes a lower limit for the merging rate at the α -polar neutral point: it must be at least as large as that necessary for almost every high polar latitude field line to have merged with the interplanetary field at least once in less than one hour; i.e., an open field merging rate not less than $\sim 1.3 \times 10^5 \mu\text{G-R}_\oplus^2/\text{hr}$.

This rate is not inconsistent with the following estimate for the maximum rate at which the interplanetary magnetic field impinges on the polar neutral points. If all of the $\sim 60 \mu\text{G}$ interplanetary magnetic field which impinges on the front of the magnetosphere is thought of as being swept up past the neutral point by the $\sim 225 R_\oplus/\text{hr}$ (400 km/sec) solar wind, then the "rate" at which the interplanetary field would impinge on each neutral point would be $\sim 1.4 \times 10^5 \mu\text{G-R}_\oplus^2/\text{hr}$.

These rates are also consistent with at least two of the theoretical maximum merging rates discussed in Section VI: those predicted by Sonnerup [87] and by Yeh and Axford [88]. The consistency with the latter predic-

tion is self-evident, since they predict that there will be no upper limit on the merging rate. In order to check the consistency of these merging rates with the prediction of Sonnerup, given by (6.2), we must estimate the solar wind conditions near the polar neutral points. According to Spreiter, *et al.* [111],

$$V_{np}/V_{sw} \sim 0.7$$

and

$$\rho_{np}/\rho_{sw} \sim 1.8$$

Also, according to Alksne [113],

$$B_{np}/B_{sw} \sim 4$$

This means that

$$V_{A,np}/V_{A,sw} \sim 3$$

and the Alfvénic Mach number of the solar wind plasma near the polar neutral point is therefore

$$(M_A)_{np} = (M_A)_{sw} \frac{V_{np}/V_{sw}}{V_{A,np}/V_{A,sw}} \\ \sim 1.9$$

Thus the idea of the interplanetary magnetic field merging as fast as it impinges on the neutral point is not inconsistent with (6.2), which specifies

$$M_A \leq 2.4$$

Assuming these constraints to be satisfied, the degree to which the OGO-4 data agree with the resultant predictions of this model is indicated in table VII-4, although the *a priori* assumption that the constraints discussed above were satisfied was begging the question somewhat. It is interesting that this model is the only type discussed here which even qualitatively provides a mechanism for generating an $L_{\alpha\beta}$ access window configuration. Although the data presented here cannot provide a conclusive test of the validity of the model in its present form, they do provide three major constraints within which more refined versions of the model will have to be developed.

Interplanetary Anisotropies

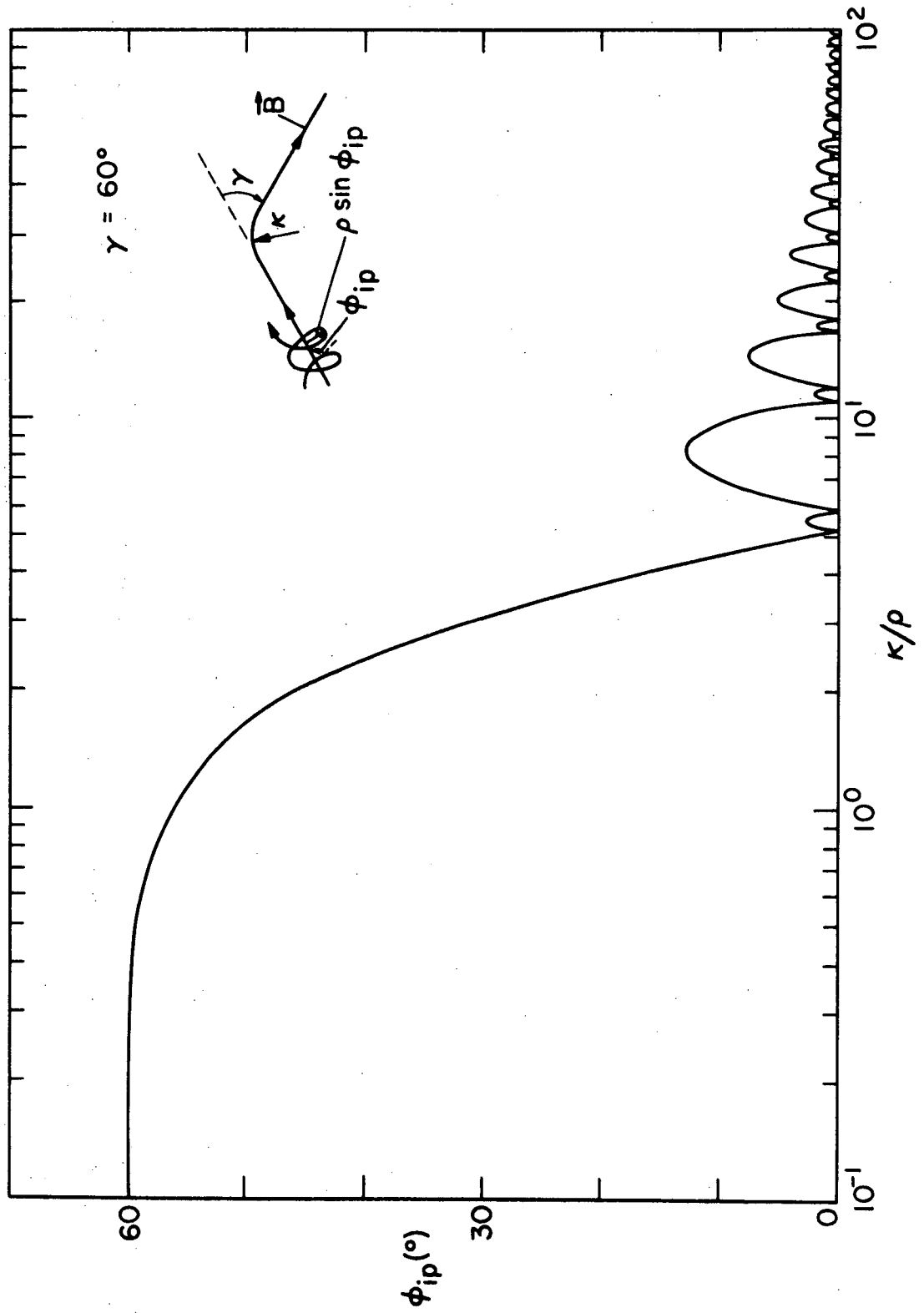
Although not directly supportable from the OGO-4 data due to a lack of interplanetary measurements, it is certainly not unreasonable to suppose that interplanetary anisotropies may have some affect on polar cap observations and may contribute to persistent features (*cf.* #8 in table VII-4). The entire role of interplanetary anisotropies in the formation of polar cap features in an open geomagnetic configuration is not at all as straightforward as it may appear at first, however. The assumption of adiabatic motion in the propagation of particles from interplanetary space to the polar regions means that the magnetic moment is conserved and that therefore the only particles observable at the altitude of OGO-4 are those with interplanetary pitch angles $\leq 1^\circ$ or $\geq 179^\circ$. Since the geomagnetic tail field and the interplanetary field are almost never parallel, the propagation of particles from interplanetary space to the geomagnetic tail

will involve the passage through a region where the magnetic field is changing direction. Since the propagation of particles in the tail between the transition region (access window) and the polar caps can be considered adiabatic, only those particles with pitch angles near zero (or 180°) in the tail will be observed at the altitude of OG0-4. If the "curvature" of the magnetic field in the transition region is sufficiently large compared to the gyroradius of the particle, then adiabatic motion might indeed be expected.

Appendix B treats this problem in some detail, dealing with the configuration of two magnetic fields equal in magnitude separated by a region in which the field changes direction with a constant radius of curvature (*cf.* figure B-1). Figure VII-5 shows typical results for the magnetic fields at an angle of 60° . In this figure, ϕ_{ip} is the interplanetary pitch angle giving a pitch angle of 0° after traversing the transition region; ϕ_{ip} is shown as a function of κ/ρ , where ρ is the particle's gyroradius and κ is the constant radius of curvature of the field in the transition region. Other values of γ give comparable results (see Appendix B). These results show that, for $\gamma=60^\circ$, unless $\kappa/\rho \geq 50$, the interplanetary pitch angle ultimately being observed at the polar caps varies drastically as a function of particle energy and as a function of the instantaneous interplanetary field configuration. One would not expect, for instance, that 3 MeV protons, which have a gyroradius of about $9.8 R_\oplus$ in a $60 \mu\text{G}$ interplanetary field, with pitch angles $\leq 1^\circ$ in interplanetary space would be observed at the polar caps, except transiently, unless κ were greater than about $490 R_\oplus$. Since the cross sectional

Figure VII-5

Interplanetary pitch angle (ϕ_{ip}) giving a pitch angle of 0° after passing through a region in which the magnetic field changes direction through an angle $\gamma=60^\circ$. The direction change is assumed to take place at a constant radius of curvature, κ . The gyro-radius of the particle in the magnetic field, whose magnitude does not change, is represented by ρ . See Appendix B for a more detailed explanation of these results.



radius of the entire tail at about $200 R_{\odot}$ is about $25 R_{\odot}$, it is hard to visualize a transition region which is at least $490 R_{\odot}$ wide. These pitch angle mapping results are, of course, relevant only in the presence of an interplanetary anisotropy; if the interplanetary flux is isotropic, it does not matter *which* interplanetary pitch angles are observed over the polar caps.

Although direct observational evidence for interplanetary anisotropies is not available from the OGO-4 data, there are three pieces of pertinent indirect evidence indicating the observation of persistent north/south differences in the absence of interplanetary anisotropies (*cf.* #10 in table VII-4):

- (a): A number of the flare events observed with OGO-4 either were associated with east limb optical flares or were possibly associated with optical flares on the other side of the solar disc. Although interplanetary anisotropies have been observed at low proton energies during *some* east limb flares, it is suggestive that persistent features (and hence north/south flux differences) were observed during all flare event observations made with OGO-4.
- (b): Persistent features are consistently observed during the decay phase of flare events, whereas anti-solar directed field aligned interplanetary anisotropies normally disappear shortly after the peak of a flare event. Interplanetary anisotropies observed during the decay phase of flare events are normally anti-solar directed and solar wind aligned. Examples of persistent β -HPL depressions are shown in fig-

ures A-3 and A-9. The β -HPL flux was as much as a factor of 10 below the LPL and α -HPL fluxes during the 8 February 1968 event (figure A-9).

- (c): Several features are observed to persist for very long periods, exceeding 40 hours in at least two of the cases shown in Appendix A. This is a much longer duration than that expected for large interplanetary anisotropies (5-15 hours, depending on the time between onset and the peak). Figure A-3 shows a persistent feature which lasted for more than 24 hours. The best example, though is probably that in figure A-9, showing a very large feature $((V_1\overline{V_3})_{LPL} : (V_1\overline{V_3})_{\beta-HPL})$ as large as 25:1) persisting for at least 31 hours *during the decay* phase of the flare event.

VIII. CONCLUSIONS

Observations of polar cap fluxes of low energy solar protons (1.2-40 MeV) and electrons (0.4-1.0 MeV) made with an experiment on board the OGO-4 satellite lead to the following conclusions.

1. Extensive observations of electron polar cap fluxes during geomagnetically quiet periods have resulted in a comprehensive mapping of the boundary between open and closed geomagnetic field lines onto the polar cap. This mapping, shown in figure V-3, is an order of magnitude more comprehensive than previously available.

2. Observations during 54 solar proton events have established that the presence of persistent features in the polar cap proton flux is the norm rather than the exception (see table A-1 and figure VII-1).

3. A comparison between the electron polar cap boundary (see conclusion #1) and persistent features in the proton polar cap flux indicate that, in general, these features represent different flux levels in the open field line region (high polar latitudes -- HPL) than in the closed field line region (low polar latitudes -- LPL).

4. There is a strong correlation between the observation of persistent polar cap features and the sector structure of the interplanetary magnetic field: in general, persistent features are observed in the south

pole during a positive sector and in the north pole during a negative sector. On the basis of this correlation, the term " β -pole" is defined in such a manner as to refer to the south pole during a positive sector and in the north pole during a negative sector; in both cases the opposite pole is referred to as the α -pole. The OGO-4 observations reported here are correlated in this fashion 91% of the time.

5. The observation that persistent features disappear within O (one hour) of a reversal in the interplanetary sector is also consistent with this sector correlation.

6. There appears to be little or no correlation between the presence of persistent features in the proton polar cap flux and the orientation of the north/south component of the interplanetary magnetic field: during the observations of persistent features this component was southward only 54% of the time and changed orientation several times with no noticeable effect.

7. Observations of solar proton events, especially those associated with co-rotating regions of enhanced flux in interplanetary space, have been used to establish the $L\alpha\beta$ access window configuration illustrated in figure VII-2, in which the LPL access window is near the earth, the α -HPL access window is a few hundred earth radii behind the earth (in the anti-solar direction), and the β -HPL access window is located $O(2000 R_{\oplus})$ behind the earth.

8. The widths of the HPL peaks observed on the EDP event profiles

imply that the extent of the α -HPL access window is about the same as that of the β -HPL access window. A comparison with the LPL peaks further implies that neither of the HPL access windows is much larger than the LPL access window (see figure VII-2).

9. Although direct interplanetary measurements are not available from the OGO-4 data, it is concluded that the following contribute to persistent polar cap features (north/south asymmetries):

- A. limited interplanetary regions of enhanced flux propagating past the earth,
- B. radial gradients in the interplanetary flux, and
- C. anisotropies in the interplanetary flux.

10. The OGO-4 observations are not consistent with the particle access mechanisms proposed by Michel and Dessler [3].

11. The access window configuration deduced from EDP event observations (conclusion #7) is not consistent with an access window configuration in which both HPL access windows are the same distance from the earth, as would be expected in an open magnetospheric configuration involving magnetic merging near the sub-solar point (*cf.* Dungey [2]).

12. An $L\alpha\beta$ access window configuration (conclusion #7) may be a consequence of an open magnetospheric model involving magnetic merging at the polar neutral points (*cf.* Frank [4]). To achieve this configuration, however, it is necessary that the model satisfies at least the following constraints:

A. The merging rate for open geomagnetic field lines at one polar neutral point (α) must be ~ 5 times that at the other polar neutral point (β). This difference between the open field line merging rates must be related to the orientation of the interplanetary magnetic field, as measured far from the neutral point, in such a way as to be consistent with the observed correlation with the interplanetary sector structure (conclusion #4) and lack of correlation with the north/south component of the interplanetary field (conclusion #6).

B. The time required for open field lines to migrate from the neutral sheet region across the polar cap to the vicinity of the neutral point must be about the same in both tails, so as to account for both HPL access windows being about the same size (conclusion #8).

C. The rate at which open field lines merge with the interplanetary field at the α -polar neutral point must be at least as large as that required for almost all of the open field lines to have merged in $O(\text{one hour})$, since β -HPL features disappear within $O(\text{one hour})$ after a sector reversal (conclusion #5).

In addition to these observational conclusions, the following conclusions are implied by the results of the theoretical investigations presented in Appendices B and C.

Appendix B: The assumption of adiabatic motion for the access of 1.2-40 MeV protons from interplanetary space to the interior of the

magnetosphere is not a good approximation. If the extent to which an interplanetary pitch angle distribution maps onto the polar cap region were to be determined from appropriate data, figure B-4 would indicate the constraints thus imposed on the configuration of the magnetic field in the vicinity of the access windows.

Appendix C: The satisfaction of constraint A mentioned above in conclusion #12 is possible if the proper assumptions are made concerning angular dependence of the probability that two field lines will merge. This can be seen by comparing figures C-8, C-9 and C-10.

Although the results outlined above are most consistent with a field configuration involving magnetic merging at the polar neutral points, the question of whether there is a significant degree of merging between the geomagnetic and interplanetary magnetic fields cannot be unambiguously determined by charged particle measurements. These observations do, however, provide a suitable platform upon which to base theoretical investigations of this question.